Title
A Study on Identification and Compensation of the Dynamic Behavior of CNC Machine Motion Error

Author
Kidani, Shinya

Publication Date
2020

Peer reviewed|Thesis/dissertation

A Study on Identification and Compensation of the Dynamic Behavior of CNC Machine Motion Error

by

Shinya Kidani

A dissertation submitted in partial satisfaction of the

requirements for the degree of

Doctor of Philosophy

in

Engineering - Mechanical Engineering

in the

Graduate Division

of the

University of California, Berkeley

Committee in charge:

Professor Kazuo Yamazaki, Chair
Assistant Professor Hayden Taylor
Professor Anant Sahai

Spring 2020

A Study on Identification and Compensation of the Dynamic Behavior of CNC Machine Motion Error

Abstract

A Study on Identification and Compensation of the Dynamic Behavior of CNC Machine Motion Error

by

Shinya Kidani

Doctor of Philosophy in Mechanical Engineering

University of California, Berkeley

Professor Kazuo Yamazaki, Chair

Computer numerical controlled (CNC) machine tools or simply machine tools play one of the most fundamental roles in modern society to produce various types of industrial and commercial products. In order to obtain high performance products, there has been a continuous requirement for high-performance parts that require tight tolerance. Thus the accuracy requirement for the machine tools has become higher and higher. As of 2020, CNC machine tools with 1μm of positioning accuracy are commercially available, and further requirement for higher accuracy is expected.

In order to achieve high accuracy of CNC machine tools, machine tool engineers and researchers have developed various technologies and techniques to eliminate the error sources at the design and assembly stage. Even though, achieving the accuracy in the order of micrometer is still challenging. Therefore, modern CNC machine tools are equipped with the functionality so called error compensation to cancel the tiny errors by slightly adjusting the motion of the machine. However, these error compensation functions are not designed to keep track of the dynamic change of accuracies, such as thermal distortion or aging deterioration, during a machining process. As machine tools are expected to produce a large number of parts with a constant quality of accuracy continuously, the accuracy deterioration must be compensated as soon as possible. However, most of the conventional error compensation procedures require manual labor to set up measurement equipment, time to execute a measurement program, data analysis, and manual updating the compensation parameters. Therefore, this study aimed to develop a novel error compensation system that enables machine tools to measure the accuracy and update the compensation parameters automatically. As a key to the automation system, a built-in automatic measurement and compensation system based on dual linear scales is proposed, and the following four points are investigated to realize the system.

1. The principle of the integrated measurement system
2. The design methodology of the built-in sensor system
3. The feasibility of the proposed system on an actual machine tool
4. The remaining technological problem to be solved and an idea of the solution for future study

Based on the analysis, a physical prototype was developed, and its feasibility was investigated by a series of experiments. The results showed that the measurement with the linear scale system agreed with a conventional measurement method within the uncertainty estimated at the design stage. Based on the accuracy deterioration detected by the scale system, the compensation of the accuracy deterioration was attempted. With the compensation, the maximum accuracy deterioration was successfully suppressed from 22 to 3 μm, which is verified by the laser measurement. This indicates that the accuracy of a machine tool can be maintained by the dynamic measurement and compensation system. Future perspective of this study is also discussed. Based on the theory of magnetic field intensity, it was explained that six DOF measurement would be possible in principle by arranging multiple read heads on the moving component. Also, in order to realize a dynamic error measurement, a data analysis scheme with k nearest neighbor algorithm was introduced, and its feasibility was assessed with a sample data. From these results, the feasibility of the proposed dual linear scale system has been verified for yaw measurement. The same kinematic model and data analysis scheme is also applicable to the remaining five DOF elements. Since the scale system has the scalability of degrees of freedom of measurement, further development of the linear scale technology still remains to improve the maturity of this system.

To all my loved ones

I would like to dedicate this dissertation to all my loved ones.

Contents

List of Figures

List of Tables

Acknowledgments

I would like to express my sincerest gratitude to Professor Kazuo Yamazaki, professor of the University of California at Berkeley and director of the Precision Manufacturing Center (PMC), Berkeley Institute, and president of the Machine Tool Technologies Research Foundation (MTTRF). His continuous support and guidance throughout my tenure as a member of the PMC laboratory has strengthened my technical foundation and expanded my knowledge of interdisciplinary engineering concepts. I will always carry his teachings with me and apply them towards further personal growth and moving forward in my professional career.

I also thank Professor Hayden Taylor, Professor Anant Sahai, professors of the University of California at Berkeley for their expert comments on the research from their specialized domain.

I also thank Dr. Masahiko Mori, president and CEO of DMG MORI Co., Ltd., for having granted me the opportunity to study at the university. Without his understanding and kind financial support from the company, this research had never accomplished.

I would also like to thank Professor Masakazu Soshi, professor of the University of California at Davis, in the Mechanical and Aerospace Engineering Department for his generous time and dedication to review of this manuscript that were applied in this research.

I would like to thank Mr. Jim Okada, director of the MTTRF for the encouragement throughout this experience.

I would like to thank Dr. Makoto Fujishima, Dr. Naoto Takayama, senior managing directors of DMG MORI Co., Ltd. for their continuous support and helpful comments on the research. Dr. Naruhiro Irino from DMG MORI Co., Ltd. gave me various technical advice from his professional viewpoint, including logical composition, presentation, and writing.

I would like to thank Dr. Toru Fujimori, Ms. Kayoko Taniguchi, Mr. Shigeaki Maruyama, Mr. Shigeru Ishimoto, Mr. Shuko Ishibashi, from Magnescale Co., Ltd., for having supplied the state-of-the-art linear encoders and data-capturing system. Their technical support made an essential contribution to this research.

I would like to thank my colleagues at DMG MORI, the PMC laboratory, and the IMS laboratory for their aid and encouragement throughout this experience.

Finally, I would like to thank my family for supporting me during the compilation of this dissertation.

Chapter 1

Introduction

1.1 Machine Tool and its Accuracy

Computer numerical controlled (CNC) machine tools or simply machine tools play one of the most fundamental roles in modern society to produce various types of industrial and commercial products. Quite many products are composed of metal parts manufactured by machine tools: automobiles, industrial robots, constructing machines, aircrafts, injection molds for plastic products, and medical devices shown in Figure 1.1 are just a few examples of them. Even a machine tool itself consists of parts that are manufactured by other machine tools. Thus, machine tools are sometimes called "mother machines" that implies "machines that create other machines" [1].

Industrial products or parts are generally produced by changing the shape of raw materials by adding, removing, or forming the materials. The manufacturing technology is broadly categorized into removal and non-removal processes, depending on if the unnecessary portion of the raw material is removed or not to change the shape. The non-removal process is further divided into the melting process and forming process. The removal process is divided into machining and unconventional process, as shown in Figure 1.2.

Machine tools mean any machines that perform any of the manufacturing process in a broad sense. However, in a narrow sense, machine tools are defined as machines to perform the removal process, more specifically the machining process [2]. Figure 1.3 summarizes the machining methods conducted by machine tools [3]. The cutting process removes metal materials from a workpiece by using cutting tools such as an endmill or drill to form a desired shape. The grinding process uses a grinding wheel as the cutting tool and fabricates a fine surface finish and very accurate dimensions. For workpiece with a specific property or geometry, other machining methods such as wire electrical discharge machining or ultrasonic machining is selected. Recently, additive manufacturing receives attention for fabricating parts with unique, intriguing, and appealing geometric forms, such as sophisticated internal features to increase functionality and improve performance [4]. The additive process is not a

machining process in the narrow sense, but major machine tool manufacturers are developing new type of machine tools for more advanced part production by integrating the additive manufacturing with the cutting process [5, 6, 7]. In this study, machine tools specifically means the machines for the metal cutting process. Typical examples of the machine tools are machining center for milling or drilling of block part and turning center for machining of cylindrical part, as shown in Figure 1.4.

Figure 1.5 shows an example of a face milling operation performed by a machining center. In metal cutting by using a machine tool, material removal is achieved by defining relative motions between a cutting tool and a workpiece during their physical interference. Due to the physical interactions, the motion of the cutting tool is directly copied on the workpiece. This interaction determines the geometric and dimensional accuracies of the machined products. The accuracy of the machined parts depends on and never transcends that of the machine tool used for the machining process. Due to this "copying principle" [8], in order to obtain highly accurate products, there has been a continuous requirement for machine tools with higher accuracy. Figure 1.6 shows tolerances on some typical mechanical components created by the machine tools [9]. High-performance parts requires tight tolerance, thus the machine tools must have high accuracy. As of 2020, CNC machine tools with 1μm of positioning accuracy are commercially available, and further requirement for higher accuracy is expected.

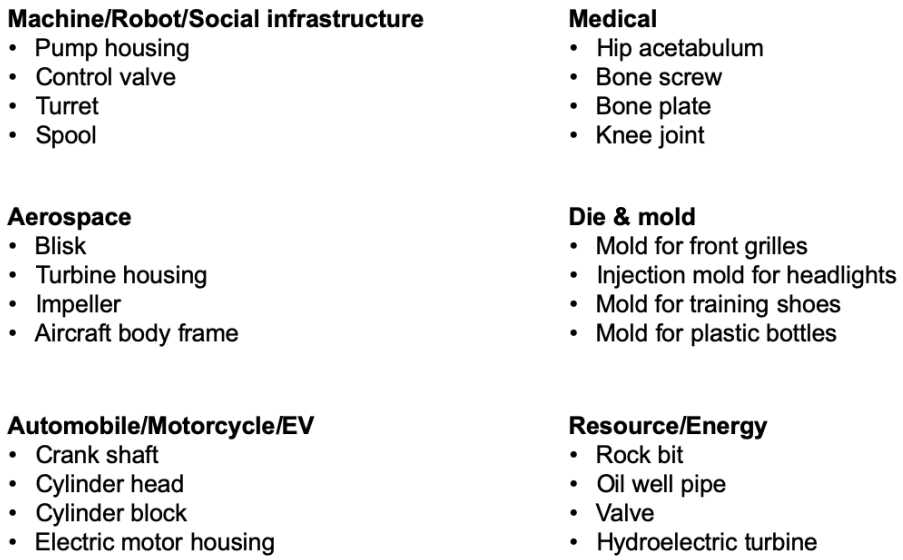

Figure 1.1: Example of products machined by CNC machine tools.

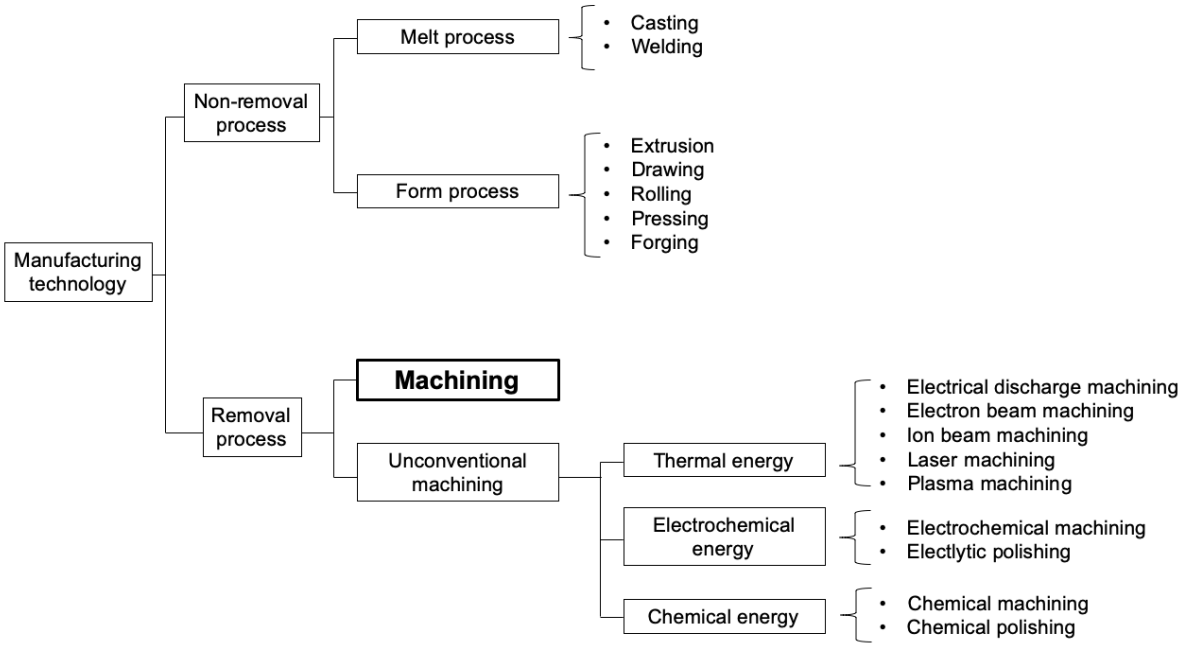

Figure 1.2: Classification of the manufacturing process (translated from [10]).

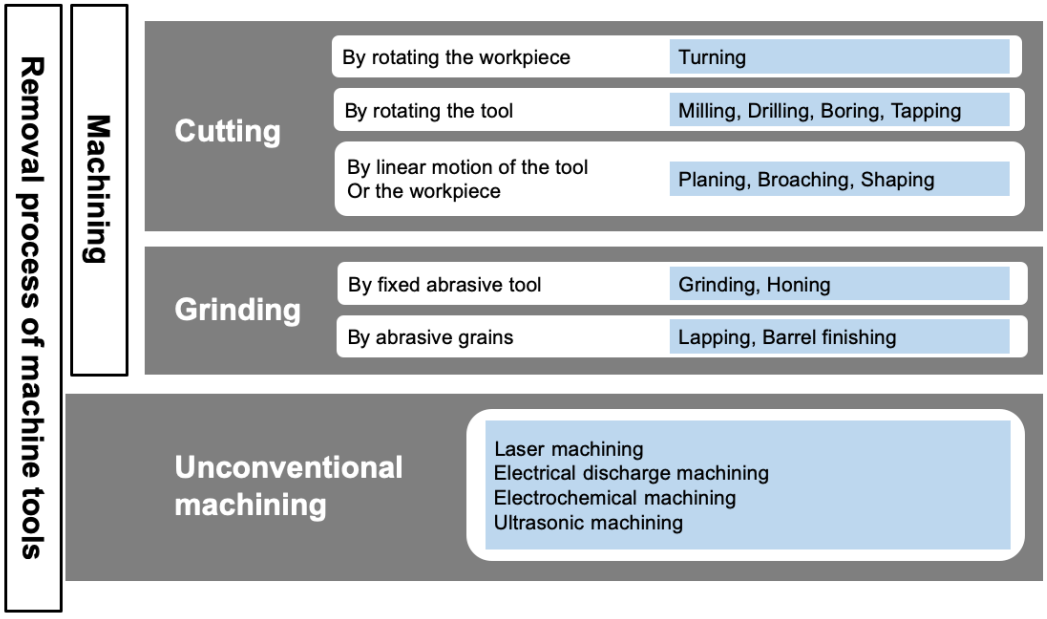

Figure 1.3: Machining methods conducted by machine tools [3].

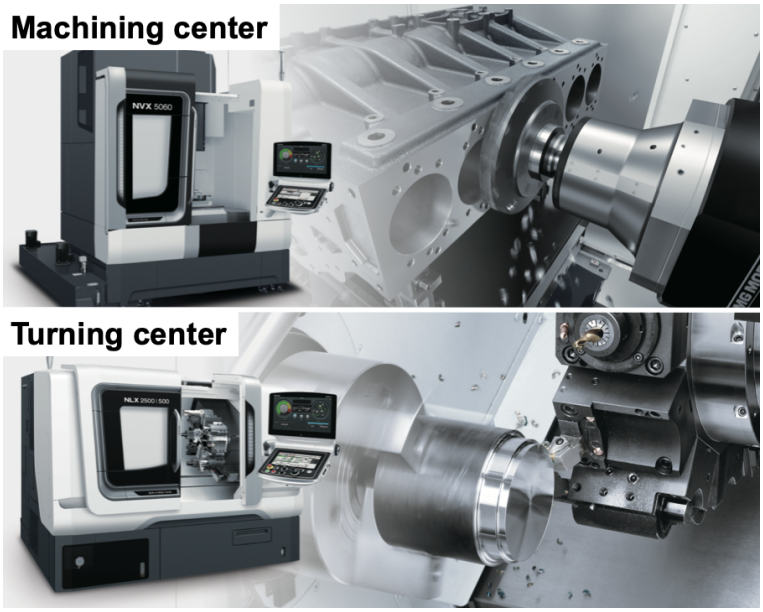

Figure 1.4: Machining center for milling or drilling of block part and turning center for machining of cylindrical part [11].

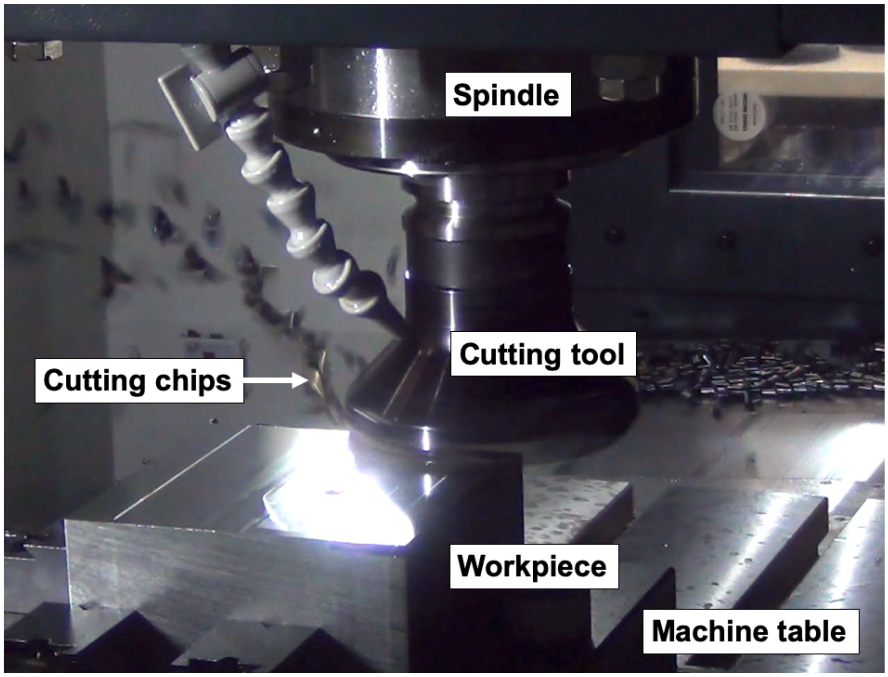

Figure 1.5: Example of a face milling operation by a machining center.

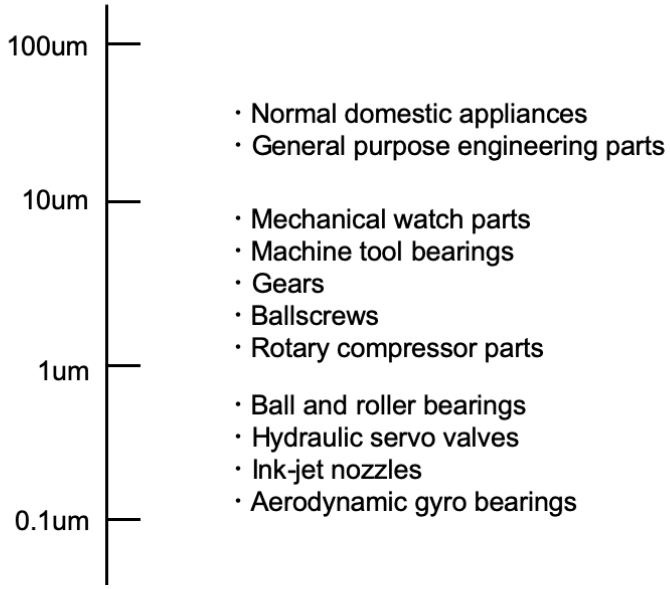

Figure 1.6: Tolerances of typical mechanical components (created based on [9]).

1.2 Technology to build a precision machine tool

1.2.1 Errors in a Machine Tool and the Classification of their Generation Mechanisms

As mentioned in the previous section, a machining process is achieved by the physical interference and relative motions between a cutting tool and a workpiece. A highly accurate machine tool can locate the cutting tool tip or tool center point (TCP) precisely at the target point on the workpiece. However, just as no mechanical system is perfect, it is impossible to make a machine tool without error, and there is always a relative displacement between the TCP and the target point. Figure 1.7 shows an example of a relative displacement between the TCP and the target point induced by a rotational error of the spindle component. In this paper, this relative displacement is called the error at the TCP. The error at the TCP generates as a combination of various types of the mechanism called error sources. Therefore, it is important to understand the individual error sources.

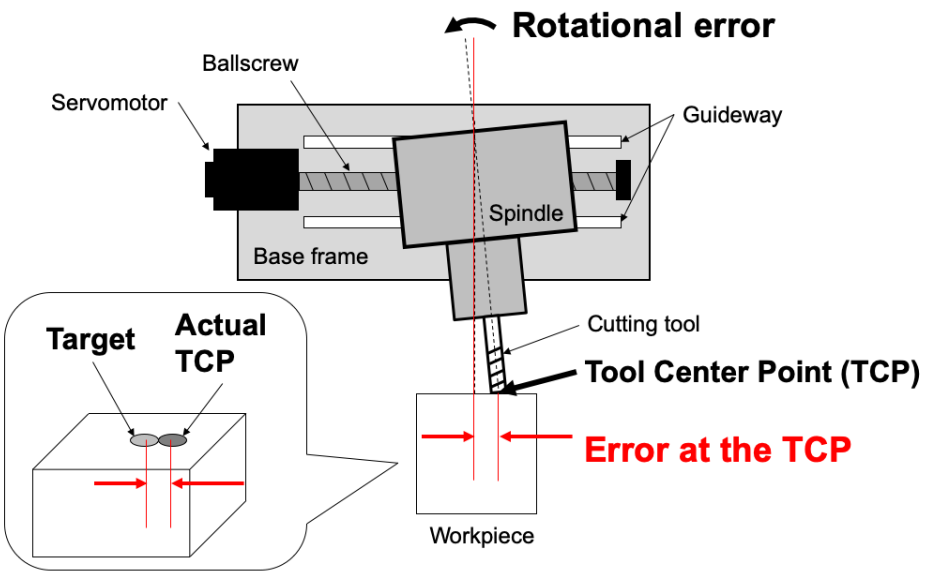

Figure 1.7: A relative displacement between the TCP and the target point induced by a rotational error of the spindle component.

Inasaki describes a machining process as a mutual interaction between the cutting process and the machine [12]. The cutting process generates the cutting force, and the force deforms the machine components. The deformation alters the relative position of the cutting tool for the workpiece, and the deviation is fed back to the cutting process. The closed loop forms the machining process, as shown in Figure 1.8. Therefore, the generation mechanisms of the errors in the machining process can also be classified into two: the cutting-process-oriented and the machine-oriented error sources. Here, the cutting-process-oriented error sources are called the external sources, and the machine-oriented error sources are called the internal sources. Each category can be further divided into small groups. Although there can be various way to classify the error sources depending on the point of view, based on some keynote papers [13, 14], the error sources can be broadly classified into four groups: Geometric and kinematics of mechanical components, heat, force, and servo control system. Then, the interaction among the error sources can be summarized, as shown in Figure 1.8.

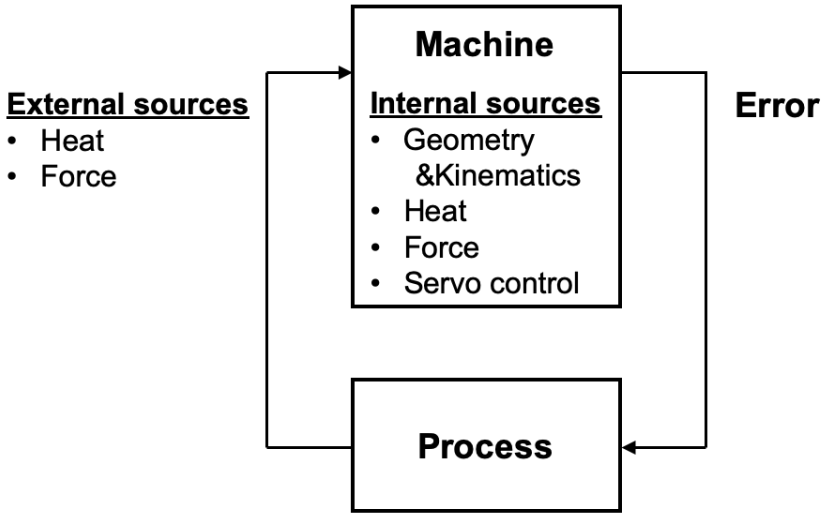

Figure 1.8: The mutual interaction between the cutting process and the machine, and the classification of error sources (created based on [12, 13, 14]).

- Geometric and kinematic errors

  Geometric errors stem from the dimensional inaccuracies of the components used for the machine or the inaccuracies of assembly. Geometric errors include elements such as straightness and flatness, inclination, squareness. Figure 1.9 illustrates the flatness, straightness, and parallelism errors of the V-groove slide ways on a machine component. The errors are initially induced by the errors in the machining process and can further develop by such as thermal distortion, internal stress, or surface wear.

  Kinematic errors are concerned with relative motion errors among several moving components. The motion errors can be induced by such as the geometric errors of the axis of the motion or insufficient rigidity of joints.

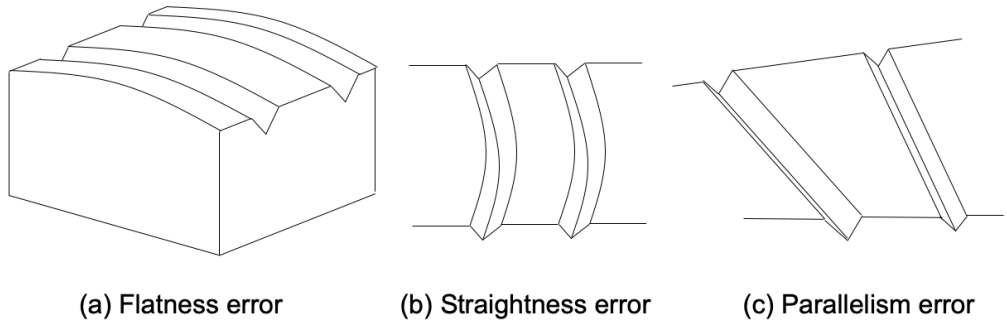

Figure 1.9: Example of the geometric errors in a machine component (based on [15]).

- Thermo-mechanical errors

  Generally, machine components are made from metal, typically cast iron, steel, or aluminum. Such materials expand or shrink with temperature. The relative expansion and bend of the machine components induces deformation of the machine component, resulting in the deformation of the toolpath. Based on the copying principle, the deformed toolpath leads to the inaccuracy of the machined geometry, as illustrated in Figure 1.10. Thermal influence is considered as one of the largest contributors to the change of the accuracy. Weck et al. addressed that thermal effects can contribute more than 50% to the overall machine error [16]. Mayr et al. estimated that up to 75% of the overall geometrical errors of machined workpiece can be induced by the effects of temperature [17].

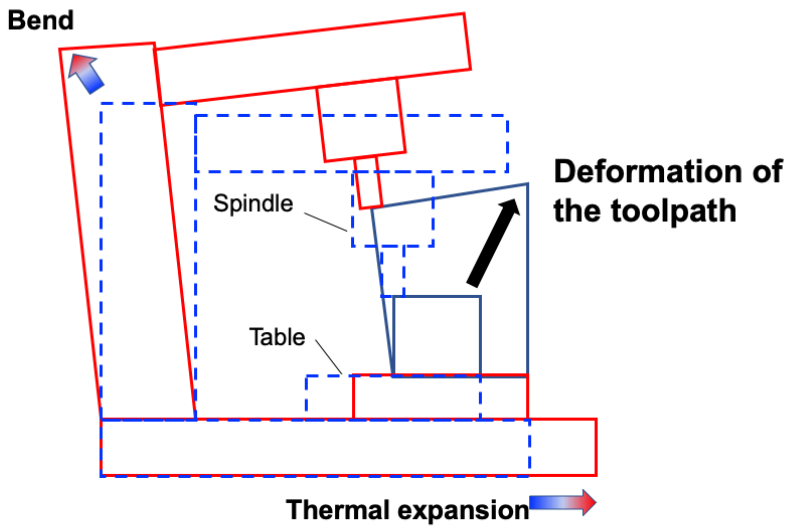

Figure 1.10: The deformation of the toolpath due to thermal influence.

- Static and dynamic forces

  A machine tool is exposed to static and dynamic forces during a cutting operation. Gravity represents a static force. A heavy workpiece on a machine bends the base structure of the machine, such as the machine bed and work table. Cutting force represents a dynamic force. During a cutting process, the cutting tool intermittently collides with the workpiece and generates forces between the cutting tool and the workpiece. Both the static and dynamic forces induce the distortion of the tool, workpiece, or other machine components.

- Servo control system

  The motion of a CNC machine tool is controlled by a servo control system. The CNC controller reads the feedback signal of the position of the moving component by using a linear encoder. Figure 1.11 is a block diagram of the position feedback loop system of the machine tool [18]. The time delay of the mechanical response of the moving component or the feedback signal to the control command causes motion errors such as contour error, as shown in Figure 1.12.

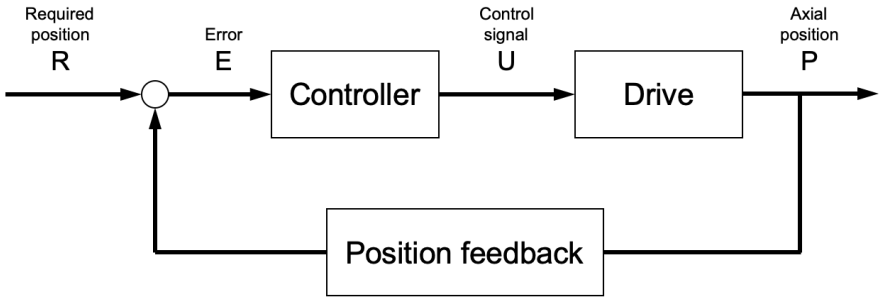

Figure 1.11: A block diagram of the position feedback loop system of the machine tool [18].

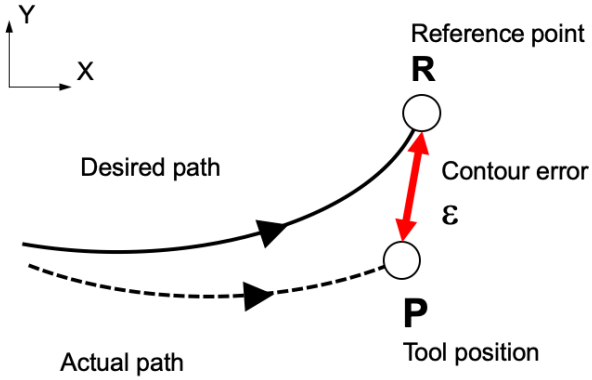

Figure 1.12: Contour error in a XY plane [18].

1.2.2 Design and Assembly Technologies to Suppress the Error Generation and Build a Precision CNC Machine Tool

As Figure 1.6 implies, today's machine tool manufacturers are required to build machine tools in the order of micrometers and further demand for higher precision would be expected in the future. In order to build such accurate machine tools careful with differentiating precision and accuracy, even under the influence of the above-mentioned error sources, machine tool engineers and researchers have developed various technologies and techniques to eliminate the error sources. Figure 1.13 shows some typical error elimination strategies employed in design and manufacturing of modern CNC machine tools.

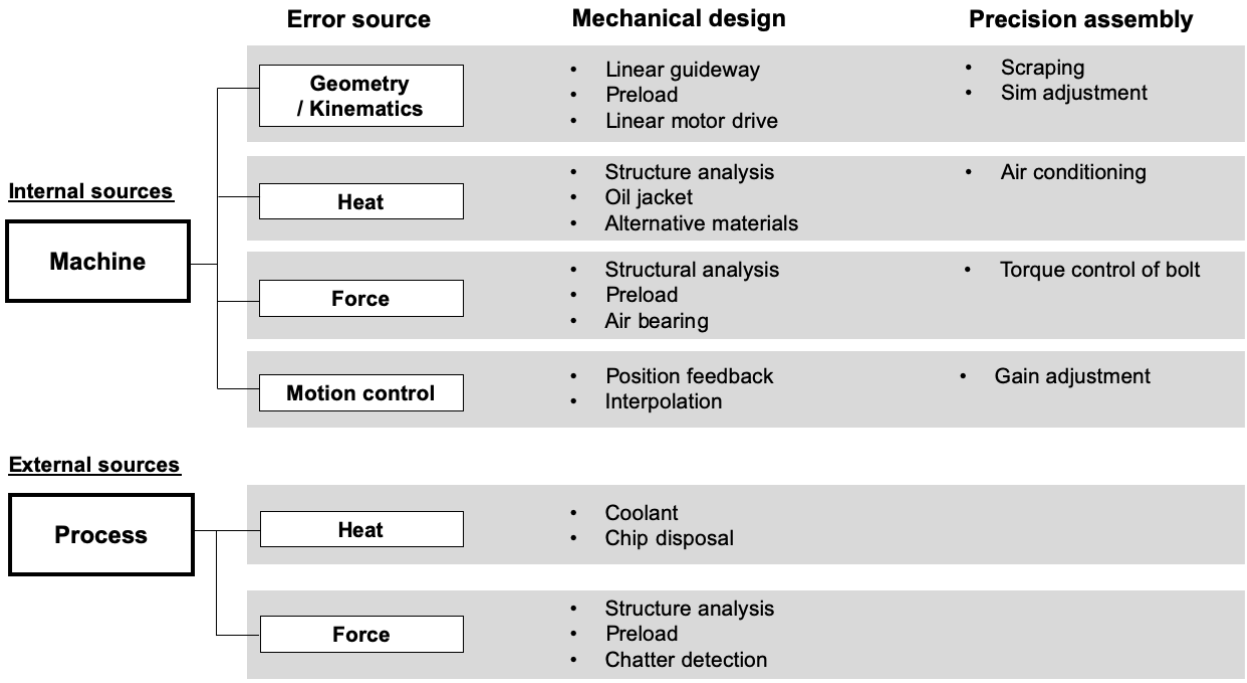

Figure 1.13: The design and assembly technologies to suppress the influence of each error source.

1.2.2.1 Geometric and kinematic error suppression

- Smooth and precision guideway system

  Flatness, straightness, or smoothness of the guideway has a significant impact on the accuracy of the machine motion [19]. The flat and straight guideway reduces the geometric error of the moving component, and the smoothness improves the response of the mechanical system, leading to the reduction of the lost motion and stick motion. There are broadly two types of guideways: friction and roller guides. In the friction guides, a moving component and the other component are physically in contact and slides on each other. Lubrication oil is supplied in the contact zone to reduce friction. When a relative sliding motion takes place in the contact zone, the lubrication oil film will be swept away by the sliding motion , leaving nothing but bare metal and the risk of seizure. In order to reduce the risk, a technique known as scraping is employed to create a smooth contact surface with high flatness and lubrication functionality. By using a hand tool called hand scraper, many shallow grooves are created on the surface, as shown in Figure 1.14. Scraping the surface will leave the original high-quality surface intact, but the shallow grooves enable the oil film to maintain its depth and surface tension [20]. Ball or roller bearings are also widely used for the linear guideway of the

machine tool. A typical roller guide consists of a linear guide rail and a carriage that has recirculating rollers inside, as shown in Figure 1.15. Roller guides are modular and do not require manual hand scraping. Thus, they are one of the most popular guideway systems. For the ultra-precision machine tool that is required to achieve the accuracy in the order of nanometers, even the tiny vibration due to the rolling of the balls or rollers is not negligible. Therefore, the magnetic bearing system is employed to eliminate the physical contact at the guideway system [21, 22].

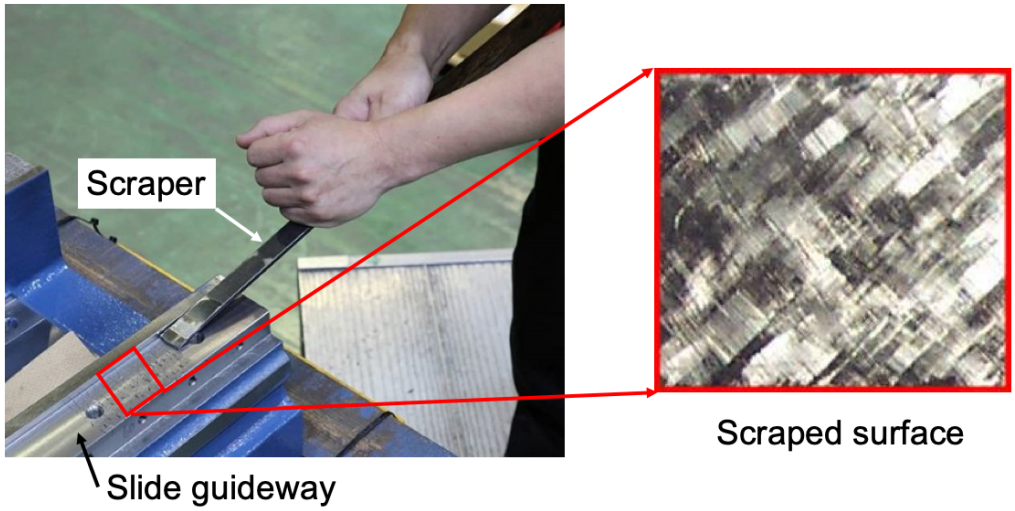

Figure 1.14: A technician performing hand scraping on a slide guideway and a magnified view of the scraped surface (created with [23, 24]).

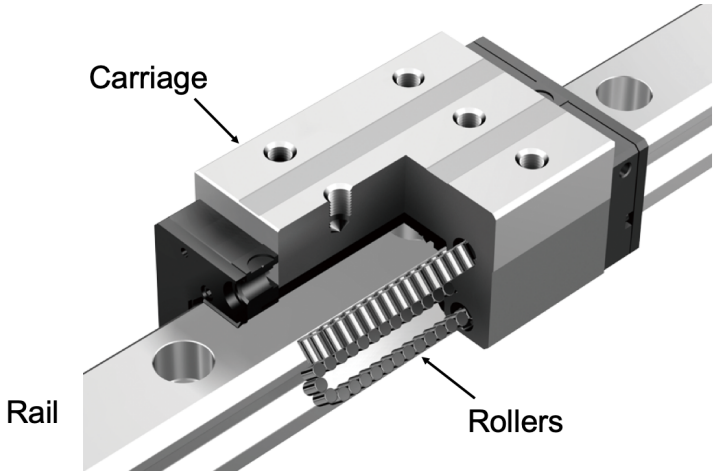

Figure 1.15: A typical structure of a roller guideway system (created with [25]).

- Preload to eliminate the backlash of mechanical components

  Backlash is generally a clearance or lost motion in a mechanism caused by gaps between the parts [26]. In a machine tool, backlash can be typically found at the bearing systems such as ball screw and linear guideways. For example, the ball screw shown in Figure 1.16 is one of the most typically used components to move a linear axis component. In a linear drive axis with a ball screw, rotation of the screw shaft is inverted to the translational motion of the ball nut that slides the moving component. The ball screw backlash is a small gap between the lead screw and the ball nut, as shown in Figure 1.18. When the machine reverses the rotation of the lead screw to alter the direction of motion, the lead screw needs extra rotation that is not inverted to the motion of the moving component.

  In order to eliminate the backlash, preload is applied to the ball nut. There are largely three types of preloading methods: adjusting the spacer, creating offset between the leads or using oversized balls [27].

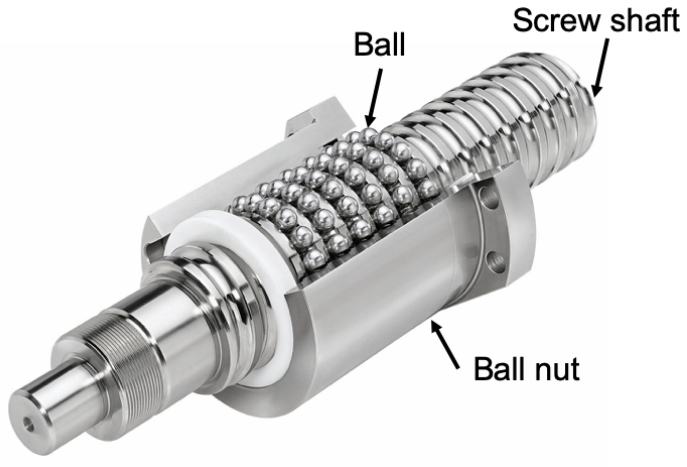

Figure 1.16: The structure of a ballscrew (edited based on [28, 29]).

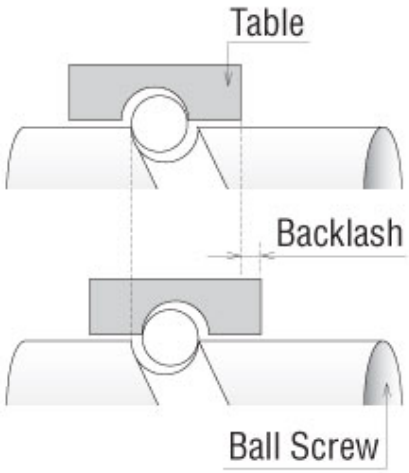

Figure 1.17: Backlash between the lead screw and the ball nut (adapted from [30])

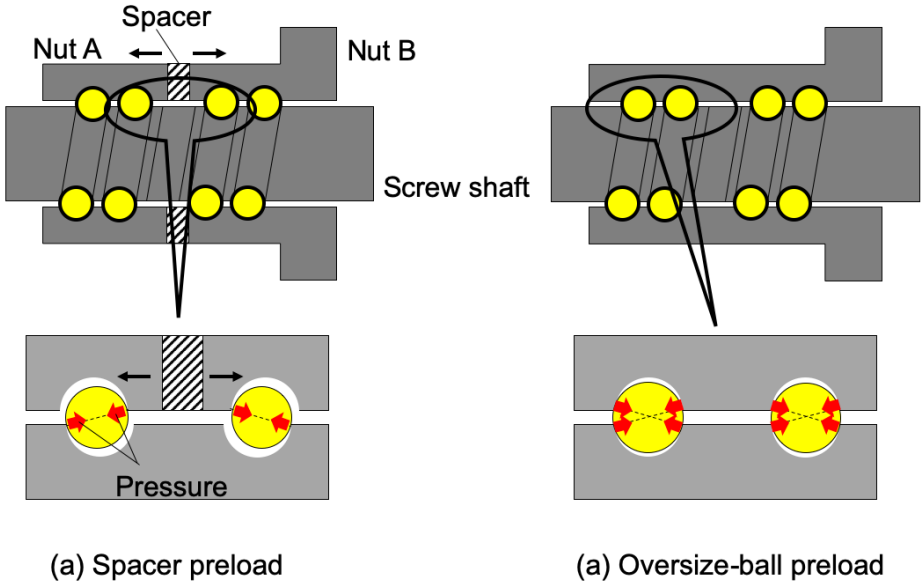

Figure 1.18: Preload methods of the ball nut (based on [27]).

1.2.2.2 Thermal error suppression

- Structural analysis
  Structural analysis is performed to analyze the rigidity of a machine tool structure

on the initial structure design at the beginning of the machine design stage. This process is important to make the machine tool frame rigid enough to satisfy the target specification. By the development of numerical analysis such as finite element method as well as computer simulation technology, today's machine tool design engineers can find structural weak points in their design and modify them without making a physical prototype, which considerably saves the cost and time [31, 32].

- Temperature control

  There is a large variety of heat sources inside and outside of a machine tool. Daily or seasonal ambient temperature of the factory [33], cutting heat, friction between various mechanical components [16], and Joule heat from electric components such as motors [34] warm up the machine components and cause thermal distortion. Figure 1.19 shows an example in which the TCP is displaced in each direction of X, Y, and Z-axis along with the variation of the environmental temperature of the machine. Thus, control of heat flow inside and outside of the machine tool is important. Figure 1.20 is an example of the oil cooling system installed into spindle and ball screw to reduce the heat transfer from the heat source to the machine frame [35]. Cutting coolant oil is used not only for lubrication at the cutting zone but also for removing the cutting heat from the machining area [36]. Cumulated cutting chips are also regarded as a heat source, thus optimization of coolant oil flow and chip conveyor is also an important issue. To keep the ambient temperature constant, some factories are equipped with an air conditioning system [37, 38].

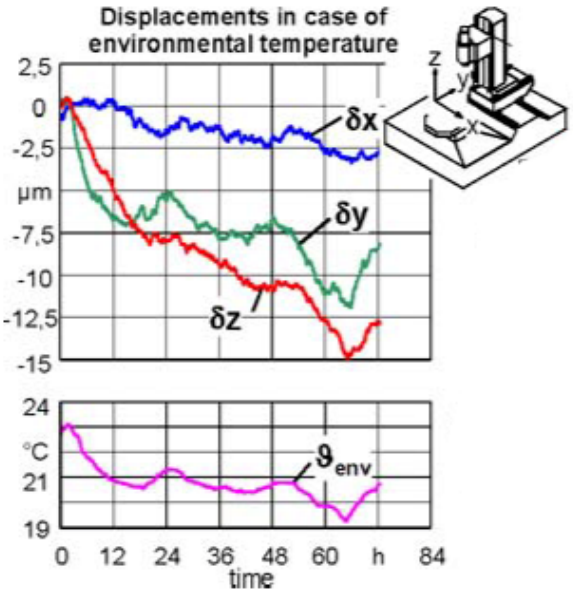

Figure 1.19: An example of the displacement of the TCP along with the variation of the environmental temperature (adapted from [39]).

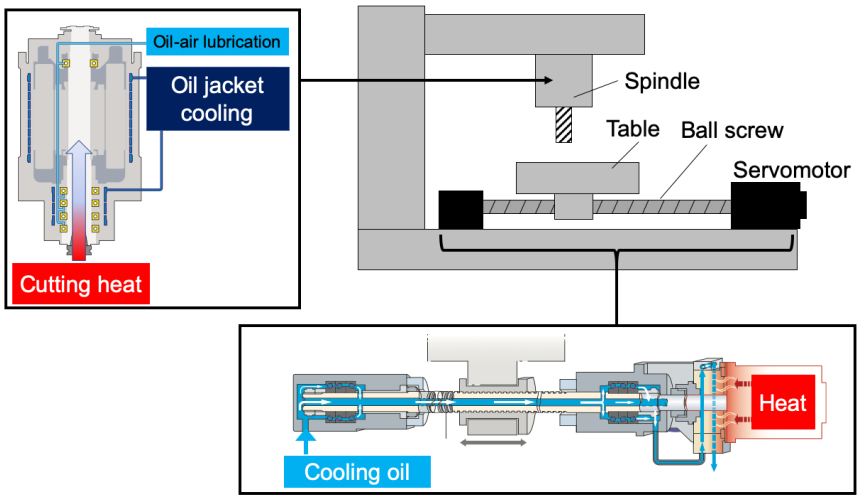

Figure 1.20: The oil cooling system installed into spindle and ball screw to reduce the heat transfer (created with [35]).

- Employment of alternative materials

  The mechanical and thermal behavior of machine tool structure strongly depends on the material properties used for the structure. Therefore, in order to improve the mechanical or thermal behavior of the machine, the employment of alternative materials such as stone, ceramics, carbon fiber reinforced polymer (CFRP) to conventional cast iron for machine tool structures has also been studied [40, 41].

1.2.2.3 Force-induced error suppression

- Structural analysis

  Structural analysis is performed to analyze the rigidity of a machine tool structure on the initial structure design at the beginning of the machine design stage. This process is important to make the machine tool frame rigid enough to satisfy the target specification. By the development of numerical analysis such as finite element method as well as computer simulation technology, today's machine tool design engineers can find structural weak points in their design and modify them without making a physical prototype, which considerably saves the cost and time [31, 32].

- Preload to increase the rigidigy

  Eliminating the backlash of the bearings by the preload leads to the elimination of the room for the mechanical component to move freely. Thus, preload also contributes to increasing the rigidity of the machine tool. Here, the preload of the linear guideway is shown. The preload of the linear guide is applied by controlling the distance between

the rail and the rolling groove of the runner block and inserting oversized balls or rollers, as shown in Figure 1.21.

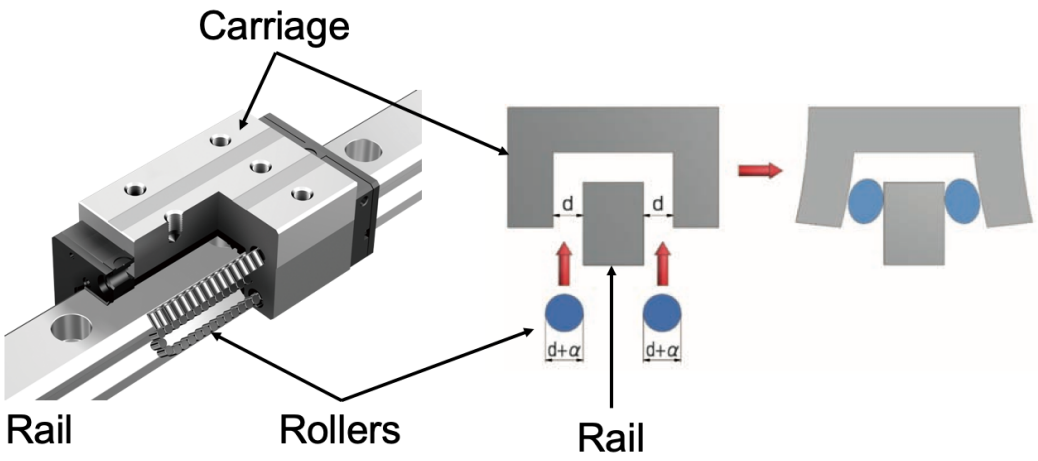

Figure 1.21: Preload of the guideway (created based on [42]).

- Hydrostatic and aerostatic bearing to reduce friction and vibration

  Figure 1.22 shows the hydrostatic and aerostatic bearing system. (a) is the aerostatic guideway that supports a linear motion table, and (b) is the aerostatic bearing that supports a rotary shaft. The hydrodynamic lubrication condition can be realized by supplying the lubricating fluid to the bearing surface as a working fluid. The lubricating fluid is typically oil or air. As a result, the following features are produced in the hydrostatic machine element: (i) friction coefficient in the bearing surface is very low compared with other bearing types, and smooth operation without stick-slip is possible, (ii) wear is not generated, and long-term maintenance of machine accuracy is possible, (iii) machining error of the bearing surface is averaged by the lubricating film, and movement with accuracy one order higher than parts accuracy is possible. Because of these features, the static pressure element is preferably used in ultra-precision machine tools and measuring instruments [43].

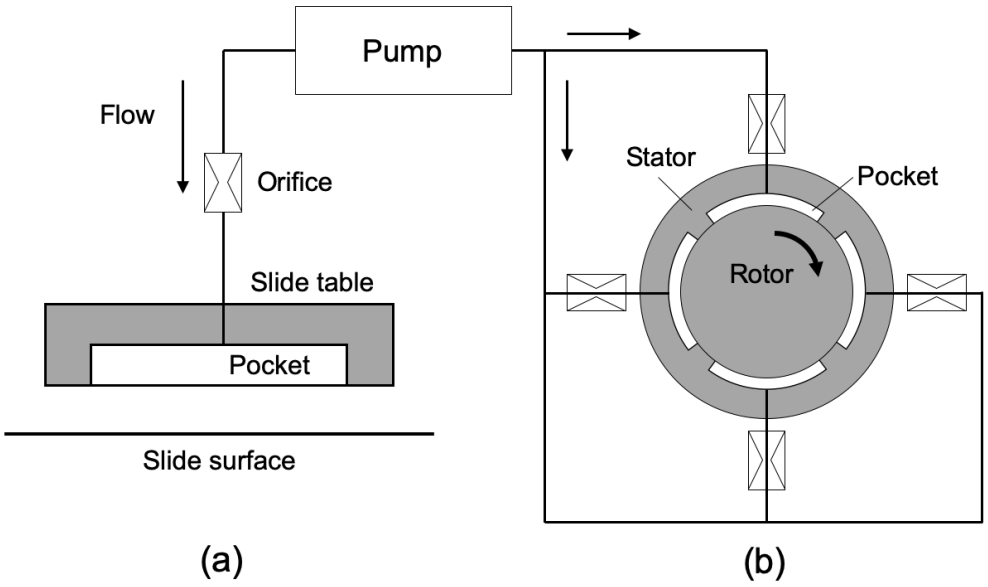

Figure 1.22: Hydrostatic and aerostatic bearing system (created based on [43]).

1.2.2.4 Motion control error suppression

- Closed loop position feedback control

  The position control system of the machine tool can be broadly classified into two types: semi-closed and full-closed loop system. The semi-closed system can be composed as in Figure 1.23 (a). The rotary encoder that is built in the servo motor detects the position and velocity of motion. The position is determined by the lead and the rotation angle of the ball screw. The lead is defined as the travel of the ball nut relative to the ball screw shaft for an angle of rotation of 2π rad (one revolution) [44]. The closed loop system is composed as in Figure 1.23 (b). A linear encoder is attached to the moving component to detect the position directly. Compared with the semi-closed loop system, whose the positioning accuracy depends on the accuracy of the lead of the ball screw, the full-closed loop system has higher accuracy by the direct measurement [45].

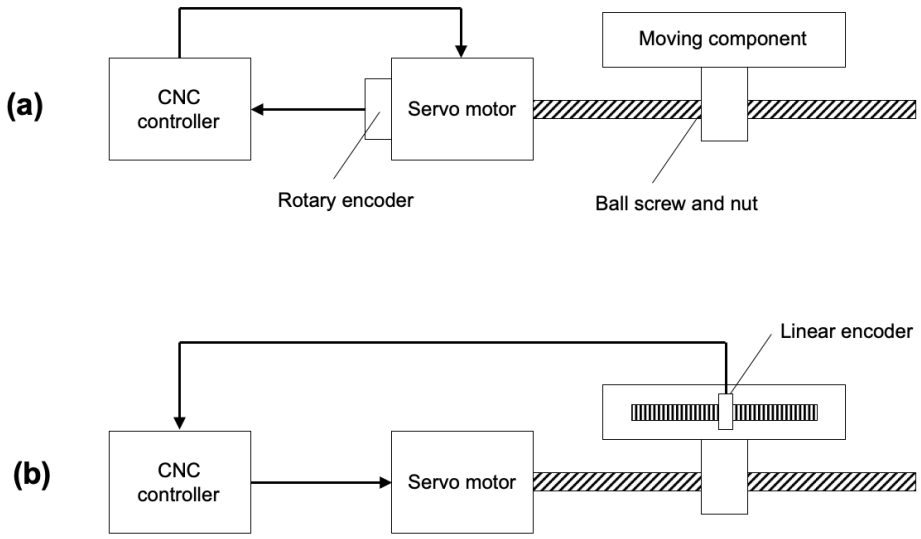

Figure 1.23: The semi-closed and full-closed loop system (created based on [45]).

- Smooth acceleration and deceleration profile generation

  Once the tool path is generated, the CNC controller generates the acceleration profile. In order to move the machine component from one position to the next within the servo control loop, sometimes too much acceleration that excess the maximum torque of the servo motor might be required, as illustrated in Figure 1.24 (a). In addition, sharp acceleration and deceleration can vibrate the machine structure, leading to the positioning error. In order to prevent this phenomenon, the CNC controller has the processor to generate the smooth acceleration or deceleration profile by controlling the jerk, the differential of the acceleration, as illustrated in Figure 1.24 (b) [46].

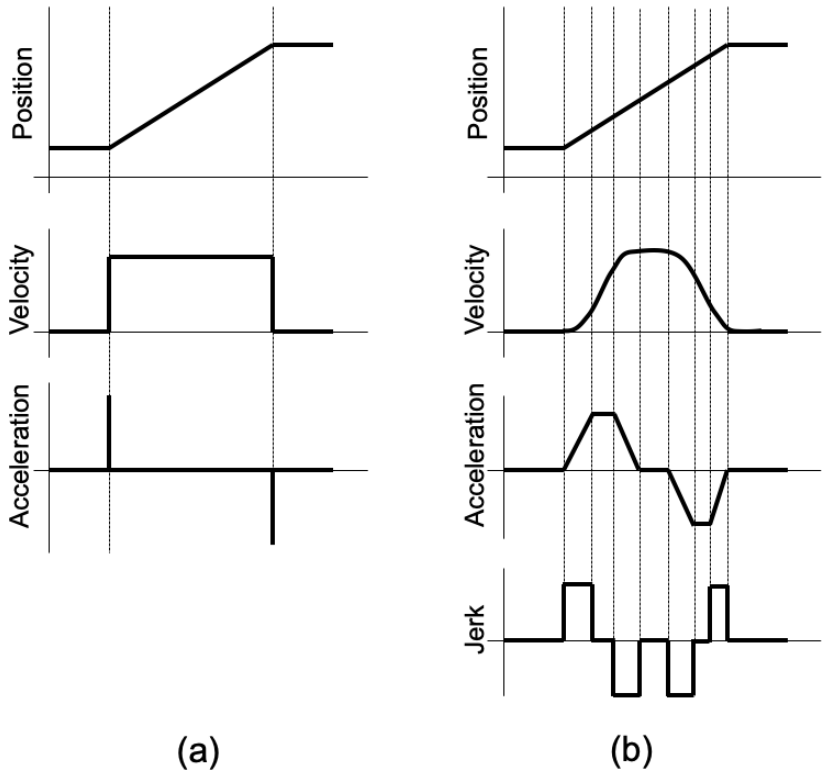

Figure 1.24: Comparison of trajectories generated with (a) simple differential and (b) jerk-limited profiles ([46]).

1.2.3 Error Compensation to Achieve Higher Accuracy

As explained, machine tool manufacturers employ the state-of-the-art machining and assembly technologies to achieve the best accuracy of their product. However, even with the technologies, achieving the accuracy in the order of 1 micrometer under any situation is challenging. A condition surrounding a machine tool differs depending on the user. The size, weight, material of the workpiece, the temperature of the factory, type of the cutting tool, cutting condition, or any other conditions can affect the accuracy of the machining. These conditions cannot be controlled by the machine builder.

Thus, another approach so called error compensation plays a vital role to achieve high precision. In the case of error compensation, errors in machine motion are measured after assembly and the information is recorded in the CNC control system. Then, the CNC controller uses the information to modify the machine motion to cancel the errors. The efficacy of error compensation was studied in 1980s to improve the accuracy performance of a coordinate measuring machine and machine tool [47, 48]. Various types of error compensation functions have been developed, depending on the type of error to compensate.

- Ballscrew lead and backlash error compensation

  The lead error is induced by the machining inaccuracy of the groove of the lead screw. The lead error induces the error of the travel length of the ball nut, as shown in Figure 1.25. The lead error compensation is the function to record the error in the CNC control system so that the CNC controller can adjust the rotation angle to cancel the error. Backlash compensation electronically compensates for backlash by adding the amount of backlash to each axis reversal [49].

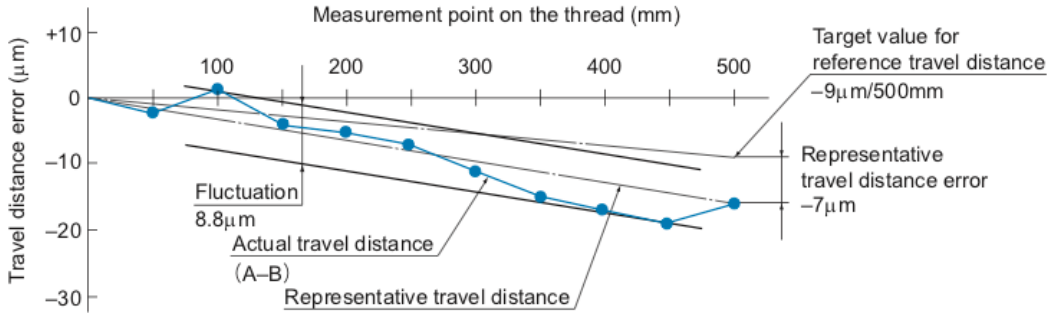

Figure 1.25: Lead error of a ballscrew (edited based on [50]).

- Straightness error compensation

  Straightness error is a tiny amount of deviation perpendicular to the principal direction of motion of a moving component, as illustrated in Figure 1.26. In the figure, the Z-axis has the straightness error in Y-axis. However, the Z-axis linear drive system does not have a function to move the table in Y-direction. Straightness error compensation is to cancel this error by moving the Y-axis component so that the relative distance in the Y-direction between the Z and Y components is kept constant. The straightness error data is measured and recorded in the CNC controller beforehand, and the controller adjusts the motion according to the data.

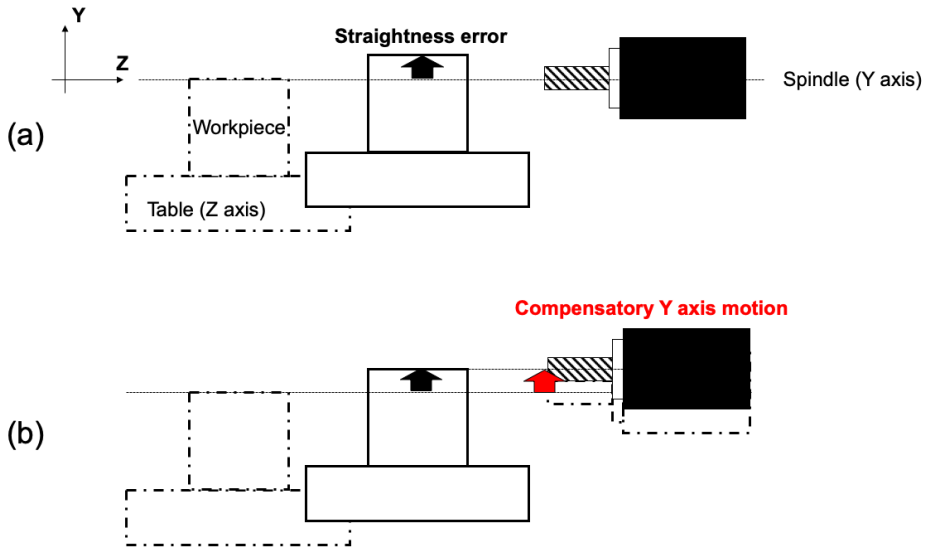

Figure 1.26: The straightness error compensation.

- Volumetric error compensation

  Three dimensional positioning error of three linear axes motion is known as volumetric error [51]. Since typical machine tools are used to cut a workpiece into a three-dimensional shape, the accuracy of the machine motion should be guaranteed for the entire machining area. In the volumetric error compensation, the positioning error of the cutting tool is measured at various measurement points that encompass the entire machining area, and an "error map" is created to visualize the magnitude of the positioning error at each measurement points. Figure is an Example of a 2D error map of a XY plane of a machine tool [52]. The error map is converted to parameters and recorded in the CNC controller. In the subsequent machining operation, the CNC controller adjusts the position command based on the error map.

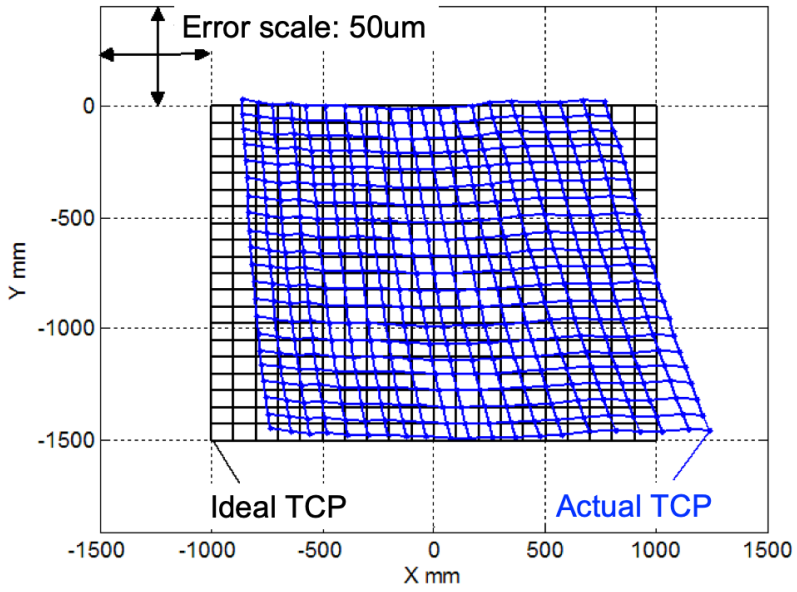

Figure 1.27: Example of a 2D error map of a XY plane of a machine tool [52].

- Quadrant glitch compensation

  Quadrant glitch is observed when a machine makes a circular motion by moving two orthogonal axes simultaneously. Figure 1.28 shows the typical quadrant glitch observed around quadrant changing points [53]. The generation mechanism of quadrant glitches can be explained as the acceleration changes due to the friction changing after the motion direction changes, which disturbs the synchronous motion control between the two axes [54], as shown in Figure 1.29. To suppress the quadrant glitch, CNC controller has parameters to adjust the acceleration of the linear axis [55].

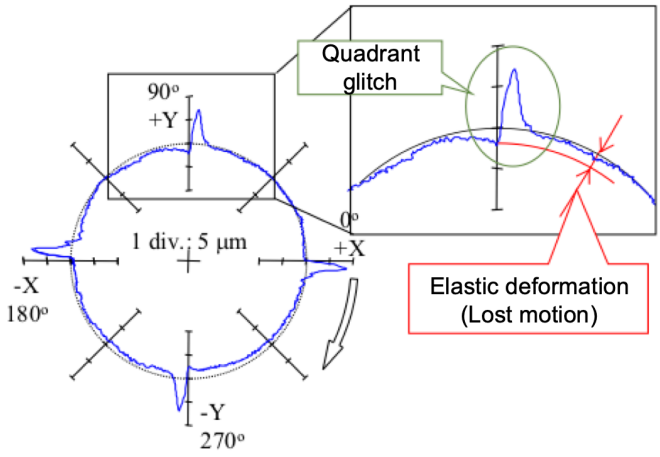

Figure 1.28: Typical quadrant glitch observed around quadrant changing points (adapted from [53]).

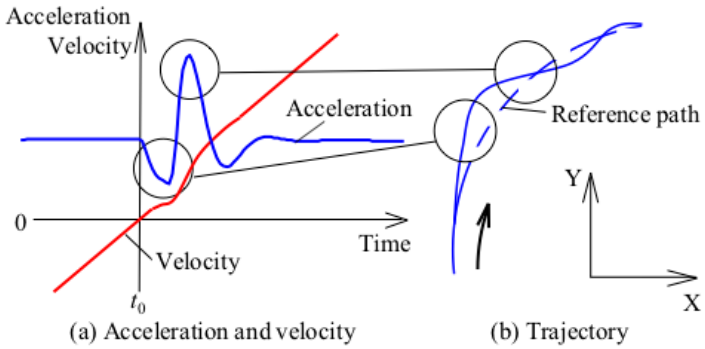

Figure 1.29: Conventional generation process model of quadrant glitches (adapted from [54]).

- Model predictive compensation

  The error compensation methods introduced above assume that the error to be compensated is measurable. The amount of the error is measured and recorded in the CNC control system, and the controller adjusts the motion of the machine based on the recorded error profile. On the other hand, the machine tool also has various types of unmeasurable errors or errors that cannot be measured easily. For example, the measurement of the deflection of a cutting tool, the machine structure due to the process force or thermal distortion is challenging because the measurement of such types of errors requires the integration of an additional complex mechatronic component into the machine tool. This integration results in higher setup time, extra costs, and limitation of the machining area. Therefore, instead of the direct measurement of

the errors, prediction of the error using a model is employed. The model is typically created based on the mechanical, dynamic, or thermal theory [56]. However, due to the complexity of the error generation mechanism, the design of an accurate model is also a challenging task. Thus, rather than building up the model from the microscopic point of view, some researchers propose to use other approaches, such as deep learning to globally characterize the error [57].

1.2.4 Precision Error Measurement Technologies for Error Compensation

In order to accurately compensate for an error, the error has to be accurately measured. In order to achieve the accuracy in the order of micrometers, errors less than one micrometer should be measured accurately. According to the third principle of measurement by Nakazawa, the measurement must be five to ten times higher [58] than the accuracy to be achieved. Therefore, measurement instruments are required to have accuracy in the order of nanometers. Today, a variety of precision measurement devices are commercially available to measure errors of machine tools. Followings are some examples of them.

- Laser interferometer

  A laser interferometer is one of the most frequently used measurement devices to check machine accuracy. It utilizes a laser beam that is directed at a reflective mirror placed on the observed object as shown in Figure 1.30 [59]. The interference between the return beam and the principle beam can be used to determine the linear position accuracy and repeatability along an axis, squareness between axes, surface flatness, rotary axis angular positioning, axial pitch, and machine tool dynamics.

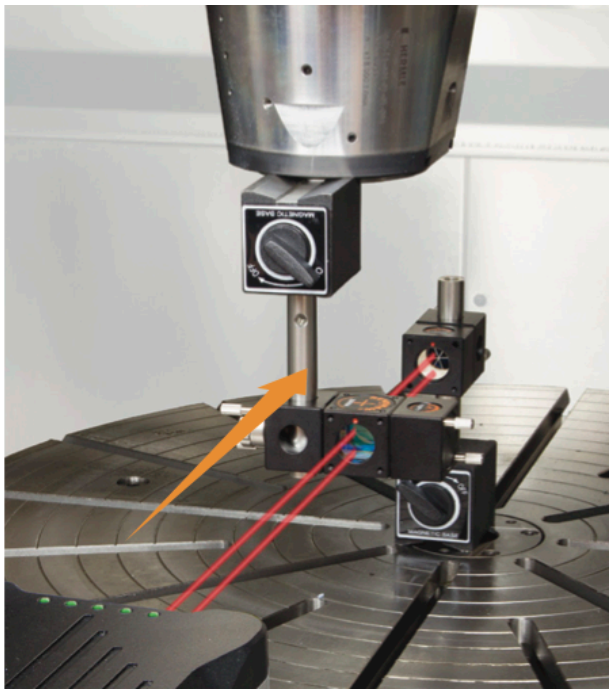

Figure 1.30: Laser interferometer [59].

- Precision level

  A precision level is apparatus to measure the level of a flat surface. A liquid such as alcohol or ether is put in a circular glass container, with a bubble left on the surface, as shown in Figure 1.31 (a). Changes in the angle of the level cause a displacement of the bubble. The position of the bubble indicates the magnitude of the level or inclination. A level is placed on the object to be measured, and when it is horizontal, the bubble is centered. Even if the level is rotated by 180 degrees in the same place, the bubble is still in the center, as shown in Figure 1.31 (b). When the right side of the object to be measured is high, the bubble moves to the right side, as shown in Figure 1.31 (c). By reading the position of the bubble, the magnitude of the inclination can be measured [60].

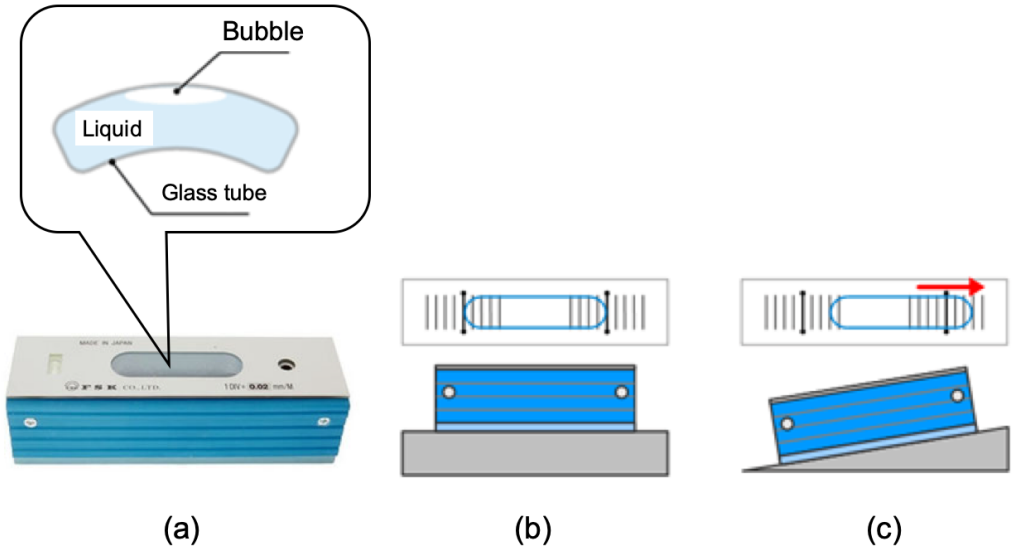

Figure 1.31: The principle of the precision level (created based on [60]).

- Double ball-bar

  A double ball-bar is widely used to determine the accuracy of two linear axes. As the name suggests, the components includes two balls, a transducer to measure the distance between them, and a fixture to secure the balls in place as shown in Figure 1.32. This accuracy measurement method is effective in determining the quadrant glitch, backlash, servo-gain misalignment, and squareness error [61]. This method is common as a criterion for acceptance testing in machine tool manufacturing for two-axis linear drives.

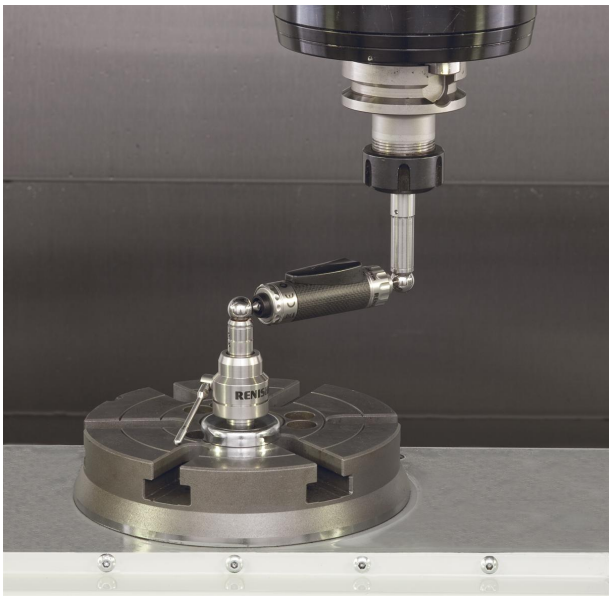

Figure 1.32: Double Ball Bar (Renishaw QC-20) [61].

- Cross grid encoder (KGM)

  A cross grid encoder, sometimes called KGM (abbreviation of a German counterpart "Kreuzgitter Messgerät") is an optical diffraction grating type encoder to measure two-dimensional position of a optical head by using a grid plate where grids are aligned orthogonal to each other. The cross grid encoder can be applied to measure two-dimensional motion errors of high-precision and ultra-precision machine tools, such as the straightness error or the squareness error [62]. Figure 1.33 shows an example of the measurement setup [63].

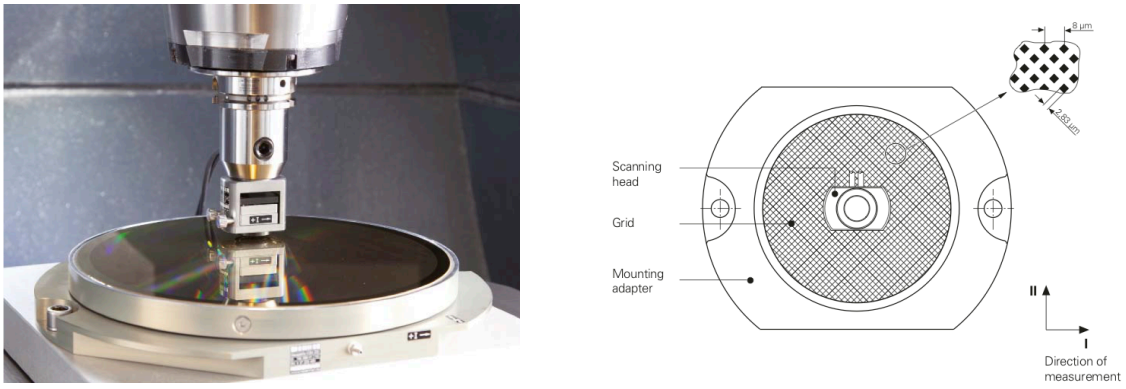

(a) (b)

Figure 1.33: Cross grid encoder [63].

- Laser tracker

  A laser tracker is a type of laser interferometer specifically designed to measure the three-dimensional position of a moving target. It is a laser tracking interferometer combined with a servo system that allows the laser to track a moving target and measure the distance and angle of the target in a polar coordinate system. The laser trackers are used in a large-scale precision manufacturing such as aerospace, shipbuilding, heavy industry as well as machine tool industry [64]. Figure 1.34 shows a setup of measurement of a coordinate measurement machine [65]. The advantageous feature of laser tracer is being able to directly measure the accuracy of the tool center point. Since laser interferometer, DBB, and KGM are limited to measure the accuracy of one-dimensional or two-dimensional motion, the measurement result provides limited information of the accuracy of machine tools. As machine tools are generally used to create three-dimensional shape, three-dimensional measurement with laser tracker serve the purpose of accuracy measurement of machine tools. [66, 67]

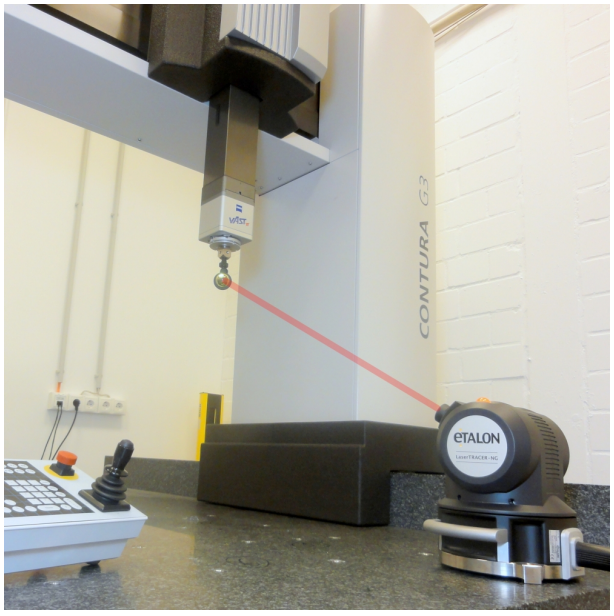

Figure 1.34: Laser tracker [65].

1.3 Issue to be Focused

1.3.1 Dynamic Change of Accuracy

By using the design, assembly, measurement, and compensation technologies mentioned above, the development of machine tools with an accuracy in the order of micrometers is now possible. In order to obtain the high accuracies achieved by machine tools, the machine

tool manufacturer measures the accuracy of the assembled machine before the shipment to preset the error data for the compensation functions. After the installation at the user's side, the accuracy is double-checked to assure that the machine satisfies the accuracy requirement. For example, assume the situation shown in Figure 1.35. The compensation parameters are registered in the CNC controller before the machine starts the first part machining. The compensation parameter at this time is represented by P_1, and the tool path is represented by the blue line e_1. e_1 is a path through which this machine can machine parts with acceptable accuracy. From a user's viewpoint, it is desirable that this accuracy is preserved for the lifetime of the machine. However, the accuracy of a machine tool continuously changes. Operating lifetime of machine tools are generally more than ten years, and machine tools in a mass production line are used for twenty-four hours a day, seven days a week. Under such operation, error sources such as thermal distortion, aging degradation of bearings continuously change the accuracy of the machine tool. Once the accuracy has been changed, the error compensation parameters set at the installation are no longer valid, and a certain amount of error will remain uncompensated. In the figure, when machining the Nth part, the tool path is changed as indicated by e_N. e_N exceeds the tolerance of the error, and the correction parameter P_1 no longer works effectively. The uncompensated errors are copied onto the workpiece, resulting in excessive variation in the accuracy of the machined workpiece geometry. This is a critical issue for the productivity of the machine user.

Therefore, in order to preserve the accuracy of the machine tool, the error compensation values should be continuously updated to keep track of the dynamic change of accuracy. In this example, by detecting that the accuracy exceeds the allowable range in the Nth machining and updating the correction parameter to P_2 to cancel this, the accuracy can be kept within the allowable range again in the $N + 1$th machining. However, conventional error compensation functions cannot make such a dynamic error compensation due to several reasons as following.

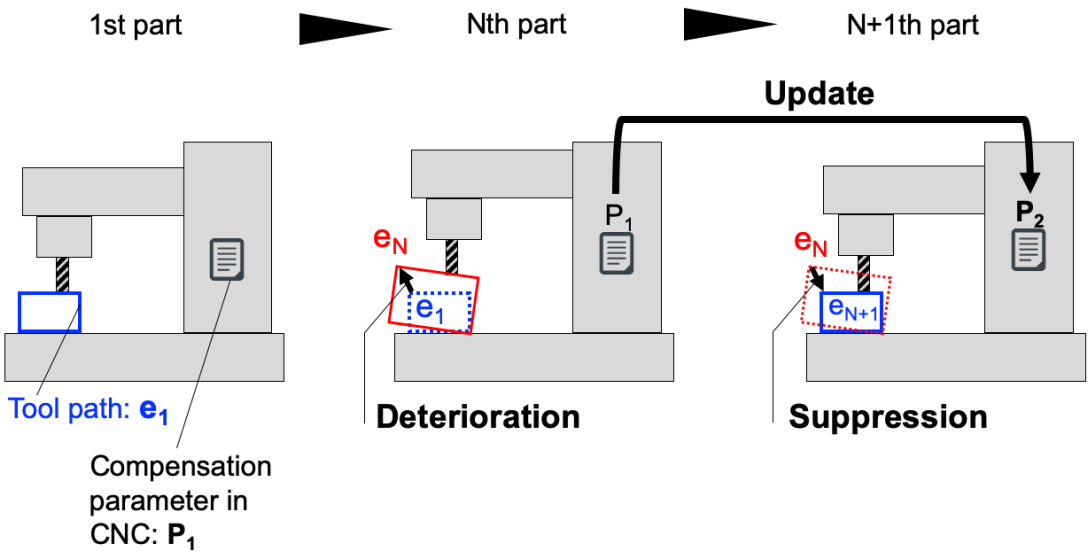

Figure 1.35: Dynamic change of accuracy and its compensation by the parameter update.

1.3.2 Limitation of the Conventional Error Compensation

1.3.2.1 The conventional error compensation procedure

Figure 1.36 shows the conventional error compensation process process. A conventional error compensation procedure flows as follows:

1. Manual setup:
   Stop the machine's cutting program and remove the workpiece and cutting tool from the machining area. Manually install a measurement device to the machine.

2. Manual measurement:
   Carry out the measurement. The measurement has to be carried out according to the measurement test code that are defied in the industrial standard such as ISO.

3. Manual compensation:
   Normally a measurement software has a functionality to analyze the measurement data and to generate a compensation parameter. The generated parameter is sent to the CNC controller by a PC or a memory card such as a USB flash media.

4. Manual setup:
   Remove the measurement device from the machine and re-install the workpiece and the cutting tool.

5. Resume the machining process:
   During the subsequent machining process, the CNC controller makes the compensation based on the recorded parameter.

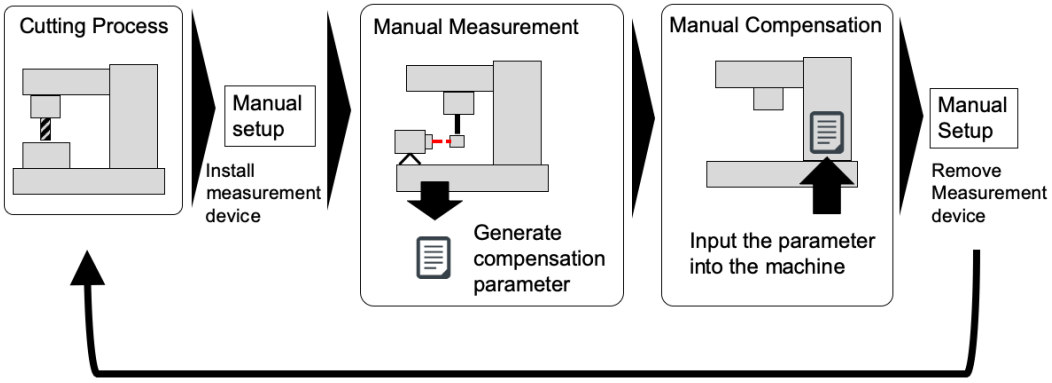

Figure 1.36: A conventional measurement procedure.

As described, the conventional approach requires many manual process and therefore time consuming. The process must be performed by a skilled technician, but the education is not an easy task for many machine users as the measurement is not their main operation.

1.3.2.2 Difficulty in applying the conventional method to the dynamic change of accuracy

In order to update the error compensation parameters with a conventional approach, user needs to perform the accuracy measurement as shown in section 1.3. However, having user's performing the tests is not an easy task for following reasons.

- High cost of the measurement devices
  Since the state-of-the-art measurement devices are typically precision electronic devices, they are expensive. Many machine tools users normally cannot afford them. For example, the price of the previously introduced devices are listed in Table 1.1.

- Low durability of the measurement devices under harsh measurement environment
  As shown in Figure 1.37 (a), the measurement must be performed under a static condition, actual cutting is done under very harsh conditions. The heavy workpiece is loaded on the machine. The cutting process generates a large amount of sludge, heat, dirty cutting oil, and violent vibration. On the other hand, the measurement must be

Table 1.1: Price of the common measurement devices.

Laser interferometer	$ 50,000
Double ball bar	$ 20,000
Cross grid encoder	$ 35,000
Laser tracker	$ 200,000

performed under static conditions, as shown in Figure 1.37 (b) because the measurement devices generally require careful handling to perform an accurate measurement. The cutting tool and workpiece must be removed, and the machining area must be cleaned up. Due to this large difference between the measurement and cutting conditions, the conventional measurement methods do not apply during an actual cutting process.

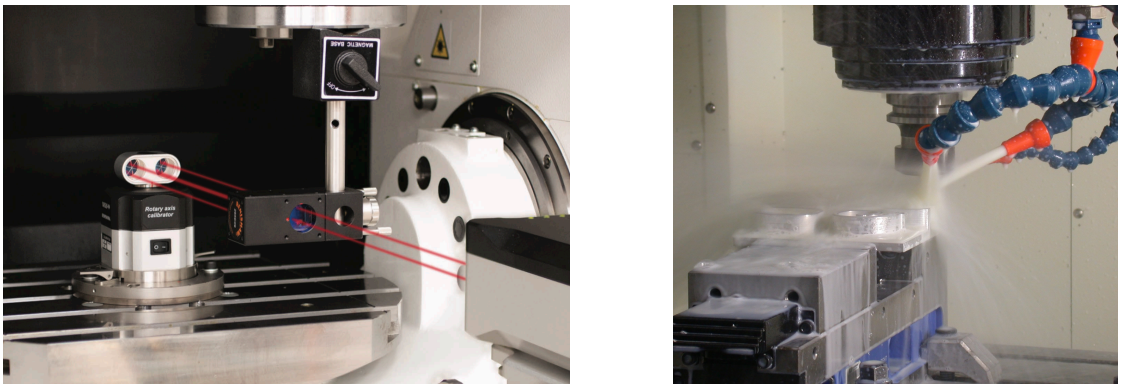

(a) Accuracy test [59] (b) Actual cutting [68]

Figure 1.37: Comparison between an accuracy test and an actual cutting environment.

- Production interruption and prolonged measurement time

  Figure 1.37 shows a comparison between an accuracy test and an actual cutting operation. As typical measurement devices are designed for offline measurement, the cutting tool and the workpiece must be removed and the machining area should be cleaned to use the measurement device. Most of the conventional measurement methods require the machine to stop any machining process during the measurement, which is an undesirable interruption in the production for the machine user. Furthermore, the measurement including the setup can take up to a whole one day. The prolonged measurement time makes it difficult to evaluate accuracy change that occurs in the short term such as thermal errors (vary in several tens of minutes) or cutting-force-induced errors (vary in a few seconds or minutes).

1.3.3 Proposal of the novel method to automate the error compensation procedure

The approach proposed in this study is to automate the procedure. By the automation, the compensation process with the new system will become as shown in Figure 1.38.

1. Automatic measurement:
   Automatically carry out a measurement by the built-in measurement system without removing the workpiece and the cutting tool.

2. Automatic compensation:
   The measurement data is analyzed by a dedicated software run on the CNC operation system. The software automatically generates and updates the compensation parameter in the CNC control system.

3. Resume the machining process:
   As the setup procedure can be skipped, the machine can start the subsequent machining process as soon as the compensation is done.

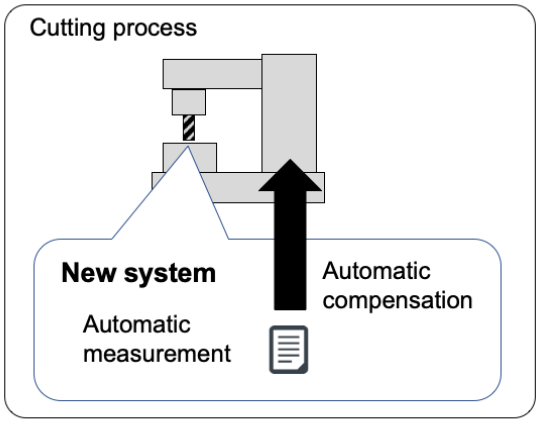

Figure 1.38: The new measurement procedure.

1.3.3.1 The advantage of the novel method: dynamic error compensation

The conventional method is based on the assumption that the behavior of the motion error of the machine tool is always the same as the behavior of the error measured. Therefore, it is a kind of static error correction in which the compensation pattern cannot be changed without changing the stored error data. The novel system proposed in this study

can detect the motion error at all times during machining by the sensors permanently installed in the machine tool, and can use the error data corrected during the machining. Thus, compensation is possible much earlier and more appropriate than the conventional method.

The elimination of the setup process enables automatic measurement without human intervention. This elimination integrates a measurement process into an automated production process. Seamless switch between a cutting process and a measurement process reduces the time required for the measurement, and then the accuracy measurement can be done more frequently. By frequently repeating the measurement, the machine can keep track of its accuracy and update the compensation parameter as soon as the accuracy has changed. In this sense, the new compensation procedure is dynamic compared with the conventional one.

1.4 Objective of This Research

As discussed so far, the accuracy of the machine tool has a direct impact on the machined workpiece and thus is one of the most important properties of the machine tool. However, machine accuracy deteriorates during the operational time due to various causes such as cutting heat, wear of bearings. Since machine tools are expected to produce many parts with a constant quality of accuracy continuously, such deterioration of accuracy needs to be detected and compensated as soon as possible. Although various error compensation methods have been proposed, most of them require manual labor to set up measurement equipment, time to execute a measurement program, data analysis, and manual updating the compensation parameters. Little research has been done for error compensation technologies without human intervention.

Therefore, this study aimed to develop a novel error compensation system that enables machine tools to automatically measure the accuracy and update the compensation parameters. As a key to the automation system, the measurement system must be composed of sensors built in a machine tool. A built-in measurement system eliminates the manual setup processes. Optimum sensor position enables measurement without interrupting machining processes. In this study, a new measurement system that can be integrated in a machine tool is proposed and the following four points are investigated to realize the system.

1. The principle of the integrated measurement system

   The measurement principle of the new measurement system is discussed. To perform a measurement without human intervention, the machine tool should be able to switch from a cutting process to the measurement seamlessly. In this research, the seamless switch is achieved by building a sensor system into a machine tool. A method is proposed to determine the TCP error by using the data collected by the sensor system. As a key theory, kinematic modeling of machine tool error by using coordinate transformation is employed.

2. The design methodology of the built-in sensor system

   Among multiple candidate sensors, linear scale has been chosen as the built-in sensor. A design of the built-in measurement system using the linear scale is proposed. To realize an accurate measurement system, impact of possible error sources in the design are analyzed by preliminary calculation. To assure the measurement accuracy, a synchronous digital data capturing system is developed. To analyze the machine tool accuracy from the time-series data captured by the data capturing system, a post-processor is designed. To evaluate the accuracy change, a key measure known as repeatability is evaluated by a statistical data analysis.

3. The feasibility of the proposed system on an actual machine tool

   The feasibility of the proposed system is investigated with a physical prototype of the hardware. Using the prototype, a series of experiments were conducted. The measurement performance of the developed system is discussed with uncertainty analysis. Thermal expansion of the linear scales is featured as a major negative impact on the measurement accuracy and the impact is carefully investigated.

4. The remaining technological problem to be solved and an idea of the solution for future study

   The remaining technological problem to be solved and an idea of the solution for future study is discussed. Recent advance of linear scale technology is expected to realize the measurement of multiple degrees of freedom error elements that is necessary to make the system complete. By integrating the technology to the system developed in this study, accurate measurement of the volumetric accuracy of machine tool would become possible.

1.5 Outline of this Thesis

This thesis consists of 5 chapters including this chapter. A brief outline of the thesis is given for a better understanding of the subsequent chapters and their context.

In Chapter 2, the theoretical background of the new measurement system with a built-in sensor is discussed.

In Chapter 3, the design methodology of the measurement system and the feasibility of the proposed system are investigated with a physical prototype of the hardwares. Using the prototype, a series of experiment were conducted.

In Chapter 4, the remaining technological problem to be solved and an idea of the solution for future study is discussed.

In Chapter 5, the contents of each chapter are briefly reviewed and the result of this study is summarized.

Chapter 2

Concept and Composition of the Novel Error Compensation System

2.1 Procedure of updating the compensation parameter with the novel error compensation system

As discussed in the previous chapter, this research aims to suppress the accuracy deterioration of the machine tool automatically. In this section, the updating scheme is designed as illustrated in Figure 2.1. The detailed process at each step is explained as follows.

Step 1 Automatic measurement

During the Nth machining operation, the accuracy of the tool path is measured. This measurement is done by a novel system that does not interrupt the machining. The detail will be explained in section 2.2. To keep track of the accuracy, the newly measured accuracy data $\boldsymbol{e}_N$ is compared with the initial accuracy data $\boldsymbol{e}_1$ to calculate the accuracy change $\Delta\boldsymbol{e} = [\Delta e_x, \Delta e_y, \Delta e_z] \in \mathbb{R}^{3\times1}$, where $\Delta e_x, \Delta e_y, \Delta e_z$ indicates the displacement of the tool center point (TCP) from the initial path.

$$\Delta\boldsymbol{e} = \boldsymbol{e}_N - \boldsymbol{e}_1 \tag{2.1}$$

The error data $\boldsymbol{e}_1$ is obtained when the machine has satisfactory accuracy (for example, when the machine assembly is completed at the machine tool manufacturer or when the machine is installed at the user's factory). The machine keeps $\boldsymbol{e}_1$ as the master data the task of the system is to preserve this accuracy.

Step 2 Judge the accuracy change

Using the difference $\Delta\boldsymbol{e}$, the accuracy condition of the machine can be evaluated

as follows:
Predefine a threshold $\Delta \boldsymbol{e}_{TOL}$ and compare with the calculated accuracy change $\Delta \boldsymbol{e}$.

- If $\Delta \boldsymbol{e} \geq \Delta \boldsymbol{e}_{TOL}$, the machine's accuracy has been changed. Compensation is needed. Go to Step 3-1.
- If $\Delta \boldsymbol{e} < \Delta \boldsymbol{e}_{TOL}$, the machine's accuracy change is negligible. No compensation is needed. Go to Step 3-2.

Step 3-1 Update the compensation parameters

The detected accuracy change will be cancelled out by modifying the relevant compensation parameters. One straightforward method is to modify the CNC command position. Assume that $\boldsymbol{p}_1$ is the position command in a CNC program, $\Delta \boldsymbol{e}$ is the accuracy change at the position $\boldsymbol{p}_1$. Then, the modified position command $\boldsymbol{p}_2$ is derived as:

$$\boldsymbol{p}_2 = \boldsymbol{p}_1 - \Delta \boldsymbol{e} \tag{2.2}$$

Then, by running the modified version of CNC command, the machine can locate the tool again at the initial point $\boldsymbol{p}_1$.

Step 3-2 Continue the cutting cycle and repeat the whole procedure periodically

If no error compensation is needed, continue the cutting process of N+1th part with the compensation parameter P_1.

By repeating this measurement and compensation cycle, the machine can update the compensation value $\Delta \boldsymbol{e}$ and preserve the initial positioning accuracy.

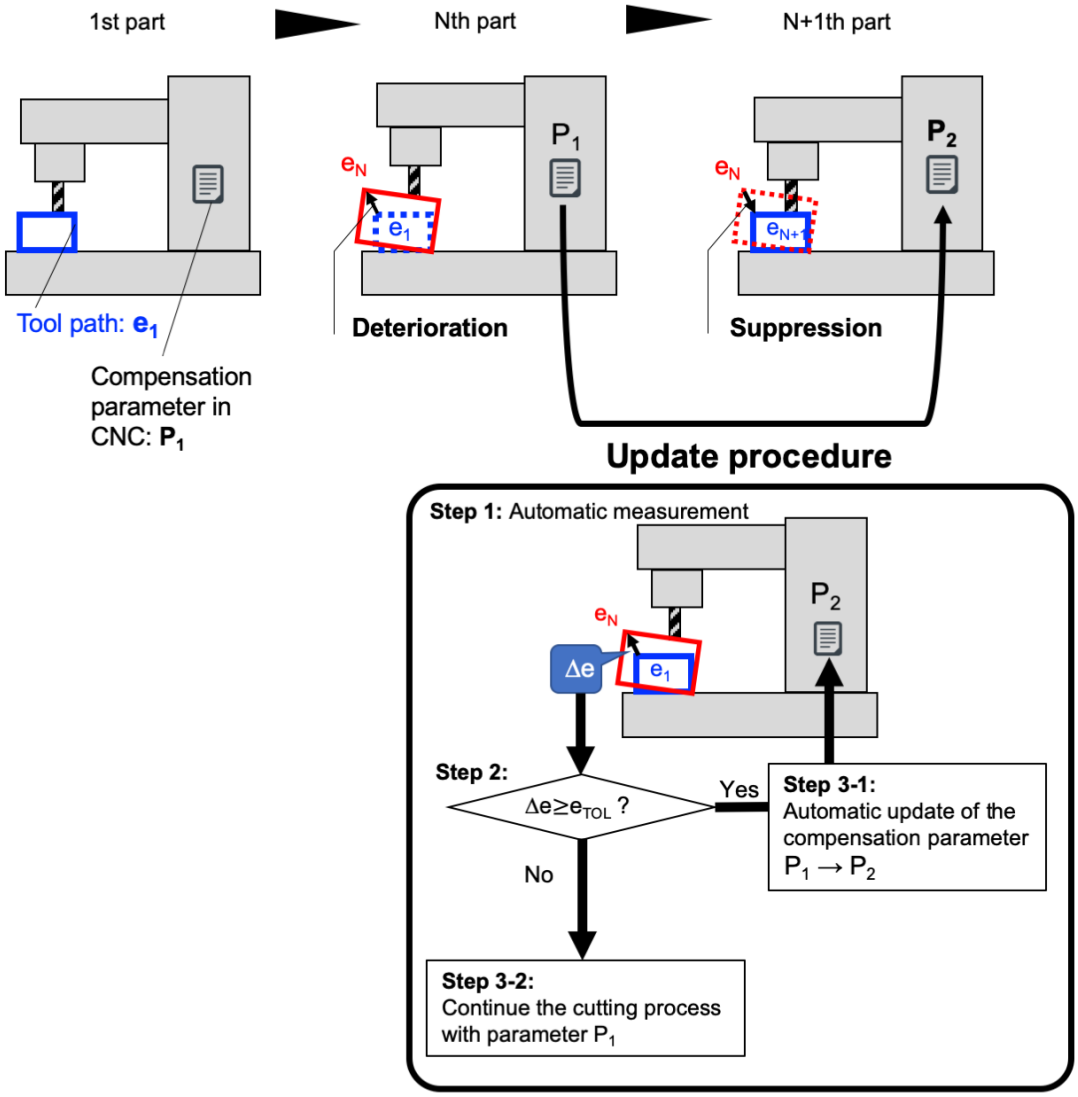

Figure 2.1: Process flow of the automatic error measurement and compensation.

2.2 Establishment of the Error Measurement Method for the Novel System – Measurement Principle

2.2.1 Problem to realize the automatic measurement

Among various errors of machine tools, machine users would mostly concern the TCP error because that determines the final dimensional accuracy of the machined workpiece.

However, as discussed in chapter 1, conventional measurement technologies are designed for manual process, and there is no technology to measure the TCP error without interrupting cutting operations directly.

In order to solve the problem, an approach shown in the next section is employed to determine the accuracy by using a kinematic model of the machine tool.

2.2.2 Kinematic model and its construction procedure

2.2.2.1 Kinematic model

A typical three-dimensional machine tool consists of three mutually orthogonal linear axis components, which are generally called X, Y, and Z-axis. Each linear axis has motion errors, which are explained in the next section. The errors are linked along with the structure of the machine, resulting in the TCP error. The kinematic model is a mathematical tool to describe how the errors in each axis are linked together and propagate to the TCP error. The advantage of the kinematic model is that the error at the tool tip can be mathematically derived even if the error at the tool tip cannot be measured directly, by knowing the errors at each axis instead. Various methods have been developed to measure the errors of a linear axis motion – for example, laser interferometer [69, 70], quadrant photo diode [71], inertial measurement unit [72]. Therefore, even though direct measurement of the TCP accuracy is still challenging, the measurement of linear axis motion errors is realizable. Based on the idea, by installing an appropriate sensor system on a machine to measure the linear axis error, the TCP error can be indirectly identified with the kinematic model. The following explanation is the procedure of kinematic modeling.

2.2.2.2 Procedure to obtain the kinematic model

i. Definition of errors in a linear axis drive motion

Errors of a single linear axis can be defined in six directions, and they are called six degrees of freedom (DOF) errors or geometric errors. Figure 2.2 is a schematic image of the six DOF error of a linear axis (e.g., X-axis). A moving component is supported by the two guideways and slides along the X-axis. Now we assume that the moving component was moved by a distance $x \in \mathbb{R}$. The actual travel distance in the X direction can have an error, as indicated by E_{XX}. This is called the linear positioning error motion of the X-axis. Other than this, translational errors perpendicular to X-axis can also occur due to the inaccuracy of the guideways. These errors indicated by E_{YX} and E_{ZX} are called straightness error motions. In addition to the translational errors, errors in rotational direction can also occur. The rotational errors are defined in three directions. In the case of X linear axis motion, rotations about X, Y, and Z-axis in Figure 2.2 are called the roll, pitch, and yaw, respectively, and indicated by E_{AX}, E_{BX}, and E_{CX}.

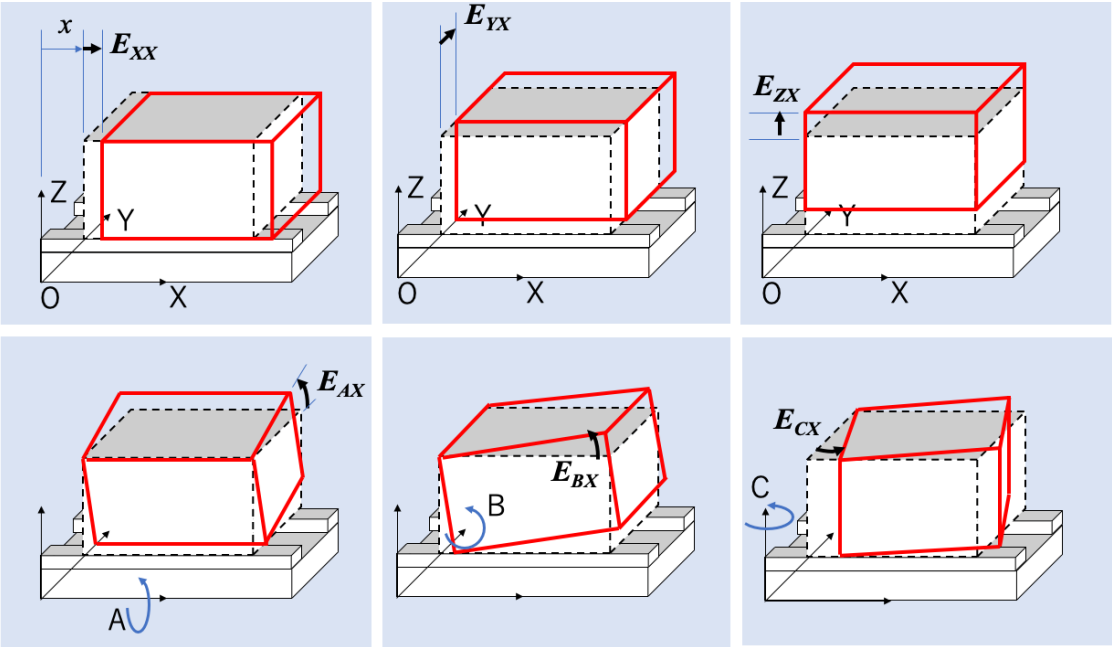

Figure 2.2: Six degrees of freedom error elements in a linear axis.

ii. Determine the kinematic chain of the machine tool

The next step of building a kinematic model is to determine the kinematic chain of the machine tool. The kinematic chain represents the order of the link of principal components (typically linear axis drives, machine bed, cutting tool, and workpiece). For example, a horizontal machining center in Figure 2.3 can be decomposed into a workpiece, the rotary table that realizes B axis motion, Z-linear axis, machine bed, column that moves along the X-axis, spindle component moves along the Y-axis, and the cutting tool. Then, the kinematic chain can be found as a path indicated by a red arrow connecting the workpiece to the cutting tool through the work fixture, table, bed, column, and spindle. In order to represent the kinematic chain, the notations as the designation defined in ISO 10791-1 industrial standard is used [73]. In this example, the kinematic chain can be represented as [w B Z b X Y t], where the upper case letters represent the axis components and the lower case letters "w", "b", and "t" represent the work holding table, the bed, and the tool, respectively. In this study, the errors in linear axis motion are focused on, so the motion in the rotary axis (B) is not considered. Then the kinematic chain can be simplified as [w Z b X Y t].

Once the kinematic chain is determined, the next step is to link the errors in each linear axis following the kinematic chain. From the next part, the mathematical method to describe the linkage among the linear axis is introduced.

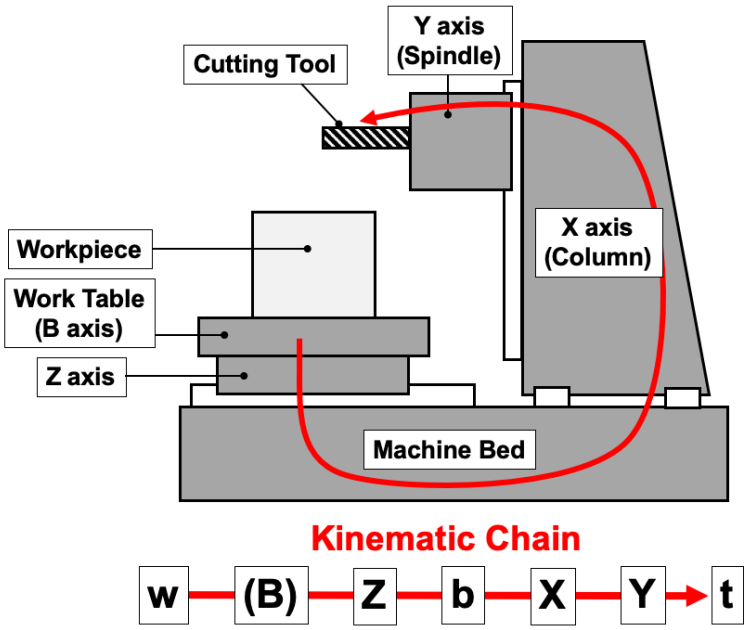

Figure 2.3: Kinematic chain of a horizontal machine tool.

iii. Homogeneous Transformation Matrix

In order to quantitatively describe the six DOF errors and their link in the machine tool structure, a mathematical tool called "Homogeneous Transformation Matrix (HTM)" is used. For example, an operation to move a vector $\boldsymbol{p} \in \mathbb{R}^3$ by a distance $x \in \mathbb{R}$ in X direction, or to rotate $\alpha \in \mathbb{R}$ about X axis can be represented as follows:

$$Translation : \boldsymbol{q} = \boldsymbol{p} + \begin{bmatrix} x \\ 0 \\ 0 \end{bmatrix} \tag{2.3}$$

$$Rotation : \boldsymbol{q} = \begin{bmatrix} 1 & 0 & 0 \\ 0 & \cos\alpha & -\sin\alpha \\ 0 & \sin\alpha & \cos\alpha \end{bmatrix} \boldsymbol{p} \tag{2.4}$$

As shown, a translation can be represented by the addition of vectors, while a rotation can be represented by multiplication of a vector with a matrix. In a machine motion, both the translational and rotational errors can occur at the same time. In order to express them with the above operations, the equation will become a complex one. An HTM is a

mathematical tool to simplify this operation. The HTMs to operate the translation in X, Y, and Z directions and the rotation about X, Y, and Z-axis are defined as in Table 2.1:

Table 2.1: HTMs to represents the transformation or rotation in each direction.

Axis	Translation	Rotation
X	$D_X(x) = \begin{bmatrix} 1 & 0 & 0 & x \\ 0 & 1 & 0 & 0 \\ 0 & 0 & 1 & 0 \\ 0 & 0 & 0 & 1 \end{bmatrix}$	$D_A(\alpha) = \begin{bmatrix} 1 & 0 & 0 & 0 \\ 0 & \cos\alpha & -\sin\alpha & 0 \\ 0 & \sin\alpha & \cos\alpha & 0 \\ 0 & 0 & 0 & 1 \end{bmatrix}$
Y	$D_Y(y) = \begin{bmatrix} 1 & 0 & 0 & 0 \\ 0 & 1 & 0 & y \\ 0 & 0 & 1 & 0 \\ 0 & 0 & 0 & 1 \end{bmatrix}$	$D_B(\beta) = \begin{bmatrix} \cos\beta & 0 & \sin\beta & 0 \\ 0 & 1 & 0 & 0 \\ -\sin\beta & 0 & \cos\beta & 0 \\ 0 & 0 & 0 & 1 \end{bmatrix}$
Z	$D_Z(z) = \begin{bmatrix} 1 & 0 & 0 & 0 \\ 0 & 1 & 0 & 0 \\ 0 & 0 & 1 & z \\ 0 & 0 & 0 & 1 \end{bmatrix}$	$D_C(\gamma) = \begin{bmatrix} \cos\gamma & -\sin\gamma & 0 & 0 \\ \sin\gamma & \cos\gamma & 0 & 0 \\ 0 & 0 & 1 & 0 \\ 0 & 0 & 0 & 1 \end{bmatrix}$

Using this, equations (2.3) and (2.4) can be rewritten as follows:

$$Translation : \boldsymbol{q} = D_X(x) \begin{bmatrix} \boldsymbol{p} \\ 1 \end{bmatrix} \tag{2.5}$$

$$Rotation : \boldsymbol{q} = D_A(\alpha) \begin{bmatrix} \boldsymbol{p} \\ 1 \end{bmatrix} \tag{2.6}$$

Thus, both the translation and rotation can be expressed with the same shape of the equation. When the translation and rotation occur at the same time, multiple of the matrices associated with the direction can be combined to express the operation. In total, six multiplications are needed to express all of the six DOF error. However, especially for machine tool error calculation, the matrix can be further simplified as follows. Generally, the errors are in the order of 10^{-6} to 10^{-5} m or rad, while machine motion is in the order of 10^{-3} to 1 m or rad. Therefore, in order to express machine motion error, the following approximation can be made by ignoring the second-order or higher terms.

$$D_X(E_{XX})D_Y(E_{YX})D_Z(E_{ZX})D_A(E_{AX})D_B(E_{BX})D_C(E_{CX}) \approx \begin{bmatrix} 1 & -E_{CX} & E_{BX} & E_{XX} \\ E_{CX} & 1 & -E_{AX} & E_{YX} \\ -E_{BX} & E_{AX} & 1 & E_{ZX} \\ 0 & 0 & 0 & 1 \end{bmatrix} \tag{2.7}$$

This approximated matrix has an advantage of expressing all of the six DOF errors with one matrix.

iv. Coordinate transformation with homogeneous transformation to obtain the kinematic model

Here, a detailed procedure to formulate a kinematic model is shown with an example. First, define a local coordinate system for each principal component in the kinematic chain. The local coordinate system is fixed to each component and moves and rotates together with the component. The six DOF errors in each linear axis are defined in this local coordinate system. The purpose of the kinematic model is to combine the errors in the local coordinate systems and map into a global coordinate system. In machine tool design, the global coordinate frame is typically fixed on the machine bed that is the base structural part of the machine tool. Therefore, in this example, the global coordinate system is fixed to the machine bed.

Now, define the TCP vector in the Y-axis local coordinate system as $\boldsymbol{t} = [t_x, t_y, t_z]^T$. Since the CNC control system needs to know the tool tip position in the reference coordinate system, HTM ${}^{X}T_Y(E_{*Y}), (* = X, Y, Z, A, B, C)$ are used to map the tool tip position vector in the Y-axis local coordinate system to X-axis local coordinate system. Here, ${}^{X}T_Y(\cdot)$ means the transformation from the Y-axis coordinate system to the X-axis coordinate system, and E_{*Y} in the parenthesis means the error elements in the matrix. Next, the HTM ${}^{b}T_X(E_{*X})$ is used to map into the reference coordinate system located at the machine bed. By the multiplication of the HTMs, the position of the tool tip to the reference coordinate system $\boldsymbol{P}_t$ can be obtained. This sequence is illustrated in Figure 2.4.

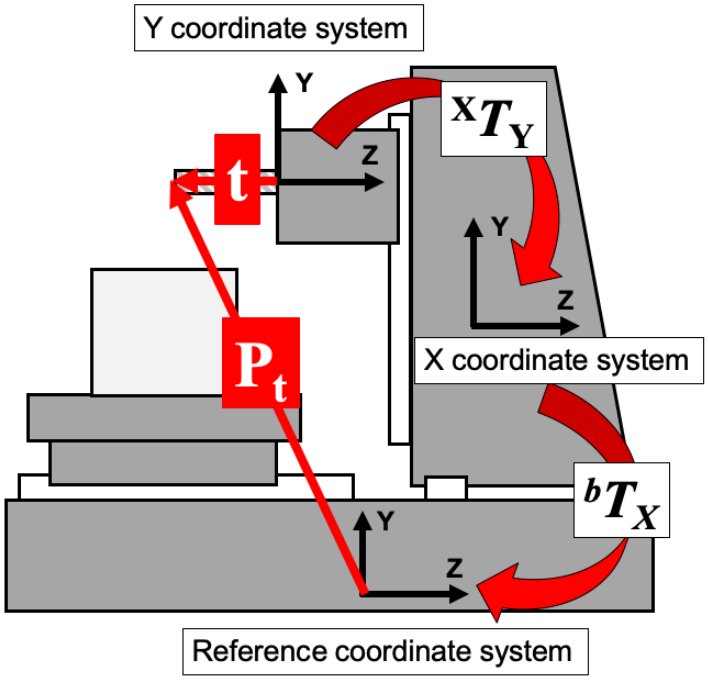

Figure 2.4: Coordinate transform of the tool tip position.

$$\boldsymbol{P}_t = \begin{bmatrix} X_t \\ Y_t \\ Z_t \\ 1 \end{bmatrix} = {}^{b}T_X(E_{*X})\,{}^{X}T_Y(E_{*Y}) \begin{bmatrix} t_x \\ t_y \\ t_z \\ 1 \end{bmatrix} \tag{2.8}$$

The target position on the work surface is also mapped to the reference coordinate system in the same way. Define the target position vector $\boldsymbol{w} = [w_x, w_y, w_z]^T$ in Z-axis local coordinate system fixed at the work table. Then, HTM ${}^{b}T_Z(E_{*Z})$ is used to map the vector into the reference coordinate of the machine. The HTM contains the six DOF error elements of the Z-axis. This sequence is illustrated in Figure 2.5. The actual coordinates of the machining point on the work surface $\boldsymbol{P}_w$ in the reference coordinate system are given by

$$\boldsymbol{P}_w = \begin{bmatrix} X_w \\ Y_w \\ Z_w \\ 1 \end{bmatrix} = {}^{b}T_Z(E_{*Z}) \begin{bmatrix} w_x \\ w_y \\ w_z \\ 1 \end{bmatrix} \tag{2.9}$$

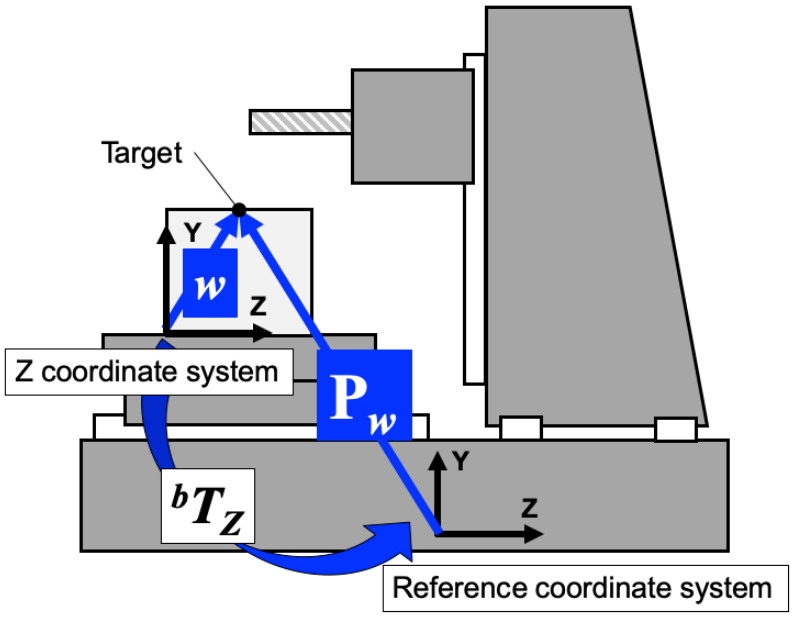

Figure 2.5: Coordinate transform of the target point on the work surface.

Then, the TCP error can be expressed as the relative displacement between the target point on the workpiece and the TCP in the reference coordinate system which can be derived by

$$\boldsymbol{e}(\boldsymbol{E}) \equiv \begin{bmatrix} e_x \\ e_y \\ e_z \end{bmatrix} = \begin{bmatrix} X_t \\ Y_t \\ Z_t \end{bmatrix} - \begin{bmatrix} X_w \\ Y_w \\ Z_w \end{bmatrix} \tag{2.10}$$

$$where \quad \boldsymbol{E} = E_{*X}, E_{*Y}, E_{*Z} \tag{2.11}$$

In the above equation, X_t, Y_t, Z_t are functions of 12 variables E_{*X} and E_{*Y}, and X_w, Y_w, Z_w are functions of six variables E_{*Z}. As shown, the TCP error vector $\boldsymbol{e} = [e_x, e_y, e_z]$ is derived as functions of 18 error elements of each linear axis. To specify that, the symbol $\boldsymbol{E}$ is defined to represent all of the 18 variables.

The kinematic model for the horizontal machining center is specifically derived as in (2.12). In the equation, L_* are constants that are determined by the dimensions of the machine components. For example, L_{ZY} means the Z directional length of the Y-axis component.

$$
\begin{aligned}
\boldsymbol{e}(\boldsymbol{E}) \;=\; & \begin{bmatrix} E_{XX} + E_{XY} - E_{XZ} + L_{ZY}(E_{BX} + E_{BY}) - L_{YY}(E_{CX} + E_{CY}) \\ E_{YX} + E_{YY} - E_{YZ} - L_{ZY}(E_{AX} + E_{AY}) + L_{XY}(E_{CX} + E_{CY}) \\ E_{ZX} + E_{ZY} - E_{ZZ} + L_{YY}(E_{AX} + E_{AY}) - L_{XY}(E_{BX} + E_{BY}) \end{bmatrix} \\
& + Z_t(E_{BX} + E_{BY}) - L_{YY}E_{CX} + L_{ZX}E_{BX} + L_{YZ}E_{CZ} - L_{ZZ}E_{BZ} \\
& - Z_t(E_{AX} + E_{AY}) + L_{XX}E_{CX} - L_{ZX}E_{AX} - L_{XZ}E_{CZ} + L_{ZZ}E_{AZ} \\
& - L_{XY}E_{BX} + L_{YX}E_{AX} + L_{XZ}E_{BZ} - L_{YZ}E_{AZ} + E_{BZ}X_w \\
& \begin{bmatrix} + E_{CZ}Y_w - E_{BZ}Z_w \\ - E_{CZ}X_w + E_{AZ}Z_w \\ - E_{AZ}Y_w \end{bmatrix}
\end{aligned} \tag{2.12}
$$

2.2.3 The limitation and target of this approach

The kinematic model assumes that every machine component is a rigid body. Therefore, errors that stem from the elastic deformation of the machine structure, tool, and workpiece cannot be described by this approach. Also, non-linear deformation due to thermal influence and errors due to the servo control system are outside of the scope of this system. As Figure 2.6 indicates, this measurement approach focuses explicitly on the kinematic error of the machine tool among the errors introduced in section 1.2.

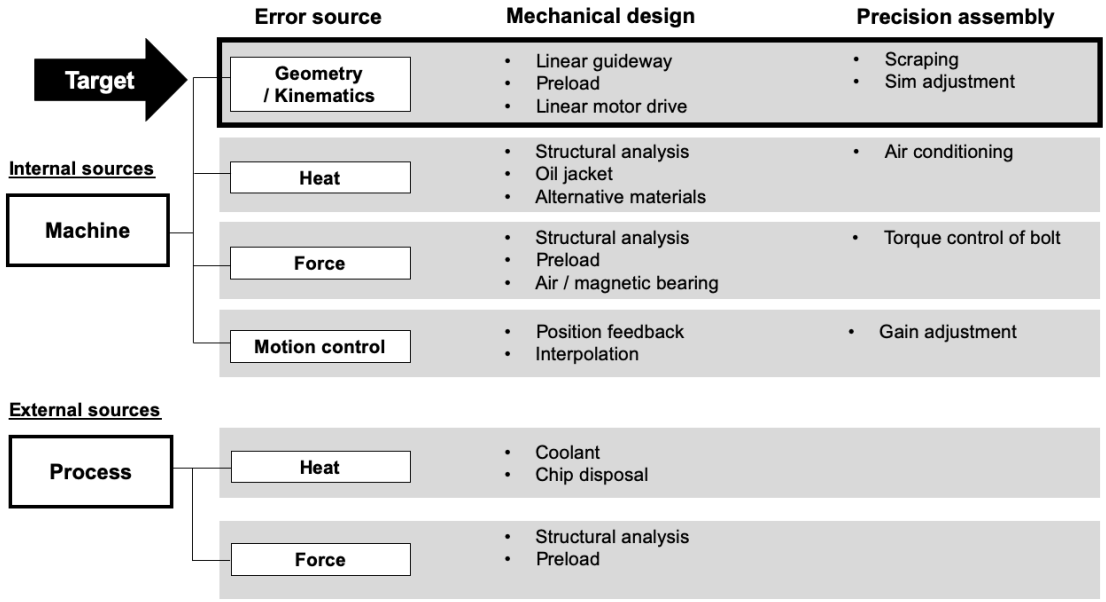

Figure 2.6: The target area of the kinematic approach.

2.3 Establishment of the Error Measurement Method for the Novel System – Hardware

2.3.1 Selection of the sensors

In order to realize the measurement of the six DOF error elements, appropriate sensors should be chosen. However, the sensors with sufficient accuracy performance are generally expensive, sensitive, and expensive, so the selection of a sensor is a challenging task. In Table 2.2, candidate sensors are listed, and their features are compared.

At present, the system which can measure the accuracy of all six DOF with sufficient resolution has only been established by using the laser [74]. However, as explained in Chapter 1, the laser measuring instrument is expensive and delicate. Thus, it is not practical to use it as a built-in sensor. Therefore, in this study, though the measurement of all six DOF is impossible at present, the sensor which is expected to be able to measure all six DOF in the future was chosen.

Among the multiple options, the use of linear scales is focused. Linear scales are commonly used on modern CNC machine tools for position feedback control, so they are already used as a built-in sensor. Although a single linear scale can only measure the position of a single axis, by using two linear scales in parallel for one axis, angular error measurement in yaw direction become possible, as shown in Figure 2.7. Recently the technologies of linear scale are rapidly growing, and a previous research conducted by Fujimori et al. [75] implies that the linear scale will be able to measure all of the six DOF error elements, as further explained in detail in Chapter 4. From this perspective, this research designed a linear-scale-based system and studied the fundamental elements to develop the system with the measurement of the yaw error element.

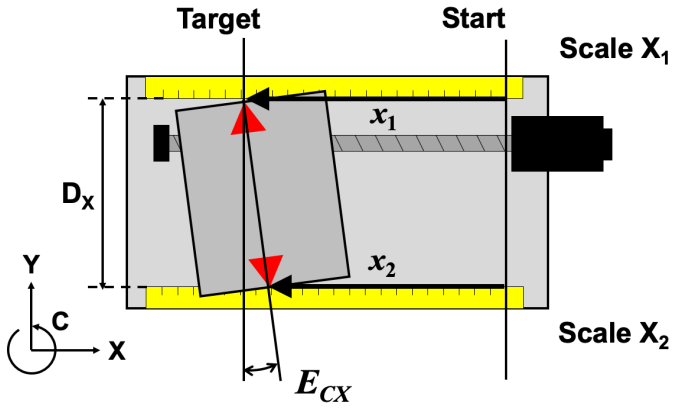

Figure 2.7: Measurement of angular error with dual linear scales.

Table 2.2: Specifications of candidate sensors ("D" in the resolution column indicates the distance between the dual linear scales, and the unit is meter. "M" in the uncertainty column indicates the measurement distance, and the unit is meter.)

Sensor	Error to be measured	Resolution	Uncertainty	Price
Clinometer [76]	Rotational	0.1μrad	1μrad	$ 5,000
Autocollimator [77]	Rotational	0.0005μrad	0.5μrad	$ 30,000
IMU[78]	Rotational	not specified	10μrad	$ 5,000
	Translational	not specified	1μm	"
Laser interferometer [74]	Translational	1nm	$\pm$0.55ppm	$ 20,000
	Rotational	0.03μrad	$\pm$0.6%$\pm$(0.5 +0.1M)μrad	"
Linear scale	Translational (single use)	10nm	(1.5+1.5M) μm	$ 1,000
	Rotational (dual use)	$(x_2 - x_1)/D$	$-$	$ 2,000

2.3.2 Design of dual linear scale system for angular measurement

The principle of the dual linear scale system is explained using an illustration in Figure 2.7. Suppose that a moving component moves along the X-axis. Two linear scales are installed in parallel on the side of the moving component. The scales are labeled as scale X_1 and X_2 to distinguish them from each other. First, the moving component is located in a start position, which is the origin of the measurement. At this point, the position and errors of the component are regarded as zero. Next, the component is moved to a target point, and the position reading of the scales X_1 and X_2 at the target is x_1 and x_2, respectively. Then, the yaw angular error E_{CX} can be calculated by the following equation. Here, the approximation $\tan^{-1}\theta \approx \theta$ can be made because, generally, the relative position difference $x_2 - x_1$ is in the order of micrometers, whereas the distance D_X between the paired linear scales indicated in Figure 2.7 is in the order of meters. In this study, scale X_1 is the primary linear scale whose position data is used for the position feedback control, and scale X_2 is the secondary linear scale just for measuring the angle. The angular deviation is calculated as the relative displacement of scale X_2 with respect to X_1.

$$E_{CX} = \tan^{-1}\left[\frac{x_2 - x_1}{D_X}\right] \approx \frac{x_2 - x_1}{D_X} \tag{2.13}$$

2.3.2.1 Required measurement performance of this linear scale system

Now let us estimate the required measurement performance of the proposed scale measurement system. In the kinematic model equation (2.12), the terms related to yaw error which is detectable with this system are:

$$\boldsymbol{e}(\boldsymbol{E}) = \begin{bmatrix} -E_{BZ}(L_{ZZ} + Z_w) + E_{BX}(L_{ZX} + L_{ZY} + Z_t) - L_{YY}E_{CY} \\ L_{XY}E_{CY} \\ -E_{BX}(L_{XX} + L_{XY}) + E_{BZ}(L_{XZ} + X_w) \end{bmatrix} \tag{2.14}$$

In the equation, L and Z are constants, so they do not have uncertainty. Therefore, the uncertainty that arises from the measurement of this system is derived as follows based on the error propagation rule for addition or subtraction [79].

$$\sigma_{\boldsymbol{e}} = \begin{bmatrix} \sqrt{\sigma_{E_{BX}}^2 + \sigma_{E_{BZ}}^2 + \sigma_{E_{CY}}^2} \\ \sigma_{E_{CY}} \\ \sqrt{\sigma_{E_{BX}}^2 + \sigma_{E_{BZ}}^2} \end{bmatrix} \tag{2.15}$$

According to equation (2.13), the accuracy of x_1 and x_2 propagates to the accuracy of the angle E_{CX}. So, let σ_{x_1} and σ_{x_2} denote the uncertainty of the measurement values. Based on the error propagation rule,

$$\sigma_{(x_2 - x_1)} = \sqrt{\sigma_{x_1}^2 + \sigma_{x_2}^2} \tag{2.16}$$

The problem is to determine the tolerable uncertainty of the linear scales. A typical positioning accuracy tolerance is set at 16 μm in ISO 10791-4 [80]. According to the principle of measurement [58], the accuracy of the measuring instrument should be at least five times higher than the expected precision of the measured object. So, the target specification is set at 3.2 (one-fifth of 16). When using the same model type of linear scales for all of the linear drive axes, the uncertainty of each linear encoders can be assumed as the same, i.e. $\sigma_{x_1} = \sigma_{x_2} = \sigma_{y_1} = \sigma_{y_2} = \sigma_{z_1} = \sigma_{z_2}$. Then, the tolerable uncertainty is calculated as follows:

$$\sigma_{\boldsymbol{e}} = \sqrt{\sigma_{x_1}^2 + \sigma_{x_2}^2 + \sigma_{y_1}^2 + \sigma_{y_2}^2 + \sigma_{z_1}^2 + \sigma_{z_2}^2} = 3.2 \tag{2.17}$$

$$\sqrt{6\sigma_{x_1}^2} = 3.2 \tag{2.18}$$

$$\therefore \sigma_{x_1} = \sqrt{\frac{10.24}{6}} \approx 1.31 \mu m \tag{2.19}$$

So, the linear scale which satisfies this uncertainty should be selected. This calculation result is used in chapter 3 to assess the measurement performance of the prototype system.

2.3.3 Hardware architecture

Figure 2.8 illustrates the architecture of the system designed for the study. To realize the measurement principle of yaw angle shown in Figure 2.7, six linear scales are installed to a machine tool.

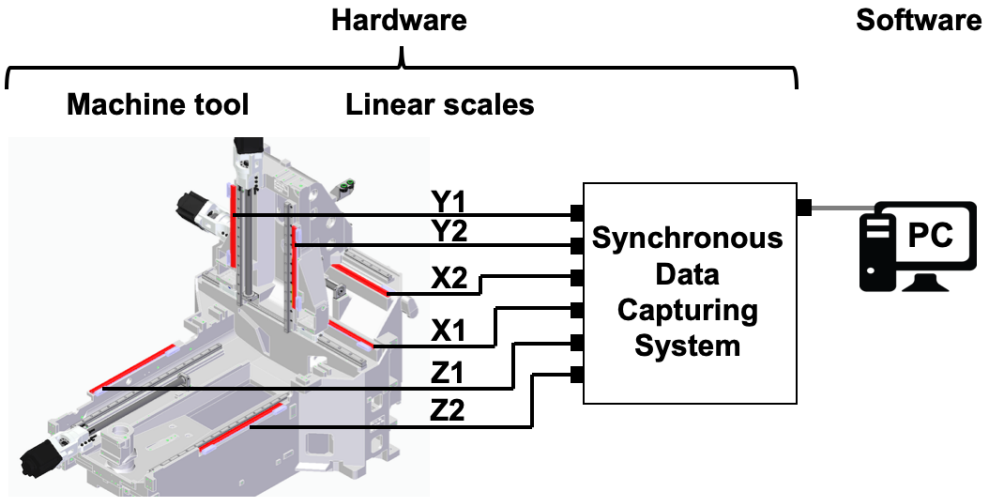

Figure 2.8: The arrangement of the scales and a synchronous data capturing system on a machine tool.

In order to measure the angle based on the principle, it is necessary to obtain the position data of the two linear scales at the same moment. Since the error calculation is done with a digital or discrete sampling system, the position data must be synchronized to obtain the accurate calculation result. Therefore, synchronous data sampling is required. In this study, synchronization is achieved by controlling the timing of the data acquisition of the read heads with the following principle.

Distribute a clock signal from the data capturing device to the read heads. Figure 2.9 (a) illustrates the clock signal sent from the synchronous data capturing device to a read head. In the figure, only one read head is shown, but the same signal communication takes place for the other read heads as well. Suppose that the digital circuits in the systems are designed such that the signal communications between the read head and the data capturing device takes place at the rising edge of the clock signal. The data capturing device send a request signal to the output interface in the read head at a certain rising edge of the clock, as shown in Figure 2.9 (b). Then, the interface sends the position data in the read head back to the capturing device at the next rising edge of the clock, as shown in Figure 2.9 (c). Since all of the read heads share the clock signal, the above step is executed at the same timing.

Thus the position data from multiple linear scales can be obtained at the same time.

The following calculation assessed the required time accuracy of this synchronization. Assume that a moving component is moving in X axis at a feed speed of F [mm/min]. The scale x_1 is sampling the position at a sampling interval of t [s], while the sampling of the scale x_2 has time misalignment with respect to x_1 by $\pm\Delta t$ [s], i.e. the sampling of the scale x_2 takes place every $t \pm \Delta t$ [s]. Then, the position reading of x_1 and x_2 is Ft and $F(t \pm \Delta t)$. Thus, the angular deviation of E_{CX} of the moving component is calculated as:

$$E_{CX} \approx \frac{x_2 - x_1}{D_X} = \frac{\pm F\Delta t}{D_X} \tag{2.20}$$

This is the measurement error caused by the time misalignment. Assuming that the feed speed is at 60m/s, which the maximum speed of the CNC machine tool, the angular error can be $\pm 60\Delta t/D$ rad. Using the kinematic model (2.21), the tool tip error caused by the error is rewritten as in equation (2.21). This equation will be used in chapter 3 to assess the measurement performance of the developed prototype system.

$$\boldsymbol{e}(\boldsymbol{E}) = \begin{bmatrix} -\frac{\pm F\Delta t}{D_Z}(L_{ZZ} + Z_w) + \frac{\pm F\Delta t}{D_X}(L_{ZX} + L_{ZY} + Z_t) - L_{YY}\frac{\pm F\Delta t}{D_Y} \\ L_{XY}\frac{\pm F\Delta t}{D_Y} \\ -\frac{\pm F\Delta t}{D_X}(L_{XX} + L_{XY}) + \frac{\pm F\Delta t}{D_Z}(L_{XZ} + X_w) \end{bmatrix} \tag{2.21}$$

2.4 Establishment of the Error Measurement Method for the Novel System – Data Analysis

So far, the measurement principle has been established, and the hardware for the measurement has selected. By making a physical prototype, the measurement would be possible. Assuming that the prototype was implemented and measurement data were obtained, the data needs to be post-processed and analyzed in an appropriate manner. In this section, the data analysis procedure suitable for this system is discussed.

2.4.1 Definition of systematic and random error elements in machine tool error

In the theory of machine tool error analysis, error data obtained by the iterative measurement is regarded as a combination of two elements: systematic error and random error [81]. Systematic error is the reproducible and predictable part of the data set and thus regarded to represent the iterative motion of the machine. Random error is the variance of the data points, which is typically due to the signal noise of the measurement, small vibration

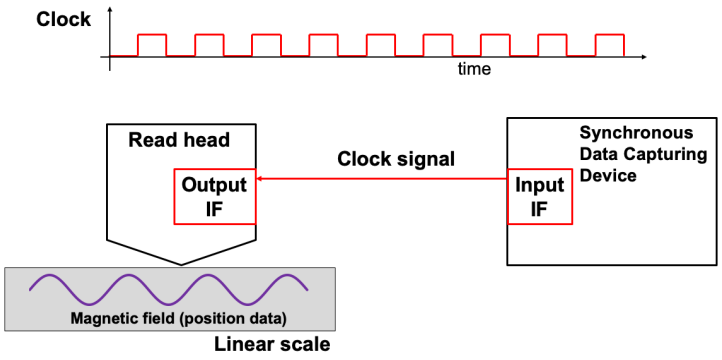

(a)

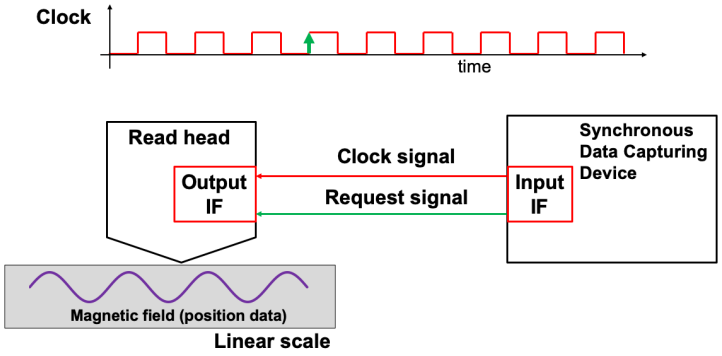

(b)

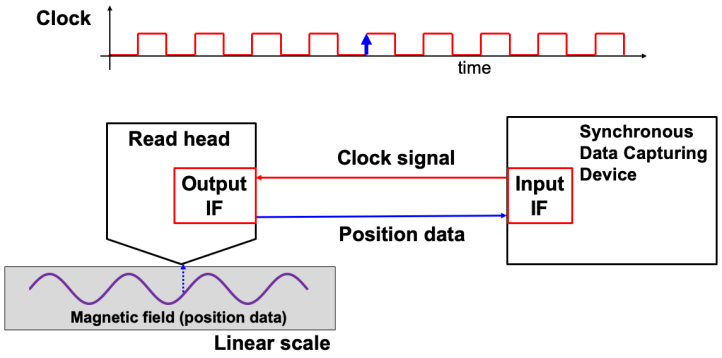

(c)

Figure 2.9: The synchronous data capturing by distributing a request signal.

of machine components, or any other disturbance of the motion or the measurement. Therefore, in order to determine the dynamic change of the repeatability, this systematic error should be extracted from the data points. Machine tool error analysis typically assumes the data distribution is subject to a normal distribution [81]. Then, the mean value represents the systematic error, and the variance of the distribution represents the random error.

Let E_{ir} denotes the raw data of an error sampled at a measurement position i, where $i = 1, ..., m$ is the index of the data point. Then, the systematic error $\overline{E}_i$ at the position i can be calculated as:

$$\overline{E}_i = \frac{\sum_{r=1}^{m} E_{ir}}{m} \tag{2.22}$$

On the other hand, the random error σ_i of the error sampled at a position i can be calculated as:

$$\sigma_i = \sqrt{\frac{1}{m-1}\sum_{r=1}^{m}(E_{ir} - \overline{E}_i)} \tag{2.23}$$

2.4.2 Example of extraction of systematic and random errors from measurement data

Figure 2.10 is an example of yaw angle data measured in this study. All data points sampled with a sampling rate of 100Hz in five iterative measurement cycles were overlaid in one figure. As can be seen, at each measurement position (horizontal axis), the measured yaw values distribute within a certain range and show certain repeatability. Figure 2.11 shows a magnified view of the data plot at position Y=-280mm and Fig. 2.12 is the histogram of the data. The histogram implies that assuming that measurement values are subject to a normal distribution is a reasonable assumption. By applying the equation, the systematic error at each measurement position was calculated. Figure 2.13 shows the systematic error extracted from the raw data plot in Figure 2.11. The random error is also derived and indicated with the vertical bars. The random error is treated as uncertainty in the measurement and will be used to evaluate the reliability of the measured result in the next chapter.

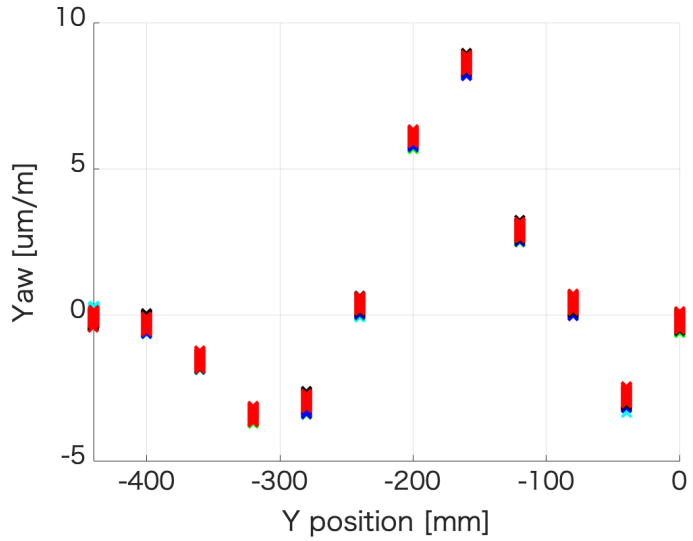

Figure 2.10: A sample yaw angle data measured with this system.

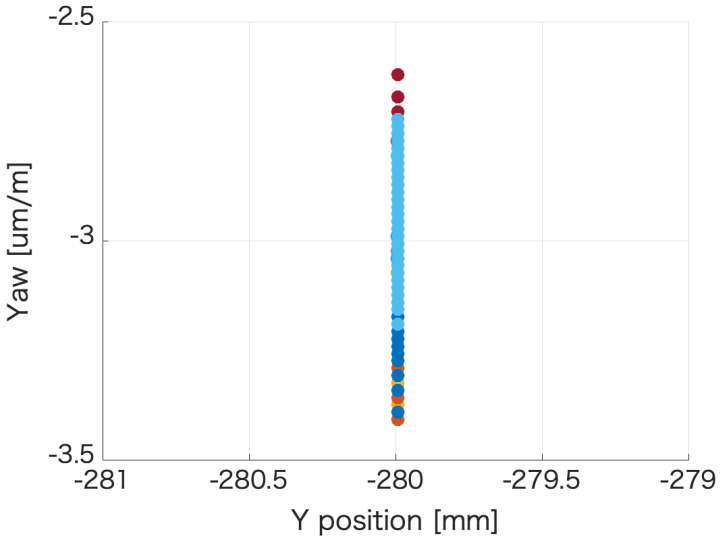

Figure 2.11: The magnified view of the yaw data plot at position Y=-280mm.

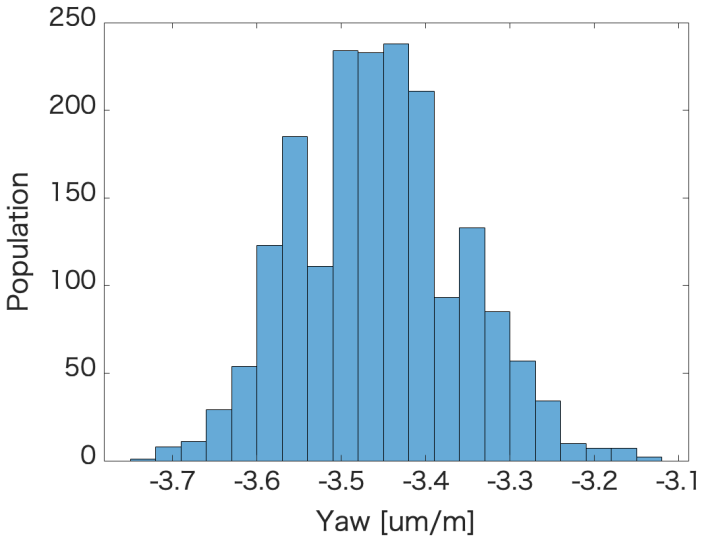

Figure 2.12: The histogram of the yaw data sampled at Y=-280mm.

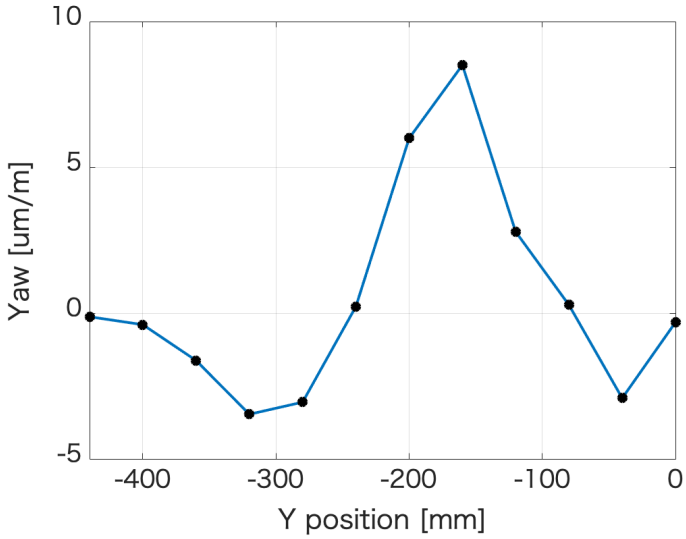

Figure 2.13: The systematic error $\overline{E}_{CY}$ extracted from the raw data.

2.5 Summary

In this chapter, the concept and composition of the dynamic error compensation system were explained.

In section 2.1, the author first pointed out that conventional error compensation is a manual procedure and proposed an approach to automate the process. For that purpose, machine tools need to detect their accuracy change and adjust the compensation parameters without human intervention. To realize that, the author proposed to evaluate the TCP accuracy by using a kinematic model of the machine.

In section 2.2, the procedure to build a kinematic model was explained in detail with an example of a horizontal machining center.

In section 2.3, the appropriate sensors to build the system were discussed, and the linear scale was selected to make a prototype system for yaw angular error. Based on the measurement principle of yaw with dual linear scales, the requirement for the measurement accuracy was discussed.

In section 2.4, the procedure of detection and compensation of machine tool accuracy with the proposed system was explained.

Chapter 3

Verification Study with a Prototype System

3.1 Prototyping

In order to investigate the effectiveness of the error measurement and compensation method, a physical prototype was required for experimentation. In this chapter, the prototype system developed for this study is introduced. The system consists of following hardware:

- Machine tool
- Linear encoder
- Synchronous data capturing device

The detailed specification of each hardware will be provided in the following sections.

3.1.1 CNC Machine Tool

For this study, a medium-size horizontal machining center, NHX4000 2nd Generation designed by DMG MORI Co., Ltd., is chosen as the test bench. Figure 3.1a is the exterior view of the machine. There are mainly two reasons for choosing this machine. One is to evaluate the feasibility of this system on a real machine in the market. Another reason is that the machining center is not an exception to general machine tools that consists of three mutually orthogonal linear axes. Figure 3.1b illustrates the axis configuration of the machine. Although the machine has a rotary axis (B axis) other than the three linear axes, in this study, the B axis is not rotated to focus on the kinematic errors of the linear axes. Thus the machine can be treated as a three-axis machine tool. The axis configuration and kinematic chain of this machine are the same as the one previously explained in Figure 2.3 in

section 2.2.2. On this machine, the linear encoders are installed. The detail of the encoder is introduced in the next section. The location of the linear encoders was decided, as shown in Figure 3.2. The stroke length and the distance between the paired scales on each axis are summarized in Table 3.1.

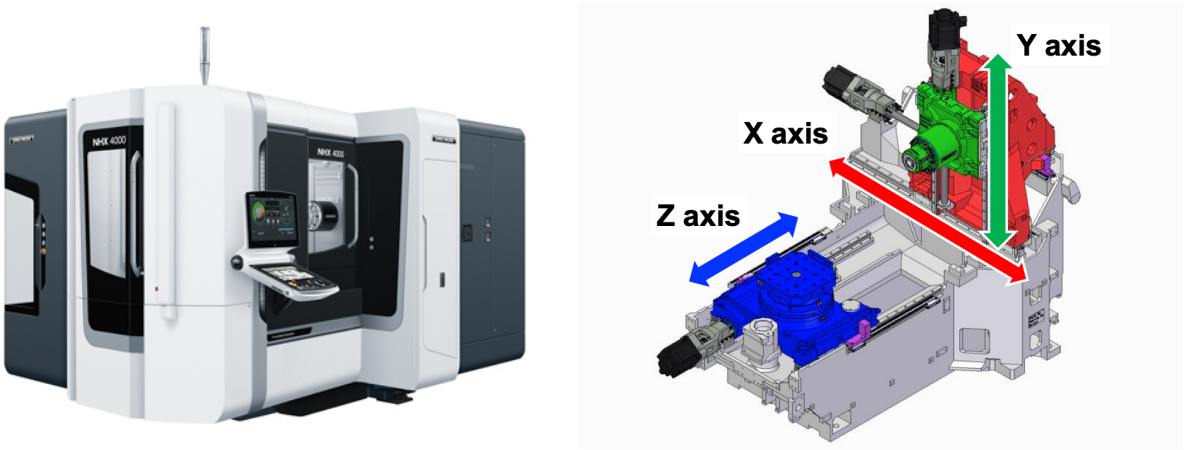

(a) Exterior [82] (b) Axis configuration

Figure 3.1: DMG MORI NHX 4000 2nd Generation.

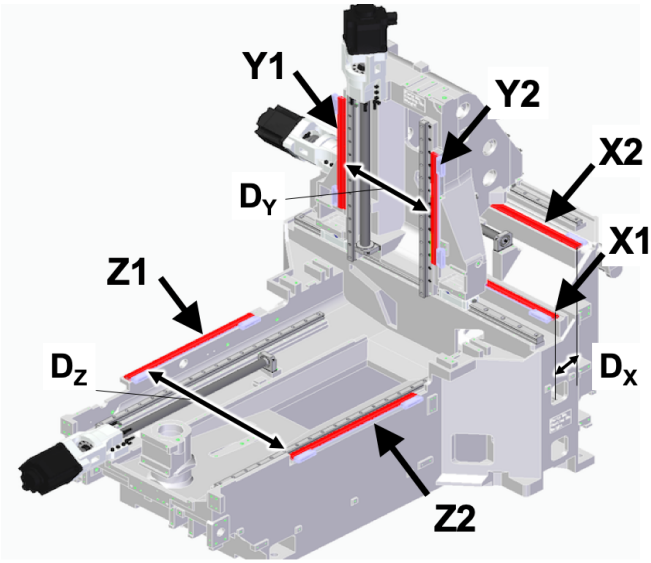

Figure 3.2: The location of the linear encoders.

Table 3.1: The stroke length and the distance between the paired scales.

Axis	Stroke [mm]	Scale Distance D [mm]
X	390	240
Y	440	600
Z	495	870

3.1.2 Linear encoder

Linear encoder plays a vital role in this system as the internal sensor to collect the machine's position data, which is necessary to calculate the angular error of the moving component. An exterior view of a linear encoder is shown in Figure 3.3. A typical linear encoder consists of two main components: a scale on which position data is recorded and a read head which read the information and convert it to an analog or digital signal.

There are mainly two types of linear encoders depending on the record and read method of the position data: optical and magnetic encoder. Generally, the optical encoder has a higher resolution because of the use of laser, but the measurement is sensitive to contamination [83]. During the machining process, a lot of coolant mist and cutting chips are generated, and they can contaminate the encoder. In order to perform precision measurement under such a harsh environment, contamination durability is required in addition to high precision. A magnetic encoder is immune to contamination in principle, and the resolution is comparable to that of optical encoder by the recent development of magnetic scale technology [83].

Linear encoders can also be divided into two groups depending on the encoding type of the position data: incremental and absolute type. For incremental type, position data are encoded with evenly separated tick marks. By counting the number of tick marks from the start position, the relative distance of motion is measured. On the other hand, for absolute type, the tick marks are encoded with a certain length of bit number so that the absolute position can be detected. The absolute type scale has several advantages with respect to the incremental type: low risk of miscounting, immune to noise, no need to find the home position, and so forth [84].

Based on these reasons, the author decided that a magnetic and absolute type linear encoder is suitable for this system. In this study, SmartSCALE, a production of Magnescale Co., Ltd., was chosen to develop a prototype system. SmartSCALE type SQ57 shown in Figure 3.3 is an absolute type magnetic linear encoder, and its specification is summarized in Table 3.2.

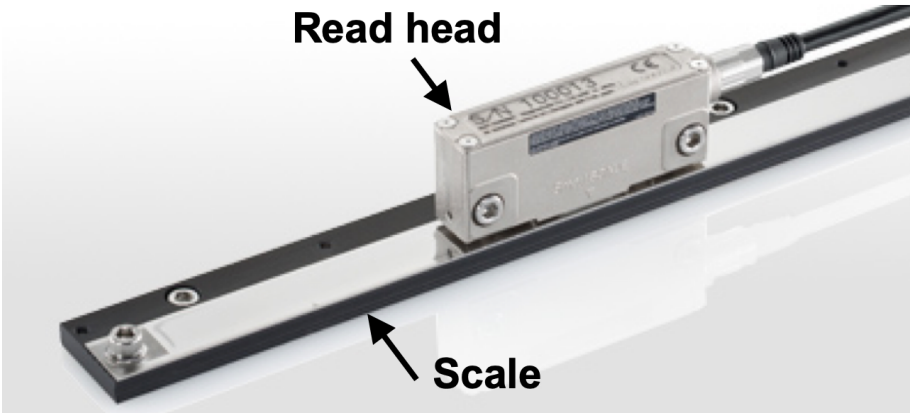

Figure 3.3: SmartSCALE by Magnescale Co., Ltd. [85]

Table 3.2: Specification of the SmartSCALE type SQ57 (L = measurement distance in meter).

Type	SQ57
Material	Steel
Accuracy	(1.5+1.5L) μm
Resolution	10 nm
Coef. of thermal expansion	12 μm/m·K
Waterproof	IP 67

3.1.3 Scale Data Capturing Device

As discussed in section 2.3.3, In order to measure the angle based on the principle, a synchronous data-capturing system is required to obtain the position data of two linear encoders at the same moment. For this study, a data-capturing device BD200 was developed by Magnescale Co., Ltd. Figure 3.4 is an exterior view of BD200 connected with six linear encoders. Figure 3.5 is the block diagram of the signal communication between the read head and BD200. The linear encoders and BD200 are synchronized with a 40MHz clock signal. The clock signal is then distributed to all read heads. By communicating with this clock signal, the position data from all of the read heads are sent to BD200 at the same moment. With this high sampling frequency, the time misalignment is reduced to 5ns. Based on equation (2.20), the measurement error of yaw angular deviation due to the time misalignment is estimated. For NHX4000, the maximum feed speed of the linear axes is 60

m/min. Then, the yaw measurement error ΔE_{YAW} due to the misalignment can be:

$$\Delta E_{YAW} \approx= \frac{\pm 60m/min \cdot 5ns}{D} = \frac{\pm 5nm}{D} \tag{3.1}$$

$$= 0.021 \quad [\mu m/m] \quad (Xaxis) \tag{3.2}$$

$$0.008 \quad (Yaxis) \tag{3.3}$$

$$0.006 \quad (Zaxis) \tag{3.4}$$

By plugging these values into the kinematic model equation (2.14), the measurement error of the TCP position due to this time misalignment is derived as up to 0.016μm (X axis), 0.004μm (Y axis), and 0.003μm (Z axis). As the measurement target of this system is errors of μm order, so this data capturing system is capable of capturing the scale position data with sufficient time accuracy.

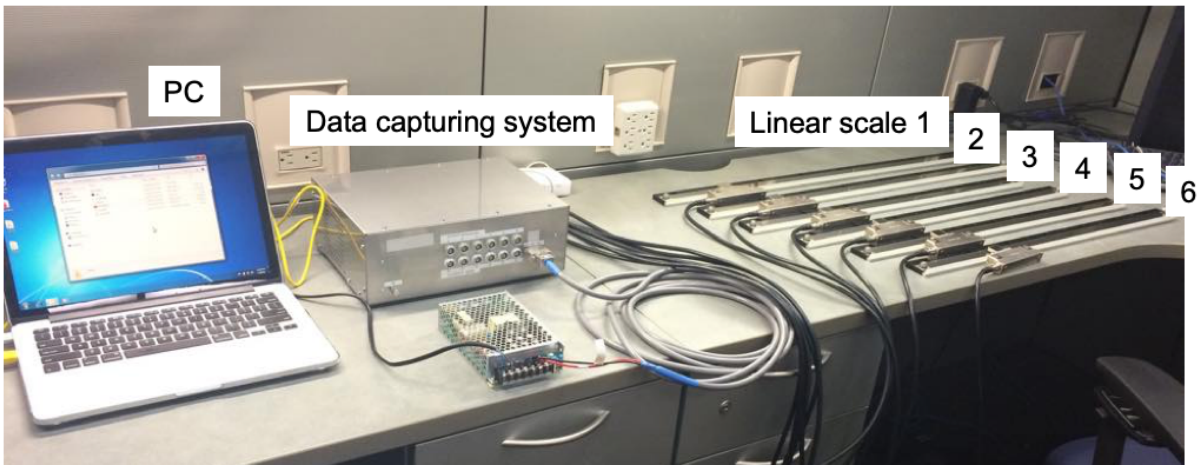

Figure 3.4: Magnescale BD200 data acquisition system.

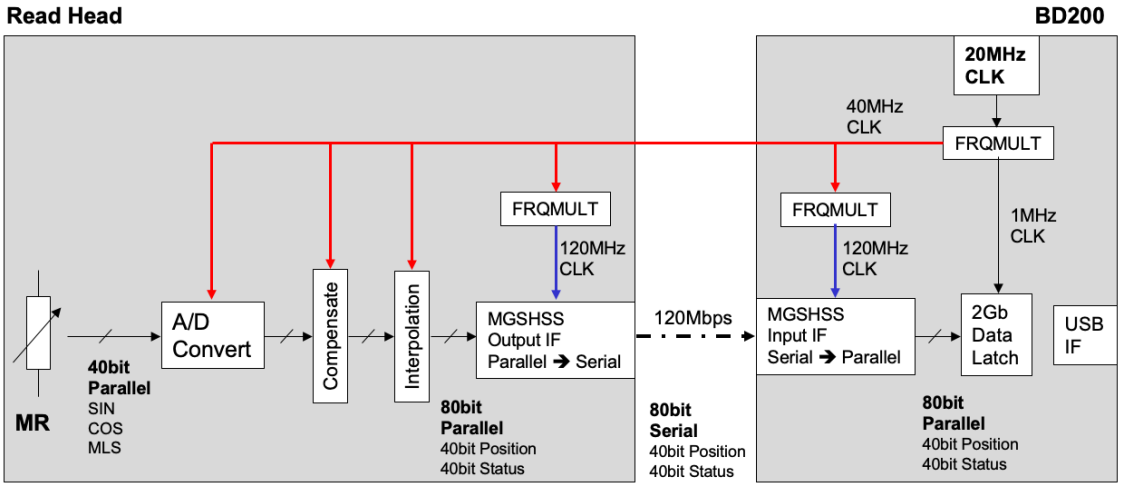

Figure 3.5: The block diagram of the data communication of the scale read head and BD200.

Data Acquisition Software for BD200

The position data collected by BD200 is exported to a PC for post-processing and further analysis. For data acquisition, a dedicated software GUI was also developed by Magnescale. The software enables a PC to communicate with BD200 via a USB Type-A connection. Figure 3.6 shows the screenshot of the GUI. The six waves in ① labeled AXIS1 through AXIS6 are the real-time-series plots of position count data sent from the six read heads. The assignment of the six linear encoders for each AXIS is as shown on the left side of the figure. The eight-digit numbers in ② is the instantaneous position count at the moment. The delta followed by eight-digit numbers in ③ are the peak-valley differences of the position counts in the window.

The user of the software can control the data sampling rate from 100Hz up to 20kHz by choosing one from the pull-down list in ④. Then, press ⑤"Select File" button to select a directory where the captured data will be saved. The start and stop of data sampling are done by clicking the ⑥"Rec" and ⑦"Stop" button on the screen. ⑧"Reset" button refreshes the GUI.

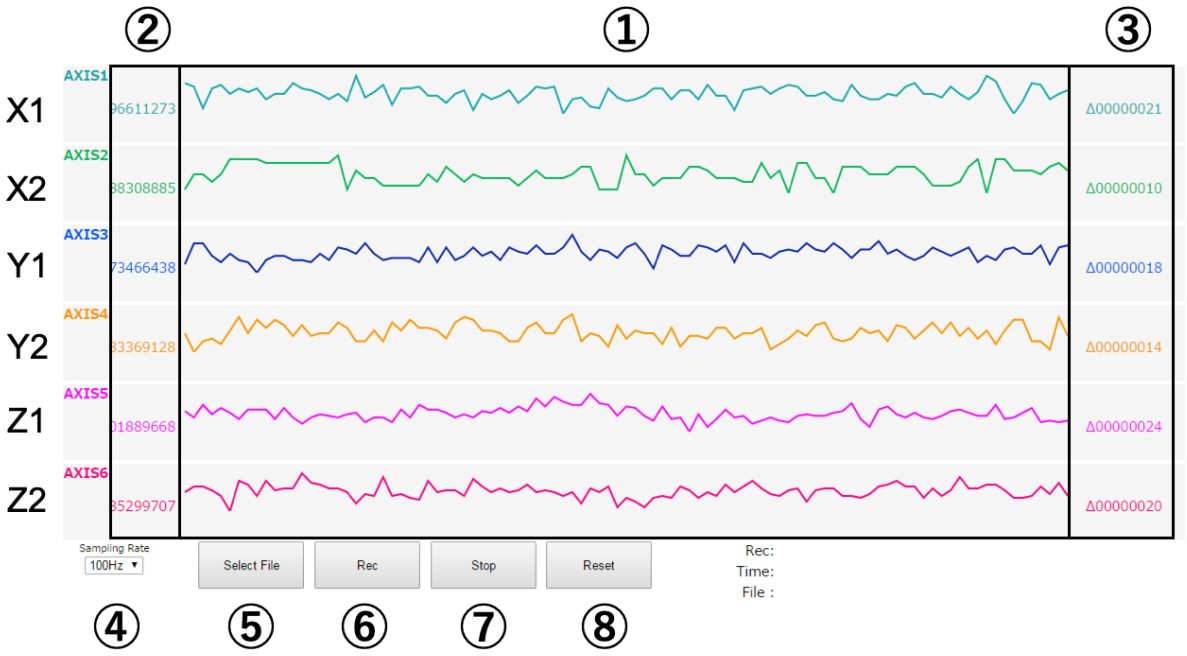

Figure 3.6: Data acquisition GUI software for BD200.

3.2 Requirement of Assembly Accuracy of the Hardware

Six linear encoders were installed on the machine tool to build the test machine. Here, additional error sources should be taken into consideration due to the difference between the conceptual design and the physical prototype.

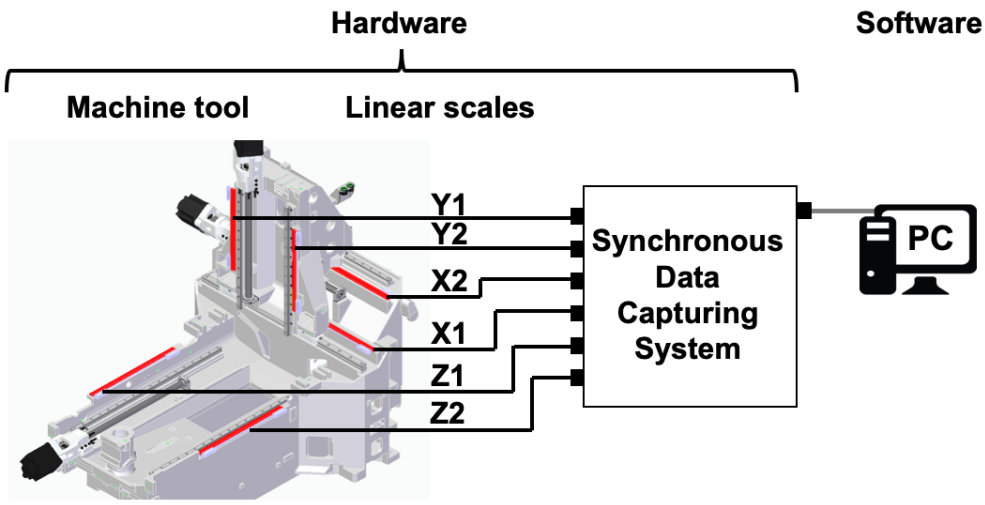

Figure 3.7: The constitution of the dual linear encoder system.

3.2.1 Parallelism of dual linear encoders

In the design of the measurement principle, the dual linear encoders are assumed to be perfectly parallel. However, it is virtually impossible to align the two scales with such perfect accuracy on a machine. Therefore, the dual linear scales are assumed to have a certain amount of parallelism error, as illustrated in Figure 3.8. The measurement error due to the imperfectness of the parallelism of the dual linear encoders should be taken into consideration. In order to evaluate the impact of the parallelism error on the measurement accuracy, the following calculation was performed.

As shown in Figure 3.9 (b), assume that the dual linear encoders are aligned with a parallelism error of δ. Assume that the table does not have any rotational or translational errors. Move the table by a distance of L. Ideally, the yaw angle error should be zero at any position over the stroke. However, in the actual case, the system has yaw measurement error due to the misalignment, and the value is:

$$\Delta E_{YAW} = \left(\frac{L}{\cos \delta} - L \right) / D \tag{3.5}$$

This equation indicates that the measurement error increases as the travel length L and the parallelism error δ become large. The maximum values of L for each axis are the same as the stroke of the axis listed in Table 3.1. Based on the drawing of the machine component, the parallelism error δ is assumed to be up to 0.61mm/m. According to equation (3.5), the yaw

measurement error due to the parallelism δ is calculated as up to 0.30, 0.14, and 0.11μm/m for the X, Y, and Z-axis, respectively. Based on the kinematic model, the resulting TCP error due to this error can be 0.20, 0.10, and 0.11μm for the X, Y, and Z-axis, respectively.

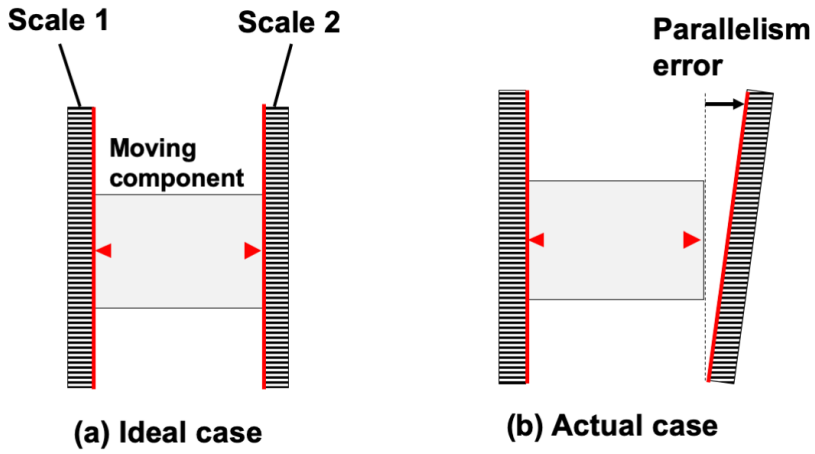

Figure 3.8: Yaw measurement error due to the parallelism error of the paired linear encoders.

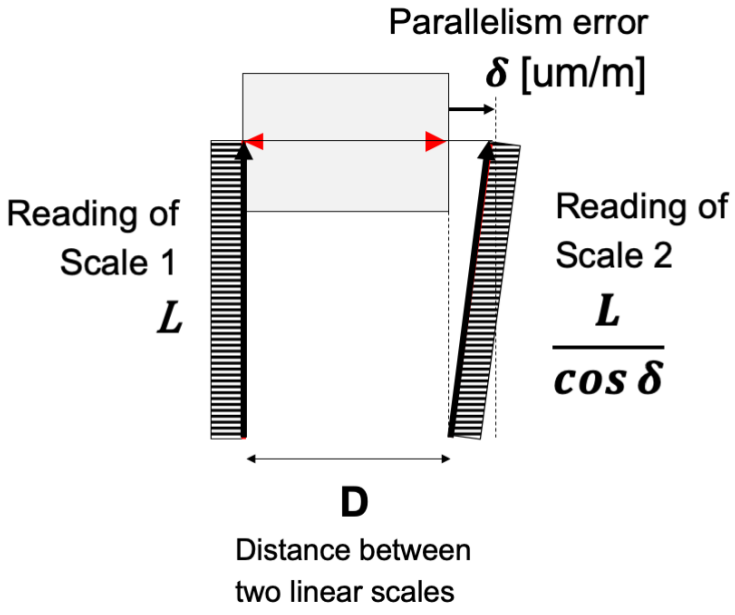

Figure 3.9: Relationship between the parallelism and the yaw measurement error.

3.2.2 Offset of zero reference position

Another point to be considered is where to set the zero point of the yaw angle. As illustrated in Figure 3.10 (a), ideally, the yaw should be zero when the moving component is perfectly perpendicular to the linear encoders. However, in reality, the moving component has a small amount of tilt and it is quite difficult to align it perfectly. Therefore, as shown in Figure 3.10 (b), the zero reference point has to be set at a point that has some initial deviation from the ideal zero reference point, and the yaw is measured as relative angular displacement from the reference point. The impact of this initial deviation on the measurement error needs to be taken into consideration.

The measurement error was evaluated as follows: As shown in Figure 3.11, assume that the reference point of the moving component is set at a position with an offset δ from the ideal zero position. This is the initial tilt of the component. Starting from the point, rotate the table with a small angle α. This is the yaw angular motion of the component, and let dx denote the change of the position reading of the scale 2. Then, the yaw angle calculated by the position reading is:

$$\begin{aligned} \frac{dx}{D} = \frac{D\sin(\delta+\alpha) - D\sin\delta}{D} &= \sin(\delta+\alpha) - \sin\delta && (3.6)\\ &\approx \delta + \alpha - \delta && (3.7)\\ &= \alpha && (3.8) \end{aligned}$$

Approximation in equation (3.7) can be made because the deviations δ and α are at most several tens of microradians, whereas D is several hundreds of millimeters. Therefore, the initial offset from the ideal orientation does not affect the measurement result.

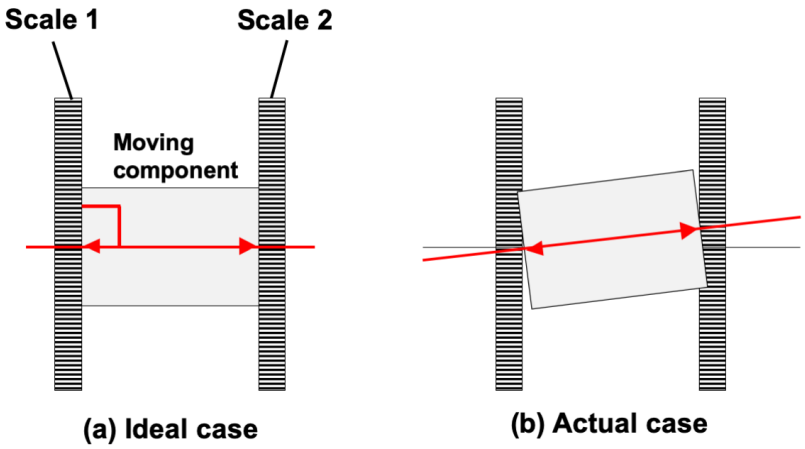

Figure 3.10: Measurement error due to zero position offset.

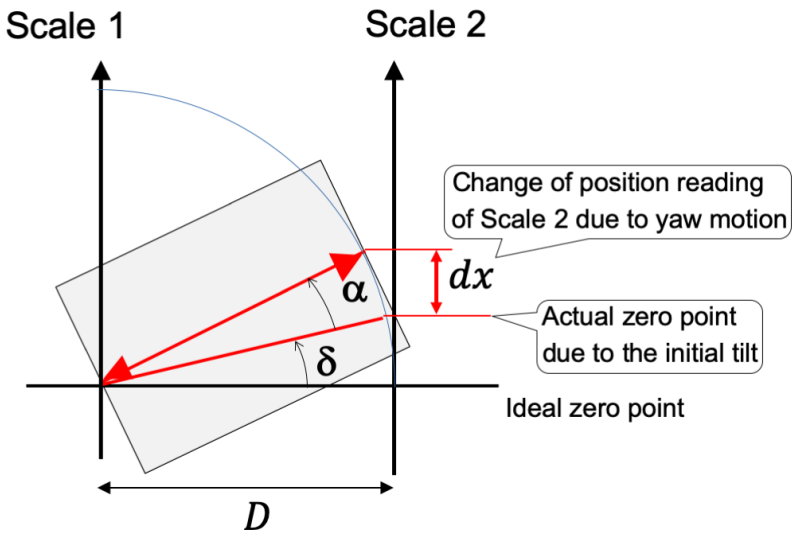

Figure 3.11: Determination of the angle α from the change of the position reading of scale 2, considering the zero position offset δ.

3.2.3 Thermal expansion of the linear encoders

The linear encoders on the machine tool are subject to heat and expand during the operating time of the machine. The expansion would affect the measurement accuracy of

the dual scale system. Therefore, the influence of the thermal expansion of the linear encoders should be carefully investigated. In this study, the impact of the thermal expansion of the linear scale is experimentally investigated. The result is explained later in section 3.3.3.

3.3 Experiments and Results

3.3.1 Proof of Concept: Evaluation of the Measurement Accuracy of the Scale System

At first, the proof of concept of this measurement system was done. The yaw error was measured by two different methods at the same time: a laser interferometer and the linear encoder system. The measurement of the scale system was validated by comparing it with the measurement of the laser interferometer, whose accuracy is assured by calibration. Figure 3.12 describes a conceptual image of the experiment.

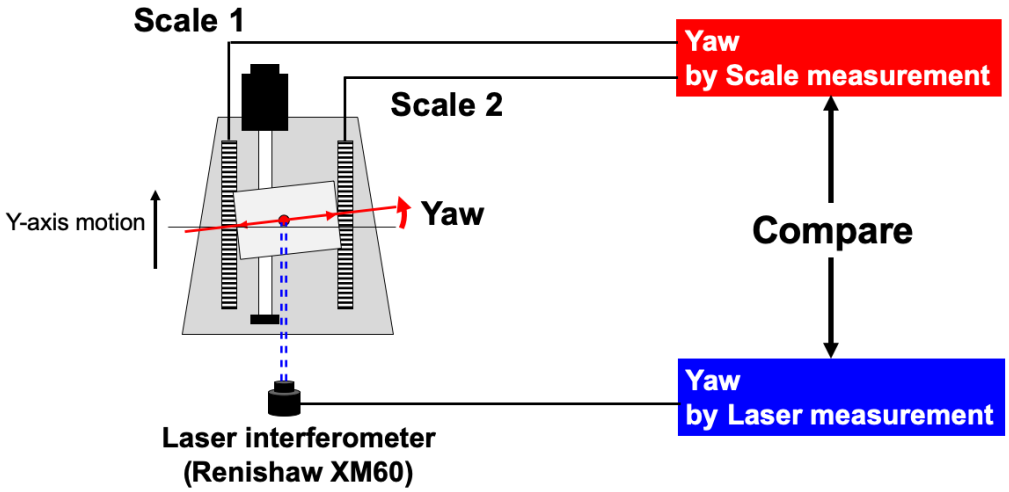

Figure 3.12: The idea of the verification measurement by a laser interferometer to prove the measurement concept of the dual linear encoder system.

3.3.1.1 Instrument for the verification measurement

For the verification measurement, XM60, a laser measurement system produced by Renishaw, is used. XM60 is capable of measuring the six DOF error elements at one time by using four parallel laser beams, as shown in Figure 3.13 [74]. The measurements are realized by a laser launcher that is mounted on the workpiece table and a reflector that is attached to the spindle. The detailed performance specifications are summarized in Table 3.3.

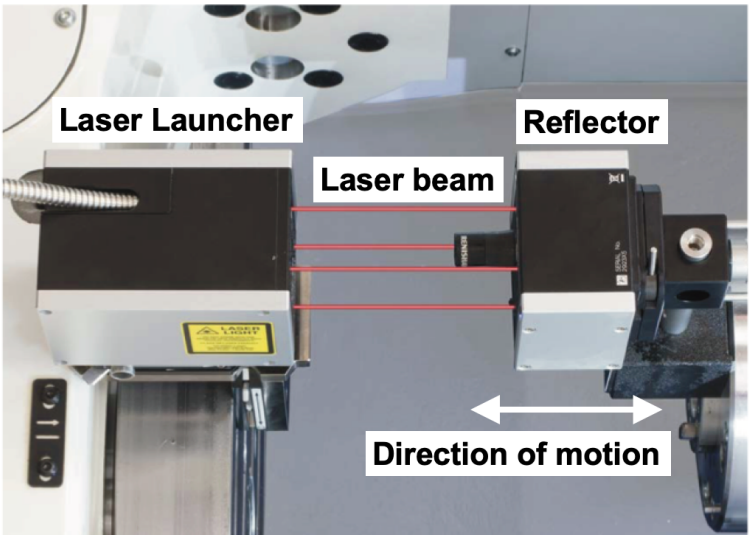

Figure 3.13: Multi axis calibrator XM60 by Renishaw [74].

Table 3.3: Performance specification of Renishaw XM60 [74].

Linear	
Accuracy	±0.5ppm (with environmental compensation)
Resolution	1 nm
Range	0 m to 4 m
Angular	
Accuracy	±0.006A ±(0.5μrad+0.1Mμrad) (A = displayed angular reading) (M = measured distance in meters)
Resolution	0.03μrad
Range	±500μrad
Straightness	
Accuracy	±0.01A ±2μm (A = displayed straightness reading)
Resolution	0.25μrad
Range	250μm radius
Roll	
Accuracy	±0.01A ±9.1μrad (A = displayed angular reading)
Resolution	0.5μrad
Range	±500μrad

3.3.1.2 Measurement procedure

The measurement setup on the test machine is shown in Figure 3.14. Figure 3.15 illustrates the measurement process. In this experiment, the Y-axis is measured. y_i denotes the Y-axis coordinate of the ith measurement position, where $i = 0, 1, 2, \cdots 11$ denotes the index of the measurement position. The 0th position is the start position $y_0 = -440$mm, and the measurement points are set at every 40mm to the 12th position $y_{11} = 0$mm. The process flows as follows:

1. At the 0th measurement point, all of the measurement values are set to zero as the zero reference (position readings of the linear scales y_{1i} and y_{2i}, the yaw measurement value of the laser interferometer XM60 E_{CYi}^{Laser} and the yaw measurement value of the linear scale system E_{CYi}^{Scale}). Every measurement value at the ith measurement position is obtained as the relative change from the 0th point.

2. At each position y_i, the position readings of the linear scales y_{1i} and y_{2i} are captured by BD200.

3. From the position readings, the yaw measurement value of the scale system E_{CYi}^{Scale} is calculated by using equation (2.13):

$$E_{CYi}^{Scale} = \frac{y_{2i} - y_{1i}}{D} \tag{3.9}$$

   At the same moment, the laser interferometer also measures the yaw and record it as E_{CYi}^{Laser}.

4. E_{CYi}^{Scale} is compared with E_{CYi}^{Laser} to verify the measurement accuracy of the scale system.

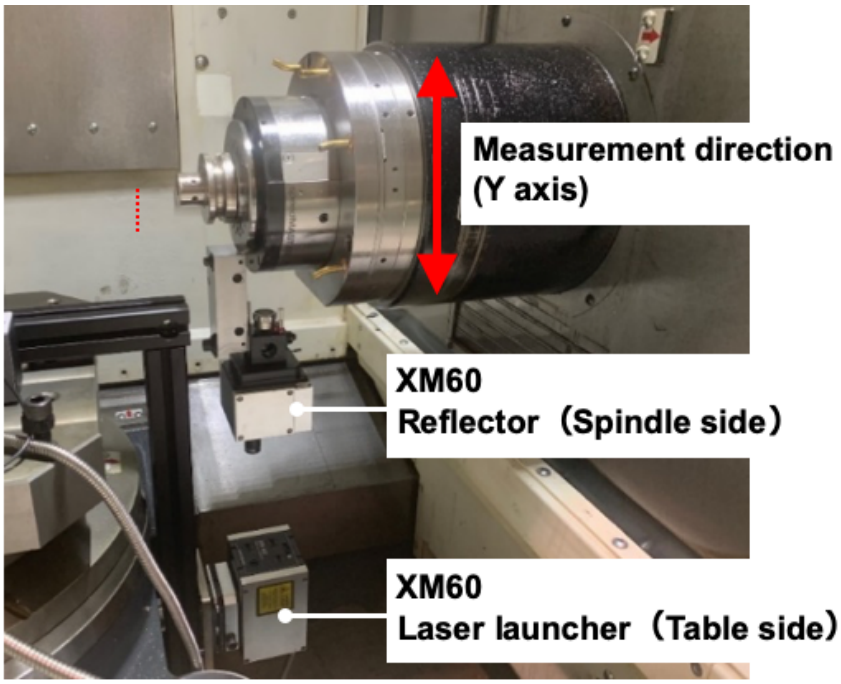

Figure 3.14: The measurement setup.

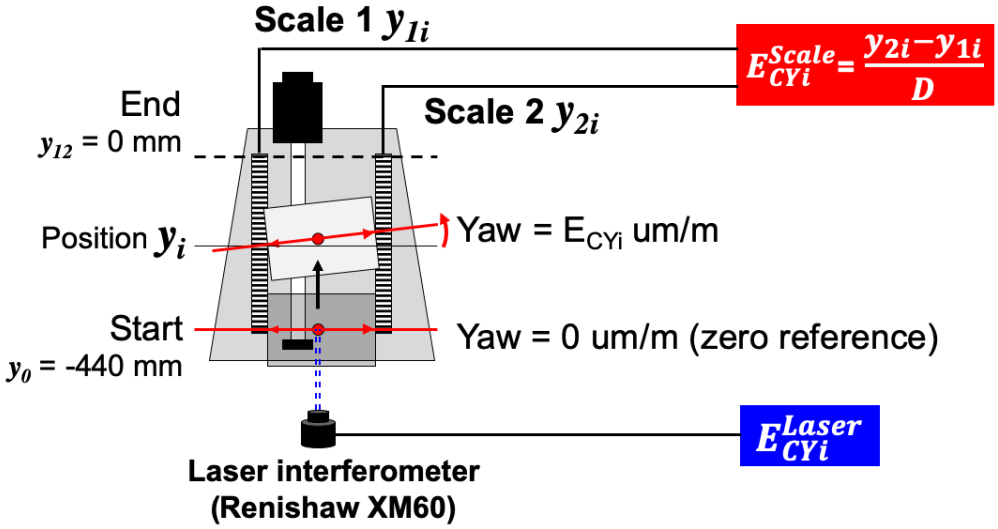

Figure 3.15: The measurement procedure.

3.3.1.3 Result and discussion

Figure 3.16 shows the comparison of the yaw measurement result. In the figure, the horizontal axis is Y coordinate y_i of measurement position, and the vertical axis is the yaw angle E_{CY} of the Y-axis component. The measurement value of the linear encoder system (E_{CYi}^{Scale}) is plotted in red, and the result of the XM60 (E_{CYi}^{Laser}) is plotted in blue. The scale measurement result shows a behavior similar to that of the laser measurement. This agreement implies that the scale system has a comparable measurement performance to the laser interferometer. The measurement accuracy was further investigated in detail as following.

The red shaded zone indicates the uncertainty of the linear encoder system ($2u$) was estimated as follows. As discussed in section 3.2, there are broadly four contributors to the overall measurement uncertainty of the scale system, as summarized in Table 3.4: linear encoder accuracy, noise in the position signal, the parallelism of the paired scales, and timing misalignment of the data sampling. They may be included in the measurement result, but cannot be identified by this experiment. Therefore, they are treated as uncertainty in the measurement. The overall uncertainty is estimated by the Type B evaluation [86]:

$$u = \sqrt{\sigma_{encoder}^2 + \sigma_{noise}^2 + \sigma_{parallel}^2 + \sigma_{timing}^2} \tag{3.10}$$

In the case of the Y-axis, plug $D = 0.6$m into the equation, and the calculated combined standard uncertainty is indicated as the red shaded zone. As can be seen, the measurement of the scale system agreed with that of XM60 within the uncertainty boundary at 10 out of 11 measurement points. This result indicates that the scale system can measure the yaw error based on the measurement principle of the dual linear scale system.

Table 3.4: Uncertainty of the error sources.

Contributor	Symbol	Standard uncertainty	Sensitivity coeff.
Linear encoder accuracy	$2\sigma_{encoder}$	$(1.5+1.5L)$ μm	1/D
Signal noise	$2\sigma_{noise}$	0.08 μm	2/D
Parallelism of the paired scales	$2\sigma_{parallel}$	$\frac{L}{\cos 0.61\times10^{-3}} - L$ μm	1/D
Timing misalignment	$2\sigma_{timing}$	0.005 μm	1/D
Combined standard uncertainty	$2u$	$\frac{1.5+1.5L}{D}$ μm/m	–

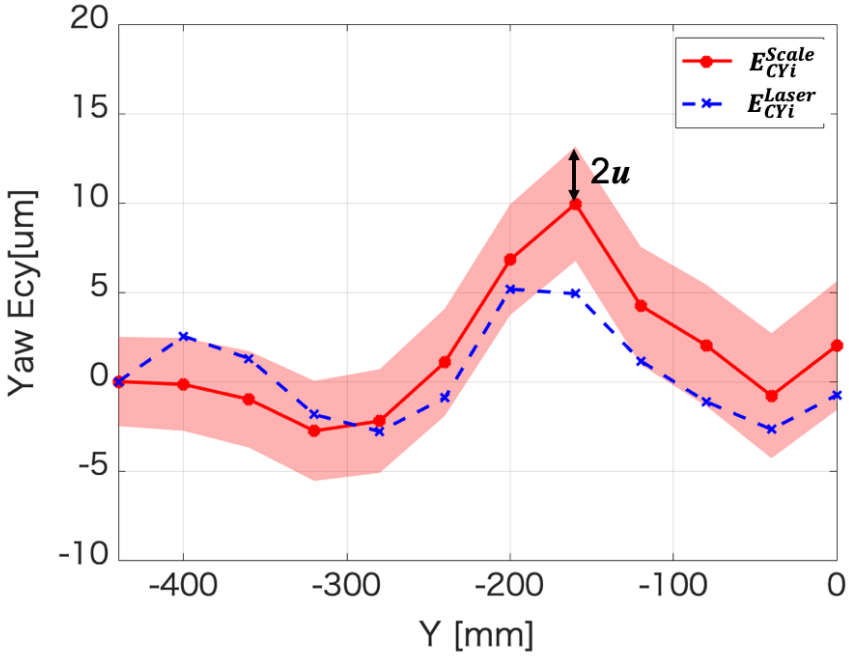

Figure 3.16: Comparison of the yaw measurement result. The red shaded zone indicates the uncertainty of the linear encoder system ($2u$).

3.3.2 Detection and Compensation of Accuracy Change

In the previous section, it is shown that the scale system can measure the yaw angular deviation of the machine component based on the proposed measurement principle. By plugging E_{CY}^{Scale} in the kinematic model of the machine (equation (2.14)), the TCP error $\boldsymbol{e}$ is determined. By periodically repeating the measurement of E_{CY}^{Scale}, the chronological change of the yaw accuracy ΔE_{CY}^{Scale} and its associated TCP error change $\Delta \boldsymbol{e}$ can be detected, as illustrated in Figure 3.17. The next test is to investigate the feasibility of the system for detection and compensation of the accuracy deterioration. In the test, a situation was assumed in which the machine accuracy deteriorated with age, and the detection and compensation for the deterioration were attempted by this system. The deterioration was replicated for the purpose of the experiment by intentionally distorting the linear guideways, as illustrated in Figure 3.18. By comparing the yaw before and after the deterioration, the deterioration of yaw can be determined, and its associated positioning accuracy deterioration at the TCP can be calculated by the kinematic model. The detected accuracy deterioration is compensated by modifying the machine motion.

The experiment assumed a situation that the machine accuracy degraded with age and tried to detect and compensate for the degradation to realize the compensation procedure

explained in section 2.1. The degradation was replicated for the experimental purpose by intentionally distorting the linear guideways. By measuring the yaw change ΔE_{CY}^{Scale}, the positioning accuracy change at the TCP Δe_y can be calculated by the kinematic model. Then, the accuracy change Δe_y is compensated. One of the most straightforward compensation schemes is to change the position command: i.e., if the positioning accuracy change Δe_{yi} was observed at a position y_i, the accuracy change can be canceled out by modifying the position command from y_i to $y_{MODi} = y_i - \Delta e_{yi}$, as shown in Figure 3.17

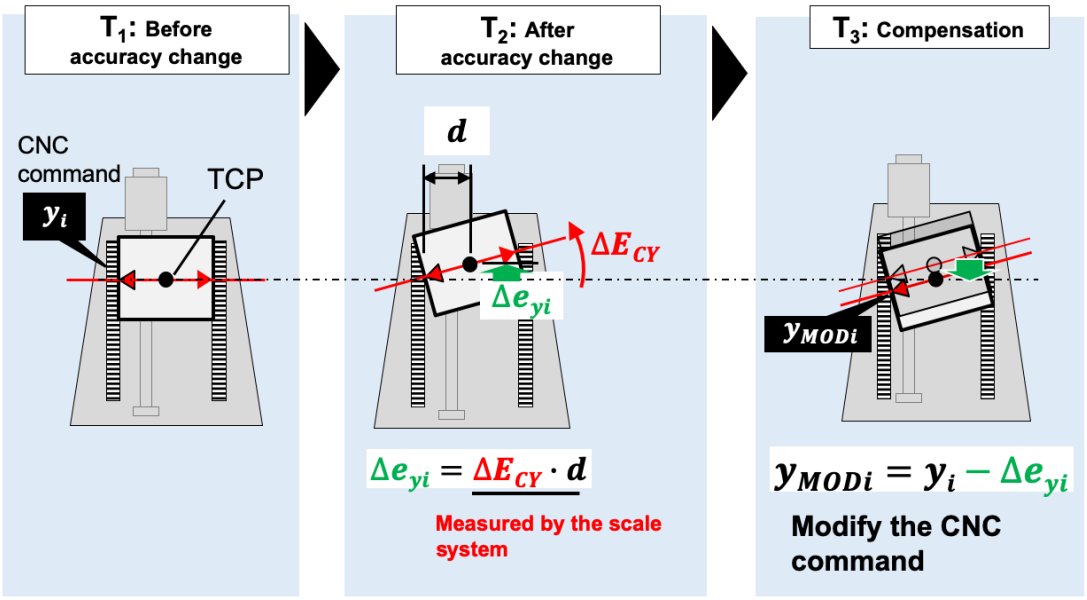

Figure 3.17: The conceptual image of the detection and compensation of the accuracy change.

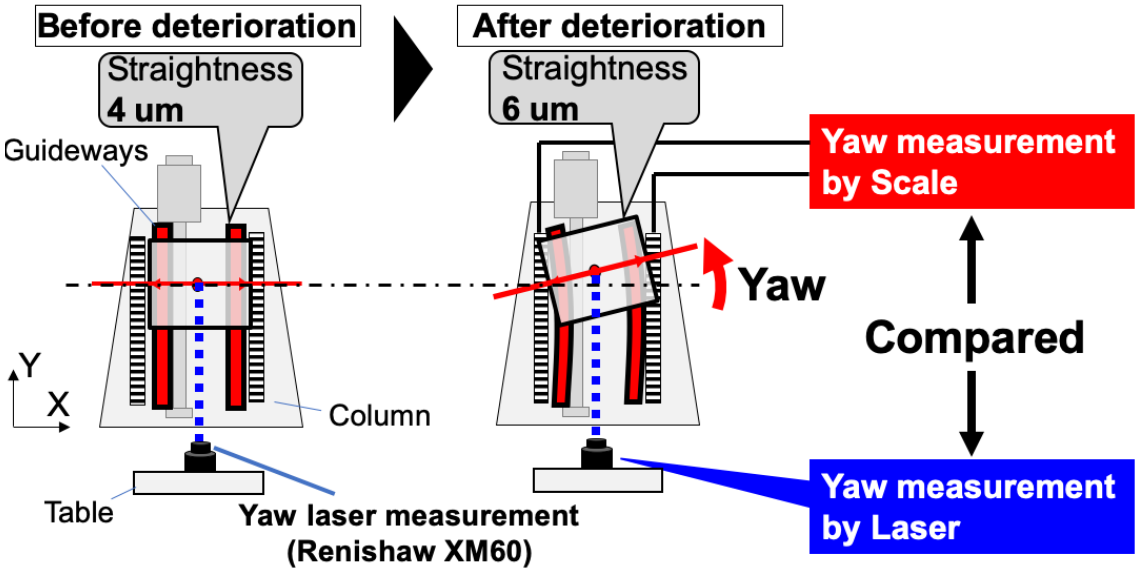

Figure 3.18: The measurement setup: The guideways were intentionally distorted to replicate degradation.

3.3.2.1 Experimental procedure

Three measurement tests verify the effectiveness of the detection and compensation of the accuracy change. Let T1, T2, and T3 indicate the test before the deterioration, after the deterioration, and after the compensation, respectively. The experiments are carried out with the following procedure.

1. Test T1: Measurement before the deterioration
   At T1, the yaw and the positioning accuracy before the deterioration are measured by the linear scale system.

2. Test T2: Measurement after the deterioration
   After T1, the linear guideways are distorted, and the measurement test T2 of the yaw and the positioning accuracy is done. Let $\overline{E}_{CY}^{(T1)}$ and $\overline{E}_{CY}^{(T2)}$ denote the yaw value measured at T1 and T2, respectively. Then, the accuracy deterioration $\Delta\overline{E}_{CY}$ is calculated as:
   $$\Delta\overline{E}_{CY} = \overline{E}_{CY}^{(T2)} - \overline{E}_{CY}^{(T1)} \tag{3.11}$$

Then, using the kinematic model, the TCP accuracy is calculated as:

$$\boldsymbol{e}^{(T)} = \mathbf{H}_Y \cdot \boldsymbol{t} - \boldsymbol{w} \tag{3.12}$$

$$\begin{bmatrix} 0 \\ e_y \\ 0 \\ 0 \end{bmatrix} = \begin{bmatrix} 1 & \overline{E}_{CY}^{(T)} & 0 & 0 \\ \overline{E}_{CY}^{(T1)} & 1 & 0 & y \\ 0 & 0 & 1 & 0 \\ 0 & 0 & 0 & 1 \end{bmatrix} \cdot \begin{bmatrix} d \\ 0 \\ 0 \\ 1 \end{bmatrix} - \begin{bmatrix} d \\ y \\ 0 \\ 0 \end{bmatrix} \tag{3.13}$$

$$= \begin{bmatrix} 0 \\ \overline{E}_{CY}^{(T1)} \cdot d \\ 0 \\ 0 \end{bmatrix} \tag{3.14}$$

This equation is derived by replacing all error elements except for $\overline{E}_{CY}$ with 0 in equation (2.12) since only Y-axis motion was considered in this experiment. Then, the TCP accuracy deterioration Δe can be determined as:

$$\Delta \boldsymbol{e} = \boldsymbol{e}^{(T2)} - \boldsymbol{e}^{(T1)} \tag{3.15}$$

$$\begin{bmatrix} 0 \\ \Delta e_y \\ 0 \\ 0 \end{bmatrix} = \begin{bmatrix} 0 \\ \overline{E}_{CY}^{(T2)} \cdot d \\ 0 \\ 0 \end{bmatrix} - \begin{bmatrix} 0 \\ \overline{E}_{CY}^{(T1)} \cdot d \\ 0 \\ 0 \end{bmatrix} = \begin{bmatrix} 0 \\ \Delta \overline{E}_{CY} \cdot d \\ 0 \\ 0 \end{bmatrix} \tag{3.16}$$

In order to compensate for the deterioration Δe_y, one of the most straightforward compensation schemes is used. The scheme is to subtract Δe_y from the initial CNC command and generate the modified command $y_{MOD} = y - \Delta e_y$, as shown in Figure 3.17.

3. Test T3: measurement after compensation
   After the compensation, the measurement T3 of the yaw and the positioning accuracy is done. If the compensation is successful, the accuracy deterioration is canceled out, and the positioning accuracy of T3 should be the same as T1.

The test setting is the same as shown in Figure 3.14. The verification measurement by XM60 was done in the three tests. In addition to the yaw change $\Delta \overline{E}_{CY}$, the TCP positioning accuracy change Δy was also measured to verify the effectiveness of the compensation. As XM60 can measure the two error elements at the same time, the measurement data are used.

3.3.2.2 Result

Figure 3.19 shows the measurement result. The graph shows the relative change in yaw induced by the distortion of the guideways for the yaw before the distortion. As can be seen, the scale measurement values E_{CY}^{Scale} well agree with E_{CY}^{Laser} in both of the measurements before and after the accuracy change. This agreement indicates that the scale system can detect the change of yaw with comparable accuracy to the laser measurement. When focusing on the relative change of the yaw $\Delta E_{CY}^{Scale} = \Delta E_{CY}^{(T2)\_Scale} - \Delta E_{CY}^{(T1)\_Scale}$, it exceeds the tolerance ΔE_{CY_TOL} at the measurement positions between $y = -160$mm and $y = 0$mm. Therefore, this system judged that the machine's yaw repeatability had been lost, and compensation was required.

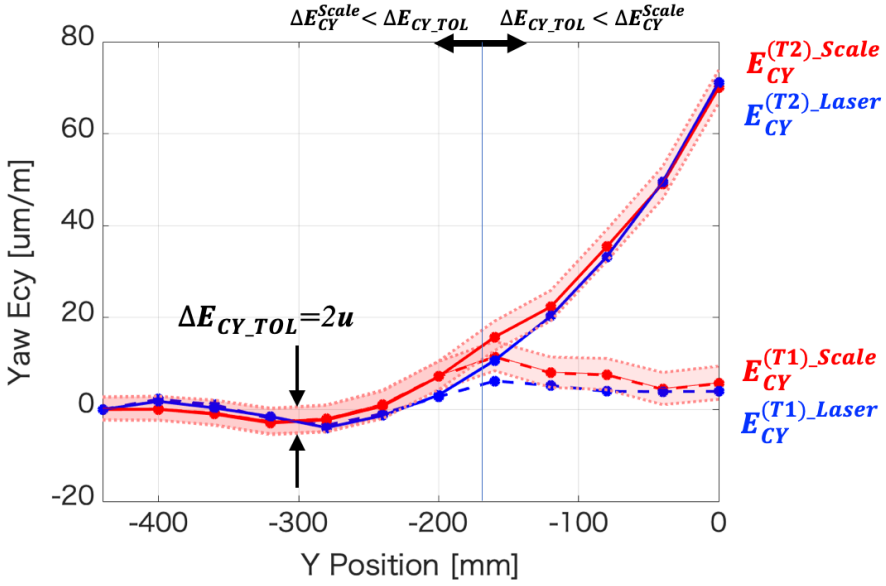

Figure 3.19: The measurement result

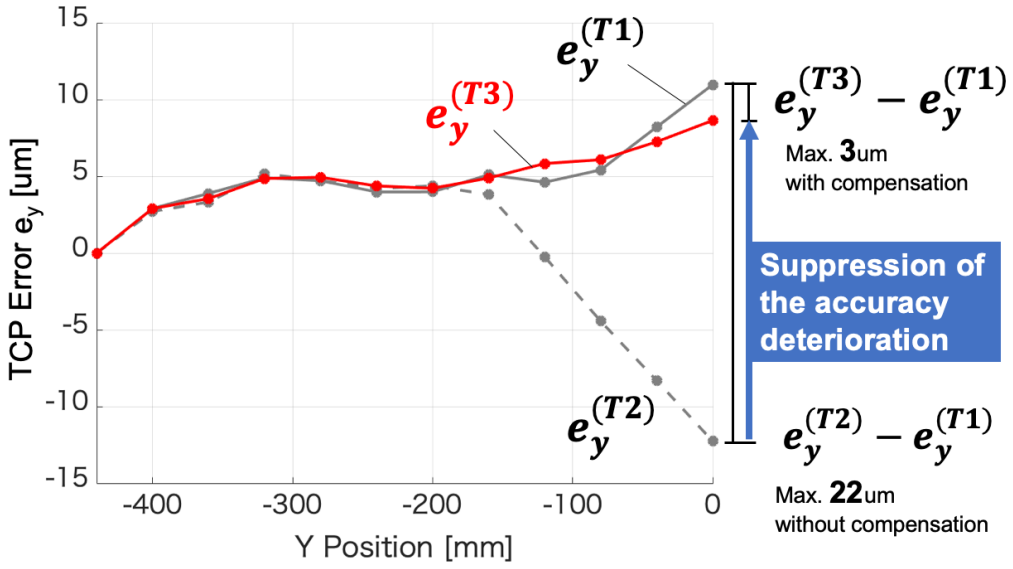

Figure 3.20: The TCP accuracy measurement after compensating the accuracy change.

Figure 3.20 shows the positioning accuracy e_y measured at each test. The positioning accuracy before the accuracy deterioration $e_y^{(T1)}$ is indicated with a solid grey line. The accuracy after deterioration without the compensation $e_y^{(T2)}$ is indicated with the grey dashed line. As can be seen, without compensation, the accuracy change $\Delta e_y = e_y^{(T2)} - e_y^{(T1)}$ was up to approximately 22μm. Since the system judged that accuracy compensation was needed at the previous step, the CNC position command was updated, and the measurement was performed again after the compensation. The accuracy with the compensation $e_y^{(T3)}$ is indicated with the solid red line. With the compensation, the TCP accuracy change $\Delta e_y = e_y^{(T3)} - e_y^{(T1)}$ was up to approximately 3μm. Therefore, the system compensated approximately 86% of the accuracy deterioration. This result shows that the linear-scale-based measurement and compensation scheme successfully suppressed the TCP accuracy deterioration.

3.3.3 Technological Issue: Thermal Influence on the Scale System and Countermeasure

As mentioned in section 3.2.3, the thermal expansion of the linear encoders is expected to have a significant impact on the measurement accuracy of the scale system. The impact can be estimated as follows.

Assume that the machine temperature is uniform at t. At the temperature, a yaw angular deviation E_{CY} was measured at a position y. Then, the machine warmed up, and the temperature of each linear encoder Y_1 and Y_2 rose by Δt_1 and Δt_2, respectively. Supposing

that the coefficient of thermal expansion of the linear encoders was C, the thermal expansion ΔL_1 and ΔL_2 of the linear encoders was calculated as $\Delta L_1 = C\Delta t_1$ and $\Delta L_2 = C\Delta t_2$, respectively. Therefore, linear encoder Y_2 relatively expands or shrinks with respect to linear encoder Y_1 by $\Delta L_2 - \Delta L_1$. If the yaw of the machine was measured again with this expanded scales, the measurement value differs as $\Delta E_{CY} = \frac{\Delta L_2 - \Delta L_1}{D}$ even if the machine's yaw accuracy did not change.

In order to use this system for the real-time measurement, the scale system should preserve its measurement accuracy during the machine is in operation. If the above estimation is correct, the measurement accuracy degradation can be calculated and suppressed by compensating for the thermal expansion of the linear encoders. The next experiment was carried out to evaluate the relationship between scale temperature and measurement accuracy. Based on the test result, thermal compensation was performed so that the scale measurement system can preserve its measurement accuracy even when the thermal expansion has occurred while the machine is in operation.

3.3.3.1 Experimental Setup

The measurement instruments and the errors to be measured are the same as the previous experiment. The measurement procedure is as follows. As in 3.3.1, the yaw of the Y-axis is measured by the scale measurement system and XM60 simultaneously. Then, the measurement values are compared. In this experiment, the measurement was performed at various temperature conditions. The change of measurement accuracy due to the temperature was calculated as explained above. Figure 3.21 is the schematic image of the experimental setup. Thermocouples are attached to the linear encoders at a constant interval of 110mm to measure the temperature of the linear encoders. At the beginning of the experiment, the machine was at a uniform temperature, and the first measurement was performed. Then, the machine's Y-axis was continuously moved back and forth for the full-stroke length. This running is done to replicate the machine's warm-up during operation. The running was paused every few hours, and the accuracy measurement was performed. After the measurement, the running was resumed. This cycle was repeated over and over again.

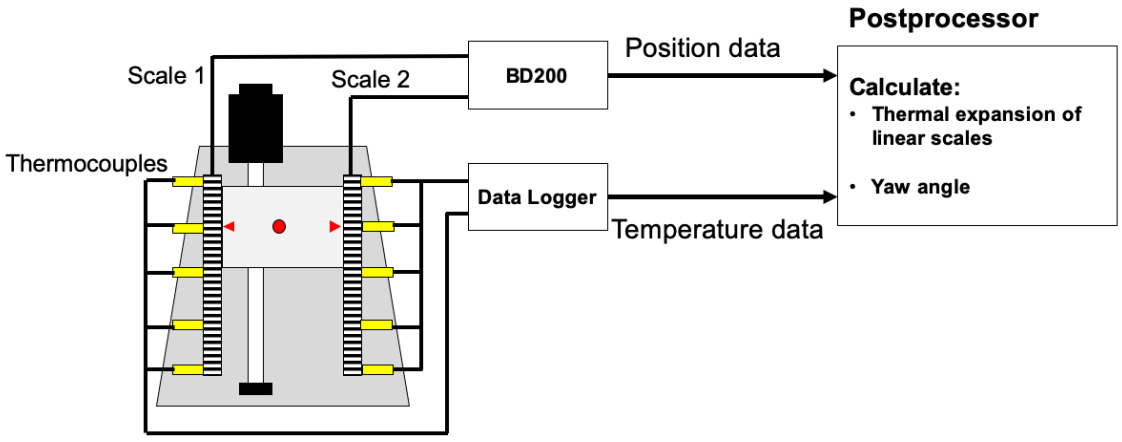

Figure 3.21: The measurement setup.

3.3.3.2 Result and Discussion

In Figure 3.22, measurement data of XM60 and the scale system are compared. The measurement of XM60 did not show a remarkable change after 20 hours of running. On the other hand, the measurement value of the scale system has changed. Since XM60 has built-in functionality to compensate for the environmental condition change automatically, the thermal influence on the measurement accuracy of XM60 can be assumed small. Therefore, it can be said that the yaw of the Y-axis did not change before and after the running. Therefore, the apparent change of the measurement result of this scale system could be induced by the change of the measurement accuracy of the system during the running.

As shown in Figure 3.23, the temperature data of the linear encoders measured with thermocouples indicates that the temperature of the linear encoder (Y1) was higher than the other (Y2). This unbalanced temperature change implies the unbalanced expansion of the linear encoders, leading to the change in measurement accuracy.

In order to verify the assumption, an analysis was performed based on the following principle. Let L be the length of the linear encoder measured at a temperature T. By comparing the length with another length data L_0 measured at temperature T_0, the amount of expansion ΔL can be derived. If thermal expansion is the cause of this expansion, the following equation is satisfied.

$$\Delta L = L - L_0 = CL_0(T - T_0) \tag{3.17}$$

The scale length was measured as follows: Move the Y-axis precisely by a distance L. The L is measured by the laser interferometer in the order of one micrometer. Meanwhile, calculate the travel distance of the read head from the reading value of the linear encoder.

Record it as $Y_{reading}$. Without thermal expansion, the position reading should be L. With the thermal expansion, the position reading does not agree with L but indicates a different value L_{read}. Then derive the deviation between the theoretical position reading and the actual reading $dL = L - L_{read}$. Although L is independent of the length of the linear encoder, L_{read} varies depending on the length. Thus, the amount of the expansion of the linear encoder can be derived. Figure 3.26 is a conceptual image of the analysis.

Based on the idea, the thermal expansion of scale Y1 and Y2 are derived, and the result is shown in Figure 3.25. Blue bars indicate the scale expansion measured by XM60. The authors also calculated the theoretical amount of thermal expansion of the linear encoders based on the temperature data. The result is shown in the same figure with red bars. On average, the two values agreed 74% for scale Y1 and 65% for scale Y2. This result indicates that the thermal expansion of the linear encoders actually occurred in the experiment and affected the measurement accuracy. The result indicates that by measuring the temperature of the linear encoders, the amount of thermal expansion can be estimated, and thus the degradation of measurement accuracy can be compensated.

By using the estimation result, the change in the yaw data of the scale system was compensated. As can be seen in Figure 3.27, the change in yaw angle error in the 20 hours was suppressed and showed similar behavior to that of the laser measurement. At the beginning of the test (0h), the difference between the measurement values of scale and XM60 was up to 3.9μm. This value became 11.7μm after 20 hours of running. After the application of the thermal compensation, the value was reduced from 11.7μm to 4.7μm. Therefore, measurement accuracy deterioration was suppressed by 90.3%. The elimination of the change indicates that the measurement performance of the dual scale system can be maintained even under the influence of heat.

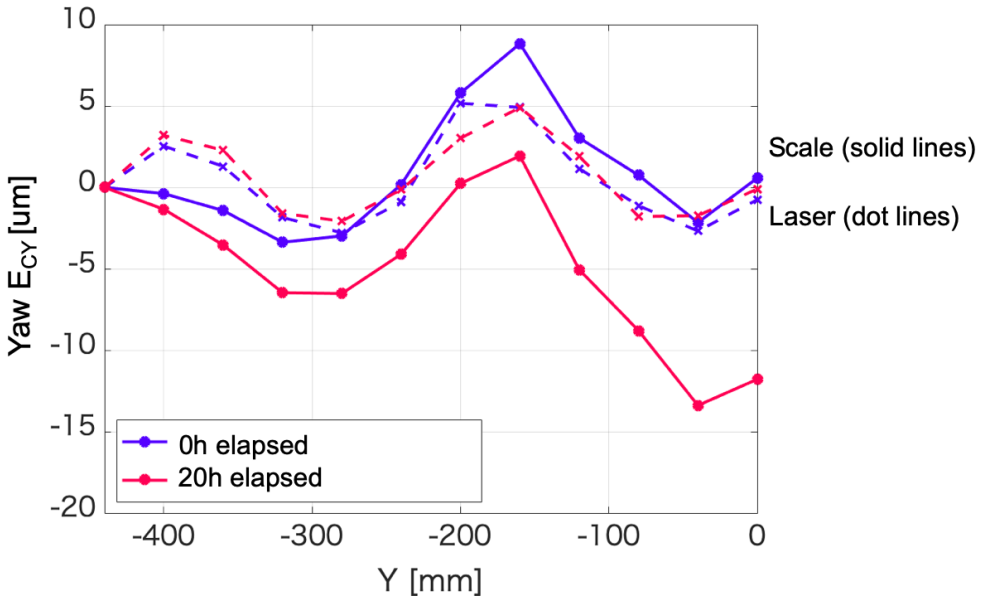

Figure 3.22: The comparison of the yaw measurement result.

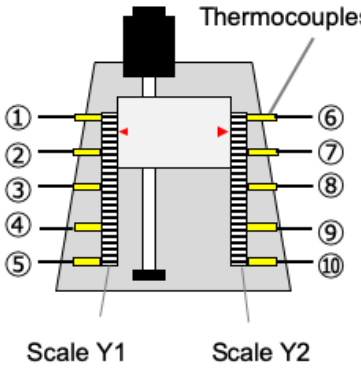

Scale Y1 Elapsed time [h]

	0	20	42	48	140	161	184	306	329	357	381
①	19.4	21.4	23.3	24.5	22.4	23.1	22.4	23.9	22.6	24.5	21.5
②	19.2	20.6	22.6	23.7	21.5	22.3	21.5	23.1	21.6	23.6	21.3
③	19.1	20.0	22.1	23.2	21.0	21.9	21.0	22.6	21.1	23.0	21.1
④	19.0	19.4	21.5	22.7	20.4	21.2	20.4	22.2	20.6	22.4	21.0
⑤	18.9	19.0	21.2	22.3	20.0	20.8	20.0	21.6	20.0	21.0	20.9

Scale Y2 Elapsed time [h]

	0	20	42	48	140	161	184	306	329	357	381
⑥	19.2	19.3	21.5	22.5	20.3	21.1	20.0	22.0	20.4	22.3	21.3
⑦	19.0	19.0	21.1	22.2	20.0	20.8	19.7	21.7	20.0	21.9	21.1
⑧	18.9	18.8	21.0	22.0	19.8	20.7	19.6	21.5	19.8	21.7	21.0
⑨	18.9	18.7	20.8	21.9	19.6	20.5	19.6	21.4	19.7	21.6	20.9
⑩	18.9	18.5	20.7	21.8	19.5	20.5	19.4	21.2	19.6	21.4	20.9

Figure 3.23: The temperature data of the linear encoders.

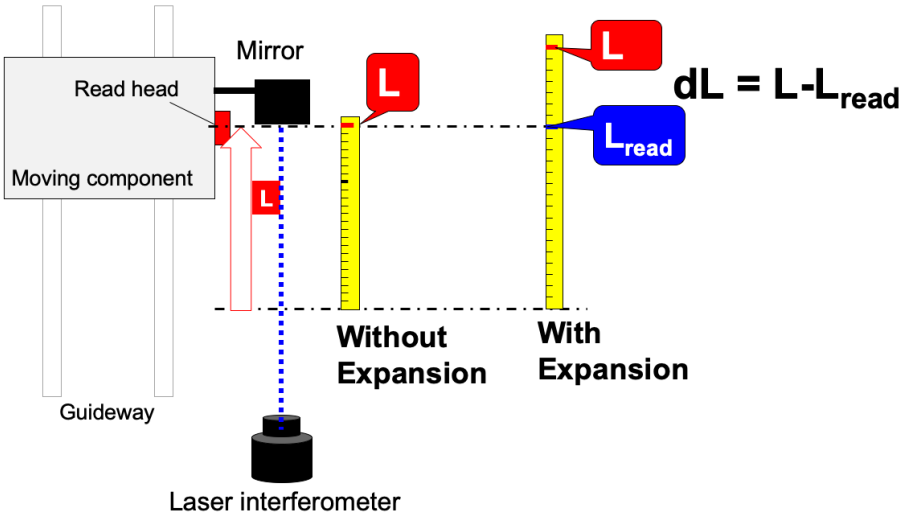

Figure 3.24: The measurement of thermal expansion (dL) of the linear scale by the laser interferometer.

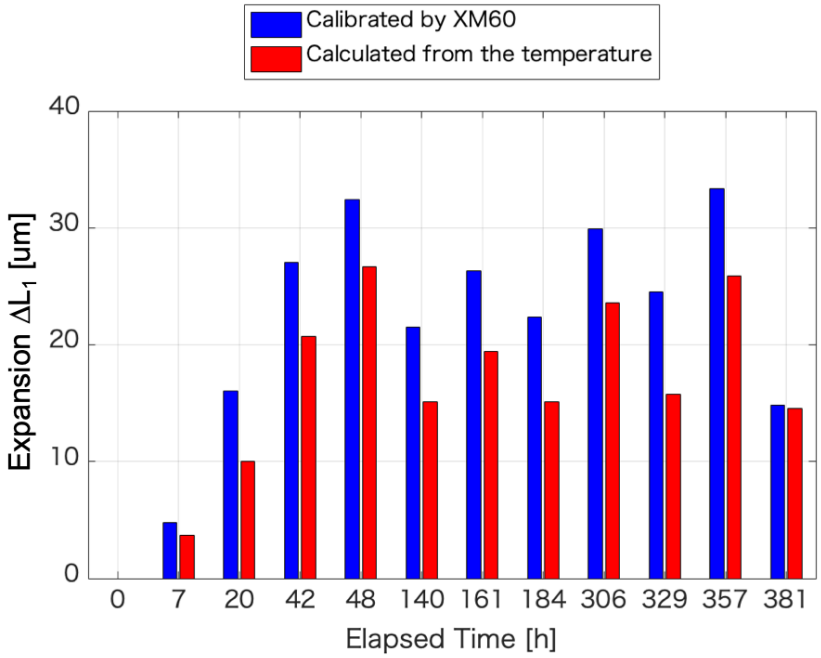

Figure 3.25: Thermal expansion of the linear encoder Y1.

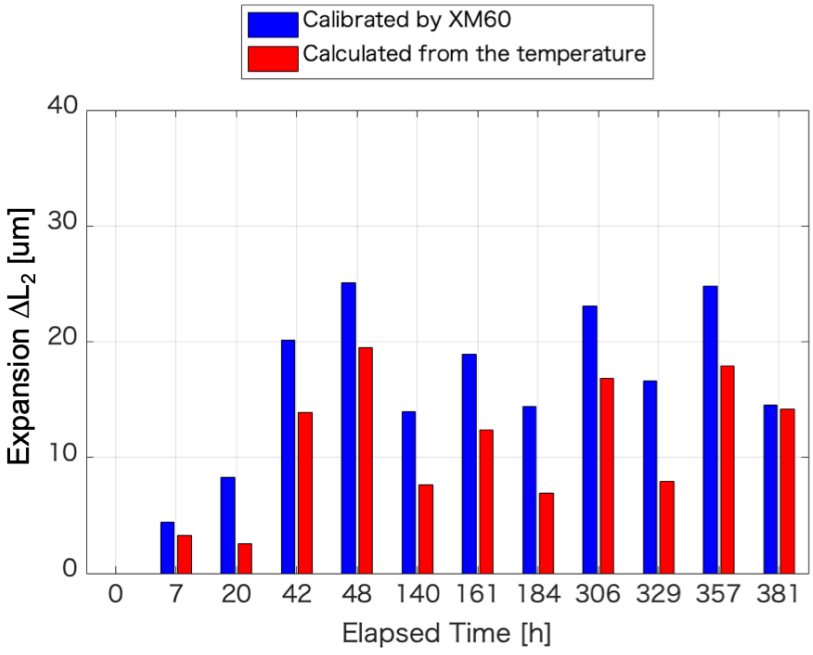

Figure 3.26: Thermal expansion of the linear encoder Y2.

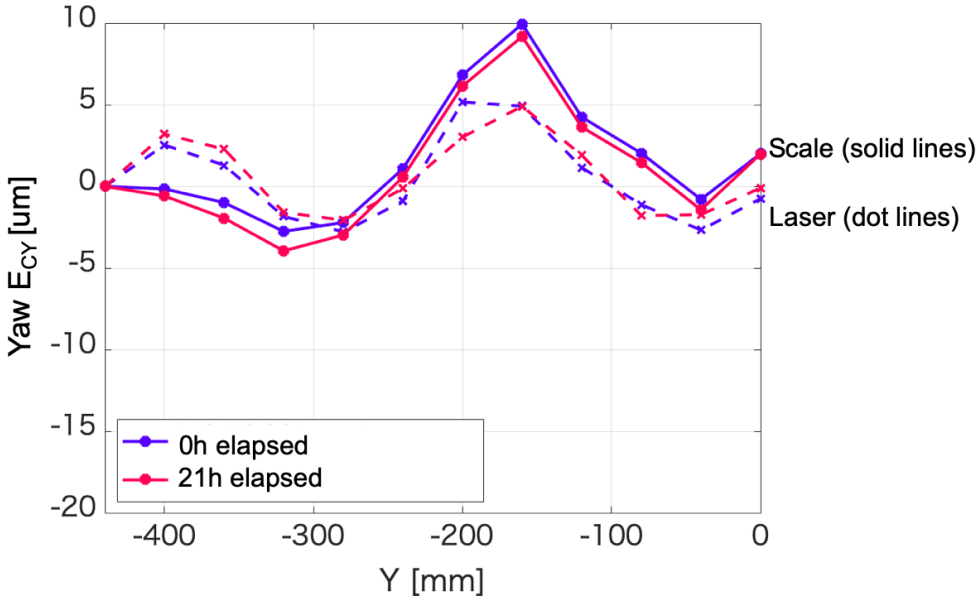

Figure 3.27: Yaw measurement result with the compensation of the thermal expansion of the linear encoders.

3.4 Summary

In this chapter, a physical prototype of the dual linear encoder system was constructed, and a series of experiments carried out to verify the effectiveness of the system was explained. Followings are the summary of this chapter.

- The physical prototype has been developed based on the design and preliminary analysis. In order to achieve sufficient time accuracy of the sampling of the position signal, a synchronous data capturing device was specifically designed.
- The basic measurement performance of the dual linear scale system was studied. The measurement of the yaw of the Y-axis component was performed by the dual scale system and a laser interferometer at the same time. The reliability of the measurement of the scale system was evaluated by comparing it with the laser measurement. The scale measurement agreed with the laser measurement within the uncertainty of $(1.5 + 1.5L)/D$, which has been estimated by the preliminary analysis.
- The TCP accuracy change detection and its compensation were conducted. Aging deterioration of yaw accuracy was replicated by intentionally distorting the linear guideways, and the scale measurement system was successfully able to detect the deterioration. The associated TCP accuracy deterioration was calculated by the kinematic model, and its compensation was attempted. The compensation was able to suppress 86% of the accuracy deterioration.
- The measurement test was conducted under time-variant temperature conditions to evaluate the thermal impact on the measurement accuracy. It has been found that the thermal expansion of linear scales had a significant impact on the measurement result of the scale system. In order to overcome this issue, thermal compensation of the measurement value was proposed, and that successfully suppressed 90.3% of the thermal impact.

Chapter 4

Outlook and Future Work of This Study

The final goal of this system is the full automation of the detection and compensation of the accuracy deterioration of the machine tool without interruption in the cutting process. There are two technological challenges to realize the goal:

- TCP accuracy measurement without interruption in the cutting process.
- Real-time measurement during a cutting process.

This study specifically focused on the first challenge, and the dual linear encoder system was proposed. As the start point, the feasibility of the dual linear encoder system was investigated for the measurement of the yaw error of the machine components. However, in order to determine the TCP error accurately with the kinematic model, all of the six DOF error elements of the linear axis need to be measured. In this section, as a future perspective, the principle of the six DOF measurement with the dual linear scale is explained, and related research is introduced.

4.1 Expansion of the Degrees of Freedom of the Measurement

4.1.1 Measurement of the pitch and roll angle

In this section, the idea to measure the pitch and roll errors is explained. Figure 4.1 illustrates an example of the dual linear encoder system that can measure all of the three rotational error elements. Two linear scales labeled as X1 and X2 are installed on both sides of the moving component, and three read heads labeled as 1, 2, and 3 are fixed to the component. If the linear encoder system could measure the gap between the linear scale

and the read head, as indicated by Z_1, Z_2, and Z_3 in Figure 4.1, the angular error can be calculated from the relative difference between the two gaps. Fujimori et al. [75] indicates that a property of the magnetic field recorded on a media can be used to measure the gap between the read head and the scale.

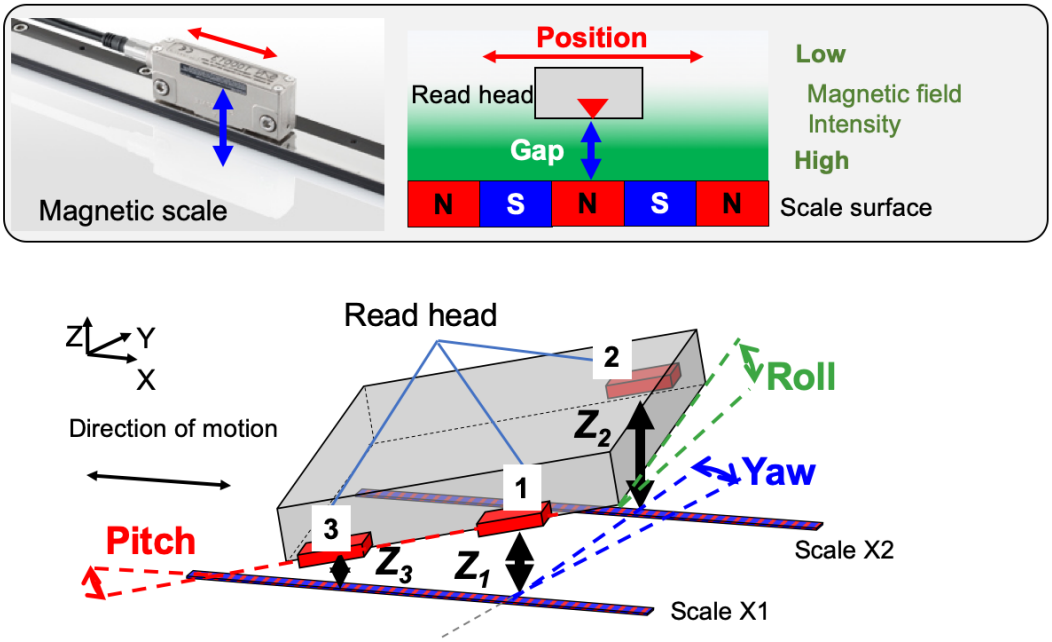

Figure 4.1: Pitch and roll measurement by multiple linear scale system.

In the vicinity of a surface of a magnetized media, the intensity of the magnetic field at a position P in Figure 4.2 is expressed with the following equations [87]. In the equations, M_r is the residual magnetization at the point P, μ_0 is the space permeability, δ is the thickness of the magnetized layer, and λ is the recording wavelength.

$$H_x = -\frac{M_r}{2\mu_0} \sin\frac{2\pi x}{\lambda} \cdot e^{-2\pi z/\lambda}(e^{\pi\delta/\lambda} - e^{-\pi\delta/\lambda}) \tag{4.1}$$

$$H_z = -\frac{M_r}{2\mu_0} \cos\frac{2\pi x}{\lambda} \cdot e^{-2\pi z/\lambda}(e^{\pi\delta/\lambda} - e^{-\pi\delta/\lambda}) \tag{4.2}$$

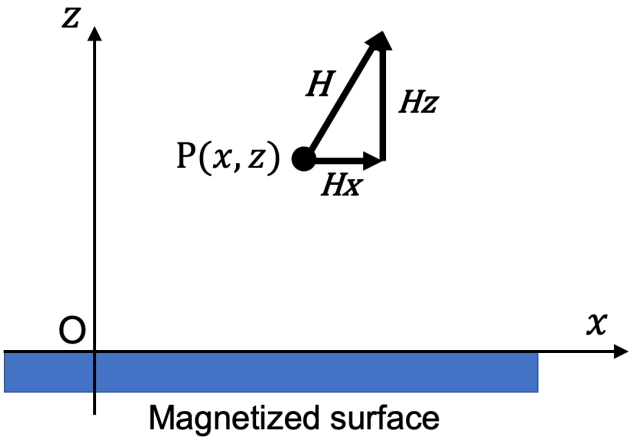

Figure 4.2: Magnetic field in the vicinity of a magnetized surface [87].

The H_z element is detected by the magnetoresistive sensor in a read head. Notice that H_z is a function of not only x but also z. Therefore, the deviation of the gap z between the read head and the surface of the scale can be detected by comparing the H_z at the same position x. Based on the principle, for example, by arranging two linear scales and three read heads, as shown in Figure 4.1, pitch and roll measurement can be achieved. In the figure, the pitch can be measured from the relative difference between Z_1 and Z_3, and the roll can be measured from that between Z_1 and Z_2.

4.1.2 Measurement of the translational error elements

With the configuration explained above, all of the three rotational error elements (yaw, pitch, and roll) can be measured. The remaining three DOF errors are the errors in translational directions, and they are measured as follows. In Figure 4.1, the X-directional deviation is straightforward. It is directly determined from the reading position. The Z-directional deviation can be determined by measuring the gap, as explained in the previous section. Y-axis measurement is challenging since the magnetic field does not change in the direction. To overcome the issue, Fujimori et al. also proposed to arrange the magnetic field in a tilted way [75]. In Figure 4.3, they proposed a linear scale that has tick marks tilted by θ to the direction of motion X.

The measurement principle of the translational error elements is as following. Let Xh_i and Yh_i denote the X and Y directional displacement of the read head i, and Sh_i denote the associated signal value of the read head i. Then, the relationship among them can be

expressed as:

$$Sh_i = Xh_i \cos\theta + Yh_i \sin\theta \tag{4.3}$$

Assuming that the distances between read head 2 and 3, 4 and 5 are very small, following approximation can be done:

$$Xh_2 \approx Xh_3, \quad Yh_2 \approx Yh_3 \tag{4.4}$$

$$Xh_4 \approx Xh_5, \quad Yh_4 \approx Yh_5 \tag{4.5}$$

By plugging (4.4) and (4.5) into (4.3), the translational displacement of the read heads can be derived as:

$$Xh_2 \approx Xh_3 = \frac{Sh_2 + Sh_3}{2\cos\theta} \tag{4.6}$$

$$Yh_2 \approx Yh_3 = \frac{Sh_2 - Sh_3}{2\sin\theta} \tag{4.7}$$

$$Xh_4 \approx Xh_5 = \frac{Sh_4 + Sh_5}{2\cos\theta} \tag{4.8}$$

$$Yh_4 \approx Yh_5 = \frac{Sh_4 - Sh_5}{2\sin\theta} \tag{4.9}$$

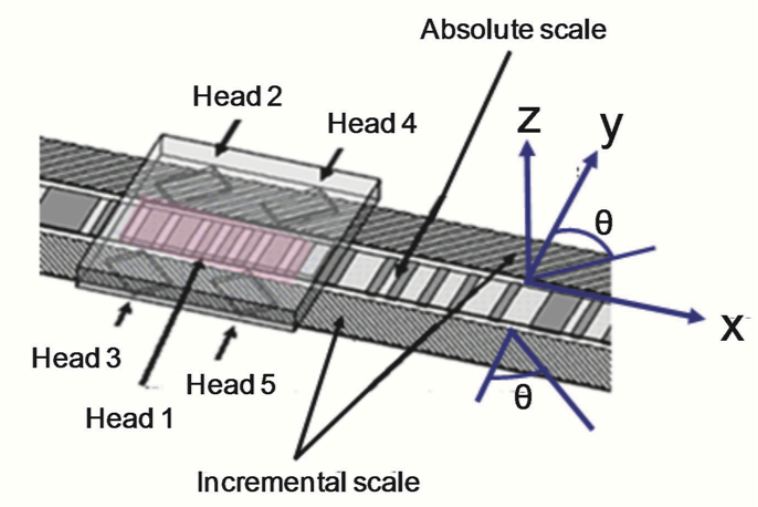

Figure 4.3: Tilting of the magnetization of tick mark for translational error detection (adapted from [75]).

By integrating the novel linear encoder technology to the dual encoder system, the measurement of the six DOF error elements is realizable in principle. Further study on the measurement accuracy of the gap and translational deviation needs be done to translate the six DOF measurement scale system into practical applications.

4.2 Real-time Measurement

With the conventional error measurement methods, the machine component needs to stand still at measurement positions to perform the measurement. The increase in the number of the measurement points elongates the measurement time. Therefore, the automatic measurement system should be able to measure the accuracy of the machine in a real-time manner during the cutting process. In this section, an approach is introduced to replace the static measurement with a dynamic one.

For example, assuming that the machine is cutting a workpiece, the yaw of the X-axis component was measured while the X-axis moved at a feed rate of 1000 mm/min. The data capturing device BD200 can capture the position data from the read heads continuously at a constant sampling rate while the machine is in motion. Figure 4.4 shows the measurement data. The data sampling rate was 100 Hz. Assuming that the machine cuts five workpieces in a row with the same geometry, the measurement was repeated five times, and all of the five measurement data are overlaid in one figure.

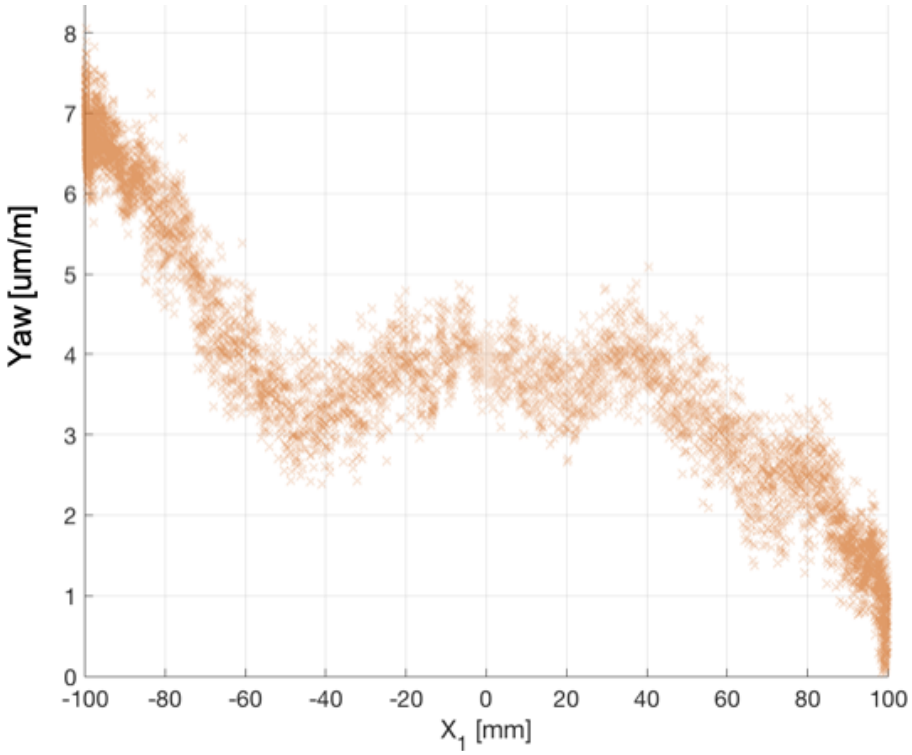

Figure 4.4: Yaw angle measured during a continuous motion of X axis.

4.2.1 Challenge in determining the systematic error element of the real-time measurement data

The plot indicates that the X-axis yaw had repeatability during the measurement. As explained in section 2.4 Based on the theory of machine tool error analysis, the random elements should be eliminated, and only the systematic elements should be extracted to measure the yaw accurately. In conventional quasi-static measurement, the systematic element is obtained by taking the arithmetic mean of iterative measurement performed at the same measurement position, as defined in equation 2.22. On the other hand, in the real-time measurement, the measurement data is obtained as scattered data points, as shown in Figure 4.4. In this case, no two data points are obtained precisely in the same position. So, the arithmetic mean cannot be used to determine the systematic element.

In order to overcome this problem and identify the systematic element from such scattered data points, the use of statistical analysis is discussed in this study. Curve fitting is one of the most commonly used methods for this type of analysis. In a typical curve fitting, it is assumed that the scattered data points are subject to a function, typically a polynomial, and the coefficients are determined by an optimization method such as the least square method. In the approach, the function needs to be defined beforehand. However, the shape of the scattered data differs depending on the machine type, axis to be measured, load on the axis, or friction of the guideways. Therefore, pre-defining a function applicable to any error data distribution would be very difficult. In order to solve the problem, an approach known as nonparametric regression has more flexibility. The advantage of this approach is that there is no need to pre-define the function (polynomial, trigonometric, exponential, etc.), which gives more flexibility of the shape of the curve. For example, Zhu et al. used a B-Spline model to extract the systematic error from a scattered machine tool error data [88]. In this study, another approach known as k-nearest neighbor (kNN) algorithm is used. kNN algorithm is one of the most straightforward nonparametric algorithms and thus it can be easily implemented with simple math. In the following section, the feasibility of the kNN algorithm to the extraction of the systematic error element is assessed.

4.2.2 k nearest neighbor algorithm for systematic error extraction from the real-time measurement data

The following example shows the systematic error extraction with kNN algorithm. Given a data set $\mathcal{D} = \{x_i, E_i\}(i = 1, ..., N)$,where x_i is the X axis position of the machine and E_i is its associated yaw error, assume that we would like to find the systematic error E_0 for a query point x_0. In the kNN algorithm, we look for k data points $x_r(r = 1, ..., k)$ closest in distance to x_0, and then calculate the arithmetic mean of the E_rs associated with the x_rs to obtain the estimation of E_0. In the example of Figure 4.5, the task is to estimate the value of E_0 for $x_0 = 2$. In this case, 1 nearest neighbor of $x_0 = 2$ is $x = 1.6$, 2 nearest neighbors are $x = 1.6$ and 1.0, 3 nearest neighbors are $x = 1.6, 1.0$, and 3.1, and 4 nearest neighbors

are $x = 1.6, 1.0, 3.1$, and 3.9. Then, the kNN estimation for each $k = 1, 2, 3$, and 4 are as indicated with the circles.

In this algorithm, the estimation result depends only on k, and k is the only parameter that determines the accuracy of the estimation. Therefore, an appropriate selection of the value of k is essential. In this study, a statistical method called cross-validation was done for the optimum selection of k.

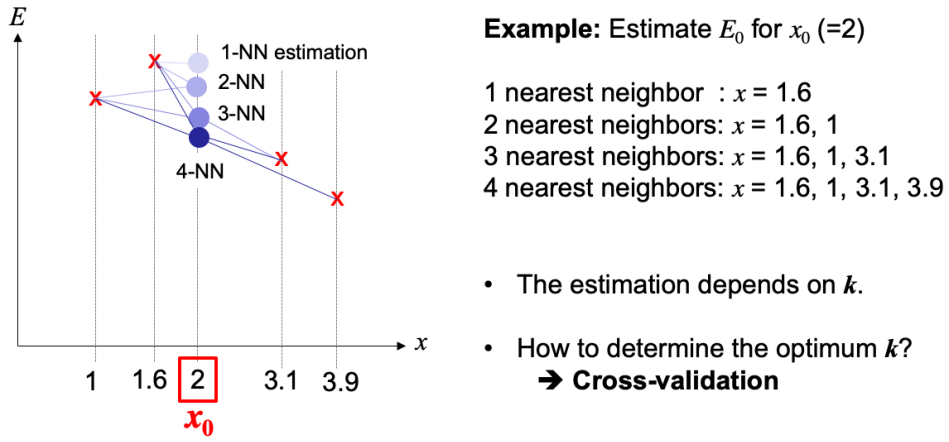

Figure 4.5: Example of the k nearest neighbor algorithm.

4.2.2.1 Cross validation to choose optimum value of k

Given a data set $\mathcal{D} = \{x_i, E_i\}(i = 1, ..., N)$, below is the flow of the cross-validation to determine the optimum value of k.

1. First, all of the data points $\mathcal{D} = \{x_i, E_i\}$ are shuffled and then randomly partitioned into K roughly equal-sized subsamples. For example, when $K = 5$, the scenario is as follows:

2. $K - 1$ (4) out of K (5) subsamples are used as training data and the other is used as validation data. Let $\mathcal{D}^t = \{x_i^t, E_i^t\}(i = 1, ..., m)$ and $\mathcal{D}^v = \{x_j^v, E_j^v\}(j = 1, ..., m)$ denote the training data and validation data, respectively. Here, m and n are the number of the data points contained in each data set, i.e. $m + n = N$.

3. Choose a value of k (the example in Figure 4.6 is $k = 2$). For each data point x_j^v in the validation data, find k nearest neighbors from the test data x_i^t.

4. Calculate the average of E_i^ts associated with the nearest neighbors x_i^t. Let $\overline{E}_j^v$ denotes the average:

$$\overline{E}_j^v = \frac{1}{k}\sum_{i=1}^{k} E_i^t \tag{4.10}$$

This is the kNN estimation value of the error associated with the target point x_j^v.

5. Compare the estimation value with the true value E_j^v for x_j^v. Compute the root-mean-squared error (RMSE) of the prediction value with respect to the true value E_j^v

$$RMSE(k) = \sqrt{\frac{1}{n}\sum_{j=1}^{n}(\overline{E}_j^v - E_j^v)^2} \tag{4.11}$$

6. Choose another subsample as test data and then repeat 3-5.

7. Repeat 3-6 for K times.

8. Take the average of the K $RMSE(k)$s.

$$\overline{RMSE}(k) = \sqrt{\frac{1}{n}\sum^{K} RMSE(k)} \tag{4.12}$$

This represents the accuracy of the prediction of the kNN estimation for k.

9. Increase the number of k as $k = k + 1$.

10. Repeat 2-9 until a stop value of k: $k = k_{lim}$ of your choice.

11. Among the $\overline{RMSE}(k)$, find the smallest value. The k which gives the smallest $\overline{RMSE}(k)$ is the optimum value of k.

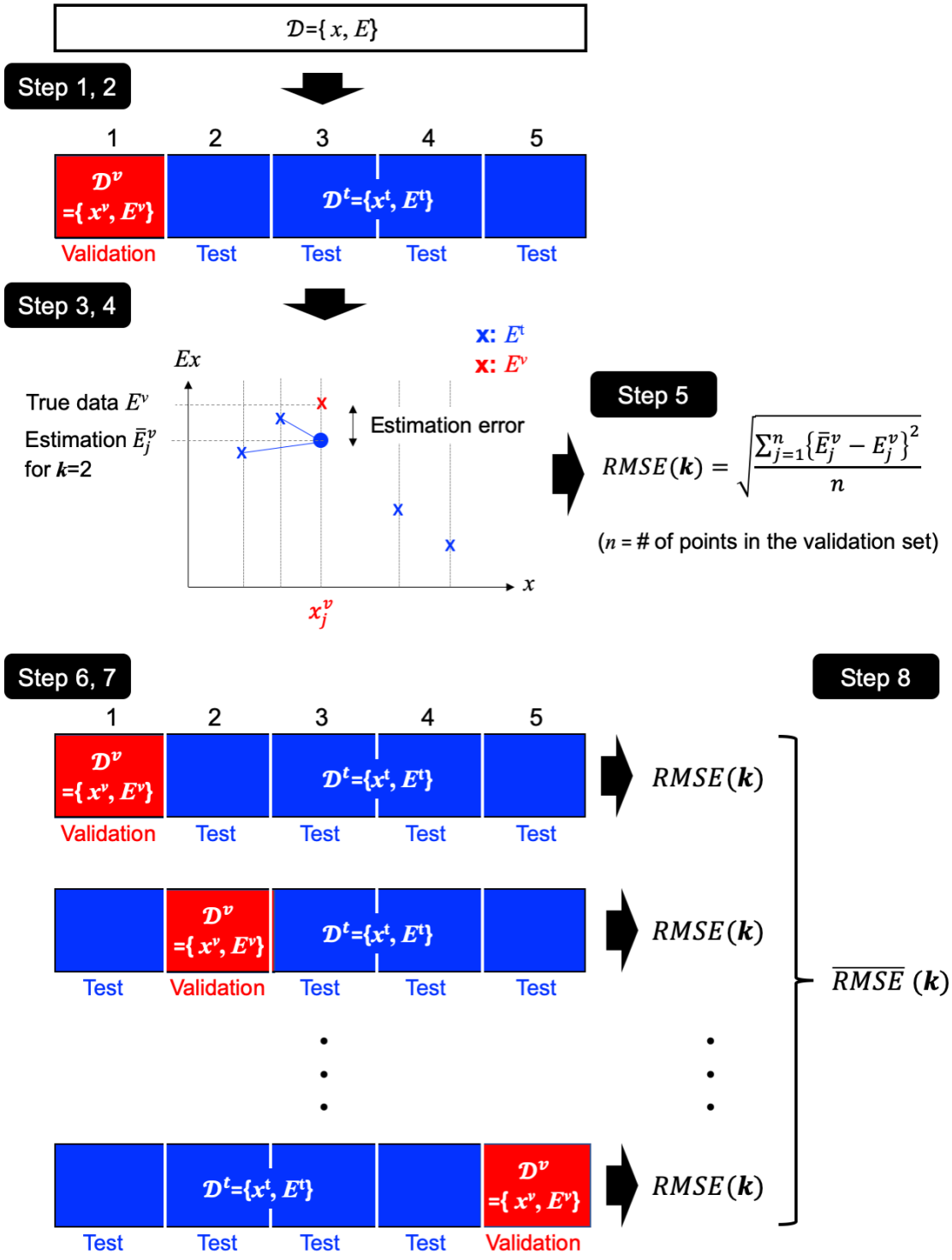

Figure 4.6: Cross-validation process.

4.2.2.2 Implementation of kNN algorithm for the error analysis

Figure 4.7 shows the cross-validation result for the measurement data. $k = 35$ was determined as the optimum value of k. Applying the kNN for the whole data $\mathcal{D}$, the systematic error was extracted from the noisy raw data points, as indicated with the blue points in Figure 4.8. The RMSE in the validation case was 0.3962μm/m. Next, the kNN regression was applied to another new data set and the resulting RMSE was 0.3907μm/m. Thus, the difference between the cross-validation and the new test was approximately 1.4%. Therefore, the kNN algorithm was able to extract the systematic element with sufficient accuracy.

Once the systematic error element is extracted for each six DOF errors, the TCP error can be derived by putting the systematic errors into the kinematic model. By repeating this process during the machine operation, the deterioration of the machine accuracy can be found, and the compensation value can be calculated, as explained in the previous chapter.

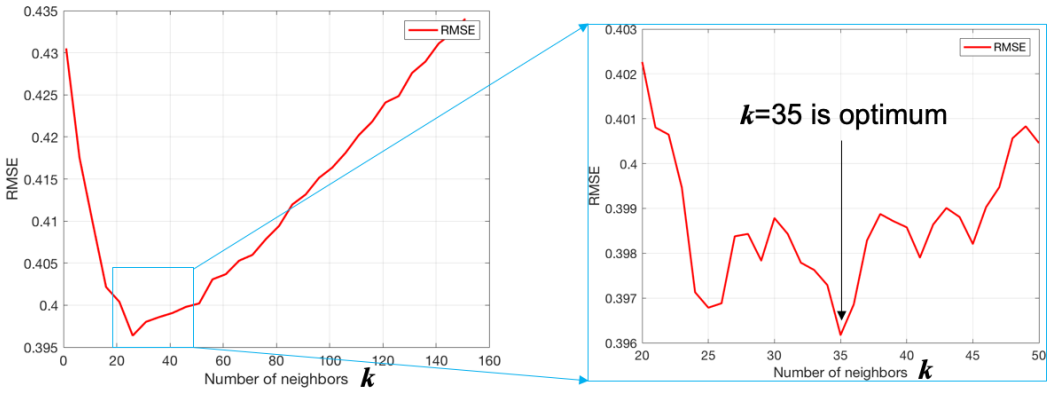

Figure 4.7: The implementation of the cross validation. The optimum k was determined as 35.

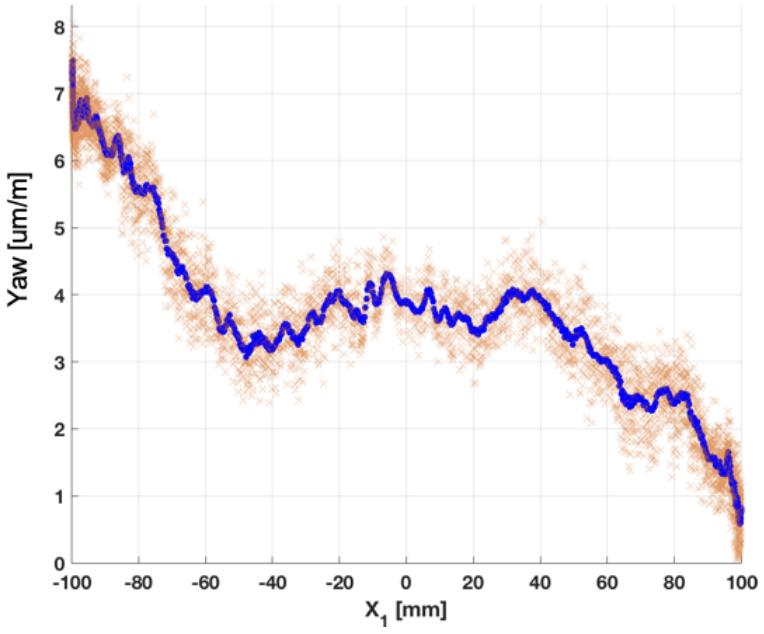

Figure 4.8: The systematic error element separated from the raw data.

4.3 Summary

In this chapter, the outlook and future work of this study were discussed. In order to measure TCP accuracy with the kinematic model, the measurement of the six DOF error elements of each linear axis is necessary. To realize the six DOF measurement with the proposed dual linear scale system, gap detection between scale and read head is a crucial feature. In section 4.1, the principle of the gap detection was explained based on the theory of the magnetic field in the vicinity of a magnetized media. By measuring the gap at three points of the moving component, pitch and roll measurement will become possible. For translational elements, Fujimori et al. proposed a unique arrangement of the magnetized tick marks. Such advance in linear scale technology would realize the measurement of the six DOF error elements.

In addition to the six DOF measurements, real-time measurement is another key to the dynamic error compensation. The measurement data is obtained as scattered data points. In order to extract the systematic error elements from the raw data, the author proposed a non-parametric regression algorithm so-called k nearest neighbors algorithm. By using a sample data set, the systematic data extraction was performed. The result showed that the kNN algorithm was able to determine the systematic error with 1.4% of accuracy in terms of RMSE. This indicates that the kNN algorithm can be used for the systematic error extraction with sufficient accuracy.

Chapter 5

Summary and Conclusion

Accuracy preservation of CNC machine tools is a key to promote factory automation. An ideal machine tool would be able to reproduce parts with the same accuracy during the operating lifetime. In order for a machine tool to be able to preserve its accuracy, accuracy deterioration should be automatically detected and compensated. In this research, a novel dual linear scale based accuracy compensation concept was proposed in order to achieve such an automatic error compensation. The physical prototype has been designed and developed to verify the feasibility of the proposed concept. The following is a summary of this study:

1. The dynamic error compensation concept has been proposed from the future perspective of automation of the manufacturing process. The key to realizing the concept was the measurement of the machine accuracy without interrupting manufacturing processes. The approach to realize the measurement was discussed, introducing the kinematic modeling of the machine tool.

2. In order to realize accuracy measurement using the kinematic model, six DOF error elements were needed to be measured, and the selection of an appropriate sensor was a challenge. Several sensors were picked up as the candidates, and a linear encoder was selected for the cost, durability, and scalability of the degrees of freedom of the measurement.

3. The design of the dual linear scale system has been performed. There were various uncertainties that affect the accuracy of measurement when using two linear scales to measure the angular deviation. Accuracy of individual linear scale, the parallelism of the two linear scales, offset of zero reference position, thermal expansion of linear scale, and time accuracy of the digital sampling of position signal were considered, and their impact was estimated by provisional calculations.

4. The physical prototype has been developed based on the design and preliminary analysis. In order to achieve sufficient time accuracy of the sampling of the position signal, a synchronous data capturing device was specifically designed.

5. The basic measurement performance of the dual linear scale system was studied. The measurement of the yaw of the Y-axis component was performed by the dual scale system and a laser interferometer at the same time. The reliability of the measurement of the scale system was evaluated by comparing it with the laser measurement. The scale measurement agreed with the laser measurement within the uncertainty of $(1.5 + 1.5L)/D$ (L is the travel distance and D is the distance between the paired linear scales) which has been estimated by the preliminary analysis.

6. The measurement test was conducted under time-variant temperature conditions to evaluate the thermal impact on the measurement accuracy. It has been found that the thermal expansion of linear scales had a significant impact on the measurement result of the scale system. In order to overcome this issue, thermal compensation of the measurement value was proposed, and that successfully suppressed 90.3% of the thermal impact.

7. Accuracy change detection and its compensation were conducted. Aging deterioration of yaw accuracy was replicated by intentionally distorting the linear guideways, and the scale measurement system was successfully able to detect the change of the yaw accuracy due to the deterioration. The associated TCP accuracy deterioration was calculated by the kinematic model, and its compensation was attempted. The compensation was able to suppress 86 % of the accuracy deterioration.

8. Future perspective of this study has been discussed. Based on the theory of magnetic field intensity, it was explained that six DOF measurement would be possible in principle by arranging multiple read heads on the moving component. Also, in order to realize a dynamic error measurement, a data analysis scheme with k nearest neighbor algorithm was introduced, and its feasibility was assessed with a sample data.

From these results, the feasibility of the proposed dual linear scale system has been verified for yaw measurement. The same kinematic model and data analysis scheme is also applicable to the remaining five DOF elements. Since the scale system has the scalability of the degrees of freedom of the measurement, further development of the linear scale technology still remains to improve the maturity of this system.

Bibliography

[1] R. L. Simison. *Mother Machines*. MIT Technology Review, https://www.technologyreview.com/s/530716/mother-machines/. [Online; accessed June 4, 2019]. 2016.

[2] JIS B 0105:2012. *Machine Tools -Designation-Vocabulary*. Japanese Industrial Standards.

[3] Japan Machine Tool Builders' Association. *Machining Methods of Machine Tools*. https://www.jmtba.or.jp/machine/introduction. [Online; accessed on February 6, 2020]. 2020.

[4] M. K. Thompson et al. "Design for Additive Manufacturing: Trends, Opportunities, Considerations, and Constraints". In: *CIRP annals* 65.2 (2016), pp. 737–760.

[5] DMG MORI Co., Ltd. *LASERTEC 65 3D*. https://www.dmgmori.co.jp/en/products/machine/id=1542. [Online; accessed on February 10, 2020]. 2020.

[6] OKUMA Corporation. *MU-8000V LASER EX*. https://www.okuma.com/mu-8000v-laser-ex. [Online; accessed on February 10, 2020]. 2020.

[7] YAMAZAKI MAZAK Corporation. *VARIAXIS j-600/5X AM*. https://english.mazak.jp/machines/technology/hybrid-multi-tasking-machine/am. [Online; accessed on February 10, 2020]. 2020.

[8] Y. Yamane and T. Childs. *Manufacturing Technology Transfer: A Japanese Monozukuri View of Needs and Strategies*. Taylor & Francis, 2018. ISBN: 9781466567641. URL: https://books.google.co.jp/books?id=xYV7DwAAQBAJ.

[9] N. Taniguchi. "Current Status in, and Future Trends of, Ultraprecision Machining and Ultrafine Materials Processing". In: *CIRP annals* 32.2 (1983), pp. 573–582.

[10] T. Nakajima and N. Narutaki. *Machining Technology*. CORONA PUBLISHING Co., Ltd., 1983, p. 2.

[11] DMG MORI Co., Ltd. [Online; accessed on February 6, 2020]. 2020. URL: https://www.dmgmori.co.jp/en/products/machines/.

[12] I. Inasaki. *Machining System*. Yokendo, 2009, p. 5.

[13] H. Schwenke et al. "Geometric Error Measurement and Compensation of Machines—An update". In: *CIRP Annals - Manufacturing Technology* 57.2 (2008), pp. 660–675.

[14] R. Ramesh, M. A. Mannan, and A. N. Poo. "Error Compensation in Machine Tools-a Review: part I: Geometric, Cutting-Force Induced and Fixture-Dependent Errors". In: *International Journal of Machine Tools and Manufacture* 40.9 (2000), pp. 1235–1256.

[15] W. R. Moore. *Foundations of Mechanical Accuracy*. The MIT Press, 1971, p. 37.

[16] M. Weck et al. "Reduction and Compensation of Thermal Errors in Machine Tools". In: *CIRP Annals - Manufacturing Technology* 44.2 (1995), pp. 589–598.

[17] J. Mayr et al. "Thermal Issues in Machine Tools". In: *CIRP Annals - Manufacturing Technology* 61.2 (2012), pp. 771–791.

[18] Y. Koren et al. "Advanced Controllers for Feed Drives". In: *Annals of the CIRP* 41 (1992), p. 2.

[19] P. Majda. "Modeling of Geometric Errors of Linear Guideway and Their Influence on Joint Kinematic Error in Machine Tools". In: *Precision Engineering* 36.3 (2012), pp. 369–378.

[20] G.T. Smith. "Machine Tool Metrology: An Industrial Handbook". In: Springer, 2016, p. 148.

[21] H. Uchida and M. Sogabe. "Linear Motor in Precision Engneering". In: *Journal of the Japan Society for Precision Engineering* 75.2 (2009), pp. 242–245. DOI: 10.2493/jjspe.75.242.

[22] Sodick Co., Ltd. *The Art of Monodukuri (Techniques for Creating Things)*. https://www.sodick.co.jp/st_en/tech/linear_motor.html. [Online; accessed on February 6, 2020]. 2020.

[23] Matsuura Machinery USA Co., Ltd. *No Substitute for Hand Scraping When It Comes to Maintaining High Levels of CNC Machining Accuracy*. http://matsuurausa.com/no-substitute-for-hand-scraping/. [Online; accessed 21-February-2020]. 2020.

[24] Wikipedia contributors. *Hand scraper — Wikipedia, The Free Encyclopedia*. [Online; accessed 21-February-2020]. 2020. URL: https://en.wikipedia.org/w/index.php?title=Hand_scraper&oldid=935543835.

[25] THK Co., Ltd. *LM Guide (Linear Motion Guide)*. [Online; accessed 21-February-2020]. 2020. URL: https://www.thk.com/?q=us/node/5197.

[26] Wikipedia contributors. *Backlash (engineering) — Wikipedia, The Free Encyclopedia*. https://en.wikipedia.org/w/index.php?title=Backlash_(engineering)&oldid=931700965. [Online; accessed 6-March-2020]. 2019.

[27] Y. Altintas et al. "Machine Tool Feed Drives". In: *CIRP Annals - Manufacturing Technology* 60.2 (2011), pp. 779–796.

[28] American Ball Screw Repair. *Ball Screw Repair Process*. [Online; accessed 21-February-2020]. 2020. URL: https://www.americanballscrewrepair.com/ball-screw-repair-process/.

[29] THK Co., Ltd. *Rotary Ball Screw*. [Online; accessed 21-February-2020]. 2020. URL: https://tech.thk.com/upload/catalog_claim/pdf/cat_blr_dir_en.pdf.

[30] Oriental Motor Co., Ltd. *Backlash, Glossary of Terms*. [Online; accessed 21-February-2020]. 2020. URL: https://www.orientalmotor.com/linear-actuators/technology/electric-linear-slides-terms.html.

[31] Y. Altintas et al. "Virtual Machine Tool". In: *CIRP Annals-manufacturing technology* 54.2 (2005), pp. 115–138.

[32] A. Hansel, K. Yamazaki, and K. Konishi. "Improving CNC Machine Tool Geometric Precision Using Manufacturing Process Analysis Techniques". In: *Procedia CIRP* 14 (2014), pp. 263–268.

[33] Y. Kakino and K. Okushima. "Study on Thermal Deformations of Machine Tools (4th Report)". In: *Journal of the Japan Society of Precision Engineering* 40.479 (1974), pp. 1105–1110. DOI: 10.2493/jjspe1933.40.1105.

[34] S. Nakamura et al. "An Analysis on Influence of Motor Heat Generation and Effect of Shaft-bore Cooling for Motor Integrated Spindle". In: *Journal of the Japan Society for Precision Engineering* 60.7 (1994), pp. 979–983. DOI: 10.2493/jjspe.60.979.

[35] DMG MORI Co., Ltd. *NVX7000 Product Catalog*. 2020.

[36] T. H. C. Childs, K. Maekawa, and P. Maulik. "Effects of Coolant on Temperature Distribution in Metal Machining". In: *Materials Science and Technology* 4.11 (1988), pp. 1006–1019. DOI: 10.1179/mst.1988.4.11.1006.

[37] DMG MORI Co., Ltd. *Constant-Temperature Factory Announcement*. https://www.dmgmori.co.jp/corporate/en/news/pdf/2006_0124_Temp_cont.pdf. [Online; accessed September 30, 2019]. 2006.

[38] YAMAZAKI MAZAK Corporation. *YAMAZAKI MAZAK Inabe Plant*. https://english.mazak.jp/our-factory/inabe/. [Online; accessed September 30, 2019]. 2019.

[39] C. Brecher, P. Hirsch, and M. Weck. "Compensation of Thermo-elastic Machine Tool Deformation Based on Control internal Data". In: *CIRP Annals - Manufacturing Technology* 53.1 (2004), pp. 299–304.

[40] H. Möhring et al. "Materials in Machine Tool Structures". In: *CIRP Annals-Manufacturing Technology* 64.2 (2015), pp. 725–748.

[41] E. Uhlmann and P. Marcks. "Compensation of Thermal Deformations at Machine Tools Using Adaptronic CRP-Structures". In: *Manufacturing Systems and Technologies for the New Frontier*. Springer, 2008, pp. 183–186.

[42] NTN Co., Ltd. *Linear Guides, Technical Explanation (Catalog No. 6108)*. Catalog, https://www.ntn.co.jp/japan/products/catalog/pdf/6108_02.pdf. [Online; accessed 6-March-2020]. 2019.

[43] H. Mizumoto. "A Fascinating World of Hydrostatic and Aerostatic Bearings". In: *Journal of the Japan Society for Precision Engineering* 73.5 (2007), pp. 537–540. DOI: 10.2493/jjspe.73.537.

[44] International Organization for Standardization. *Ball Screws – Part 1: Vocabulary and designation*. [Online; accessed 21-February-2020]. 2006. URL: https://www.iso.org/obp/ui/#iso:std:iso:3408:-1:ed-2:v1:en.

[45] Japan Machine Tool Builders' Association. "Design of Machine Tools (in Japanese)". In: Japan Machine Tool Builders' Association, 1998, p. 160.

[46] Y. Altintas and A.A. Ber. "Manufacturing Automation: Metal Cutting Mechanics, Machine Tool Vibrations, and CNC Design". In: *Appl. Mech. Rev.* 54.5 (2001), B84–B84.

[47] G. Zhang et al. "Error Compensation of Coordinate Measuring Machines". In: *CIRP Annals-Manufacturing Technology* 34.1 (1985), pp. 445–448.

[48] M. A. Donmez et al. "A General Methodology for Machine Tool Accuracy Enhancement by Error Compensation". In: *Precision Engineering* 8.4 (1986), pp. 187–196.

[49] MACHINETOOLHELP.COM. *What Exactly is Machine Backlash? Ballscrew Backlash, Ballscrew Slop, Bearing Backlash and More.* http://www.machinetoolhelp.com/Repairing/What_is_backlash.html.

[50] THK Co., Ltd. *Ball Screw General Catalog, Support Book*. Catalog. [Online; accessed 6-March-2020]. 2019.

[51] Renishaw plc. *Volumetric Error Compensation*. https://www.renishaw.com/en/volumetric-error-compensation--24159. [Online; accessed 6-March-2020].

[52] S. Ibaraki. *Soichi Ibaraki Laboratory Homepage*. https://home.hiroshima-u.ac.jp/ibaraki/morikita_jp.html. [Online; accessed on February 4, 2020]. 2020.

[53] R. Sato. "Generation Mechanism of Quadrant Glitches on Circular Trajectories (in Japanese)". In: *Proceedings of JSPE Semestrial Meeting* 2016S (2016), pp. 473–474. DOI: 10.11522/pscjspe.2016S.0_473.

[54] R. Sato. "Generation Mechanism of Quadrant Glitches and Compensation for It in Feed Drive Systems of NC Machine Tools". In: *International Journal of Automation Technology* 6.2 (2012), pp. 154–162.

[55] R. Sato. "Generation Mechanism of Quadrant Glitches on Circular Trajectories (in Japanese)". In: *Keynote Speech in Japan's Society of Precision Engineering* (2016), pp. 473–474.

[56] "Structure Model Based Correction of Thermally Induced Motion Errors of Machine Tools". In: *Procedia Manufacturing* 14 (2017). 17th Machining Innovations Conference for Aerospace Industry, MIC 2017, 6-7 December 2017, Garbsen, Germany, pp. 128–135. ISSN: 2351-9789. DOI: https://doi.org/10.1016/j.promfg.2017.11.015.

[57] M. Fujishima et al. "Thermal Displacement Reduction and Compensation of a Turning Center". In: *CIRP Journal of Manufacturing Science and Technology* 22 (2018), pp. 111 –115. ISSN: 1755-5817. DOI: https://doi.org/10.1016/j.cirpj.2018.04.003. URL: http://www.sciencedirect.com/science/article/pii/S1755581718300166.

[58] H. Nakazawa. *Principles of Precision Engineering*. Oxford University Press, USA, 1994.

[59] Renishaw plc. *Brochure: XL-80 Laser Measurement System*.

[60] F.S.K. Co., Ltd. *The Principle of the Precision Level*. https://www.fsk-level.com/. [Online; accessed 6-March-2020]. 2020.

[61] Renishaw plc. *QC20-W on Machine*. [Online; accessed September 27, 2019]. 2019.

[62] S. Ibaraki et al. "Self-calibration of a Cross Grid Encoder". In: *Journal of the Japan Society for Precision Engineering, Contributed Papers* 72.8 (2006), pp. 1032–1037. DOI: 10.2493/jspe.72.1032.

[63] Heidenhain. *Measuring Devices For Machine Tool Inspection and Acceptance Testing 01*.

[64] NIST Public Affairs Office. *NIST's Role in Laser Measurements and Applications*. https://www.nist.gov/director/pao/nists-role-laser-measurements-and-applications/1980s. [Online; accessed September 27, 2019].

[65] ETALON GmbH. *Testing and Calibration of Coordinate Measuring Machines*. https://www.etalon-gmbh.com/en/applications/testing-and-calibration-of-coordinate-measuring-machines/. [Online; accessed September 30, 2019]. 2019.

[66] H. Schwenke et al. "On-the-fly Calibration of Linear and Rotary Axes of Machine Tools and CMMs Using a Tracking Interferometer". In: *CIRP Annals - Manufacturing Technology* 58.1 (2009), pp. 477–480.

[67] S. Ibaraki et al. "Measurement of Thermal Influence on a Two-dimensional Motion Trajectory Using a Tracking Interferometer". In: *CIRP Annals - Manufacturing Technology* 65.1 (2016), pp. 483–486.

[68] Glenn McKechnie / CC BY-SA (https://creativecommons.org/licenses/by sa/2.0). *Thin-wall milling of aluminum using a water-based cutting fluid on the milling cutter*. https://upload.wikimedia.org/wikipedia/commons/1/16/Makino-S33-MachiningCenter-example.jpg. [Online; accessed March 20, 2020]. 2020.

[69] G. E. Sommargren. "Linear/Angular Displacement Interferometer For Wafer Stage Metrology". In: *1989 Microlithography Conferences* 1088 (July 1989), pp. 268–273.

[70] W. Gao et al. "Measurement of Multi-degree-of-freedom Error Motions of a Precision Linear Air-bearing Stage". In: *Precision Engineering* 30.1 (Jan. 2006), pp. 96–103.

[71] N. Imai and S. Shimizu. "Simultaneouse Measuring Method of Linear Motion Error of the Machine Tool Table". In: *Journal of the Japan Society for Precision Engineering* 67.1 (2001), pp. 126–130. DOI: 10.2493/jjspe.67.126.

[72] G.W. Vogl, M. A. Donmez, and A. Archenti. "Diagnostics for Geometric Performance of Machine Tool Linear Axes". In: *CIRP Annals - Manufacturing Technology* 65.1 (2016), pp. 377–380.

[73] ISO 10791-1:2015. *Test conditions for machining centres – Part 1: Geometric tests for machines with horizontal spindle (horizontal Z-axis)*. International Organization for Standardization.

[74] Renishaw plc. *User guide: XM-60 and XM-600 multi-axis calibrator*. https://www.renishaw.com/en/xm-60-and-xm-600-multi-axis-calibrator-performance-specification--39927. [Online; accessed October 2, 2019]. 2019.

[75] T. Fujimori et al. "A Study on Multi DOF Magnetic Scale for Motion Control Compensation of Machine Tool". In: *TRANSACTIONS OF THE JAPAN SOCIETY OF MECHANICAL ENGINEERS Series C* 79.806 (2013), pp. 3993–4001. DOI: 10.1299/kikaic.79.3993.

[76] Jewell Instruments. *Model A701-2A/B High-precision Platform Tiltmeter*. http://jewellinstruments.com/wp-content/uploads/2016/01/L00209-A701-2-Rev-B.pdf. [Online; accessed October 2, 2019]. 2019.

[77] Taylor Hobson. *Autocollimators and Accessories*. [Online; accessed October 2, 2019]. 2019.

[78] G. W. Vogl, B. A. Weiss, and M. A. Donmez. "A Sensor-based Method for Diagnostics of Machine Tool Linear Axes". In: *Proceedings of the Annual Conference of the Prognostics and Health Management Society. Prognostics and Health Management Society. Conference*. Vol. 6. NIH Public Access. 2015.

[79] G. T. Smith. "Machine Tool Metrology: An Industrial Handbook". In: Springer, 2016, p. 148.

[80] ISO 10791-4:1998. *Test Conditions for Machining Centres – Part 4: Accuracy and Repeatability of Positioning of Linear and Rotary Axes*. International Organization for Standardization.

[81] D. Dornfeld and M. M. Helu. *Precision Manufacturing*. Springer US, pp. 37–56.

[82] DMG MORI Co., Ltd. *NHX4000 2nd Generation Product Catalog*. 2015.

[83] T. Fujimori. "A Study on Linear Scale System for High Precision Motion Control of NC Machine Tools". In: *Ph.D. Dissertation* (), pp. 29–37.

[84] W. Gao. "New Encoder Technologies". In: *Journal of the Japan Society for Precision Engineering* 82.9 (2016), pp. 773–777. DOI: 10.2493/jjspe.82.773.

[85] Magnescale Co., Ltd. *Product Information of SmartSCALE SQ57*. http://www.magnescale.com/mgs/product/SQ47_57.html. 2019 (accessed December 9, 2019).

[86] National Institute of Standards and Technology. *Evaluating uncertainty components: Type B*. https://physics.nist.gov/cuu/Uncertainty/typeb.html. [Online; accessed on May 6, 2020]. 2020.

[87] K. Matsumoto, A. Ito, and A. Morisako. *Magnetic Recording Engineering (in Japanese)*. Kyoritsu Shuppan, 1990. ISBN: 978-4-320-08488-9. URL: https://www.kyoritsu-pub.co.jp/bookdetail/9784320084889.

[88] W. Zhu, Z. Wang, and K. Yamazaki. "Machine Tool Component Error Extraction and Error Compensation by Incorporating Statistical Analysis". In: *International Journal of Machine Tools and Manufacture* 50.9 (Mar. 2015), pp. 798–806.